Elasticity and disorder in irreversible deformation of materials

Paolo Moretti

A thesis submitted for the degree of Doctor of Philosophy.
The University of Edinburgh.
October 2005

Abstract

The role of elasticity and disorder and their interplay in plastic deformation processes is investigated on different length scales. Random disorder, in the form of impurities, fluctuations of defect densities and spatial heterogeneities, is responsible for a wealth of phenomena including surface roughening, non-linear dynamic response, stick-slip behaviour and temporal intermittency, which are observed in a wide variety of physical systems. A theoretical description of these phenomena is provided by theories of pinning and depinning transitions. In this work, these aspects are investigated in the context of plastic deformation of random media, such as real crystals with disordered microstructures or disordered elastic continua. Under the effect of an external force, these systems exhibit a complex behaviour arising form the competition between elasticity and disorder. Disorder tends to perturb the system, which reacts by opposing elastic restoring forces. This complex small scale dynamics determines the macroscopic behaviour of irreversibly deforming materials. These aspects are studied on different length scales.

The problem of the depinning transition occurring in dislocation assemblies is first investigated. Dislocations are microstructure defects mediating plastic deformation. Under the effect of external forces, they are driven through disordered landscapes and rearrange into complex assemblies. A theory of pinning and collective behaviour of linear and planar dislocation arrays is formulated. Non-local elastic properties arise naturally form long-range dislocation interactions and influence dramatically statics and dynamics of these systems in the presence of disorder. Comparison with numerical results and experimental data confirms the validity of this approach.

An application to vortex lattices in Type II superconductors is then considered. Dislocation assemblies such as low angle grain boundaries are often observed in these systems, determining the emergence of a polycrystalline phase. A theory of vortex polycrystals is proposed, in the conceptual framework of grain boundary pinning. Several aspects, including grain growth, transport properties, hysteretic behaviour and vortex lattice melting are investigated. Results are found in agreement with numerical simulations and experimental observations.

On larger length scales, a theory of plastic flow in the presence of random stress fluctuations is discussed. The problem proves to be described by a continuum mean-field pinning model, where disorder is produced by randomness in dislocation densities. Such a description provides a theoretical framework to understand the origin of the critical behaviour often observed in plastically deforming crystals in the form of self-affine surface roughening and intermittent avalanche motion.

The problem of interface failure is finally investigated and its applications to landslides and slab avalanches are discussed. It is shown that randomness can decrease the strength of a snow or clay slope by inducing crack nucleation, or increase it by promoting crack pinning. Failure is proven to be the result of this complex interplay.

Declaration of originality

I hereby declare that the research recorded in this thesis and the thesis itself was composed and originated entirely by myself in the School of Engineering and Electronics at The University of Edinburgh.

Paolo Moretti

Acknowledgements

"When the sun beats down and I lie on the bench, I can always hear them talk.
Me, I'm just a lawnmower - you can tell me by the way I walk."

The author would like to thank M. Zaiser for his patience and support and for the invaluable contribution given to this work.

Precious collaboration of M.-C. Miguel and S. Zapperi as well as contributions to this work by B. A. Fyffe are gratefully acknowledged.

Kind supervision of V. Koutsos and financial support of EPSRC under Grant No. GR/S20406/01 are equally acknowledged.

Thanks to all my friends, whom I met here or far away.

Thanks to my family, for their unreplaceable and unconditional support over the years, and to Chiara, for her sympathy, affection and understanding.

Contents

List of figures

List of tables

Acronyms and abbreviations

AFM	atomic force microscopy
BrG	Bragg glass
CDW	charge density wave
FC	field cooling
FRG	functional renormalisation group
GB	grain boundary
HTSC	high temperature superconductor
LAGB	low angle grain boundary
MF	mean field
MSG	Martin-Siggia-Rose
RG	renormalisation group
RM	random manifold
STM	scanning tunneling microscopy
SWLI	scanning white-light interferometry
ZFC	zero-field cooling
2D	two-dimensional space
3D	three-dimensional space

Nomenclature

This list contains notations which are used repeatedly.

a	vortex lattice spacing
$\tilde{a}$	lowest order in k expansion of elastic kernel
$\mathbf{b}$	Burgers vector
B	magnetic induction
$\tilde{B}$	reduced magnetic induction
B_{c_2}	second critical magnetic induction
$B_{ij}(...)$	Vortex lattice displacement correlator
c	pinning centre density
$\tilde{c}_{eff}$	effective pinning centre density (two dimensions)
c_{eff}	effective pinning centre density (three dimensions)
c_{11}	compression modulus (vortex lattice)
c_{44}	tilt modulus (vortex lattice)
c_{66}	shear modulus (vortex lattice)
$C(...)$	displacement correlator
C_{ijkl}	Hooke tensor
d	manifold dimension
d_c	critical manifold dimension
$\mathbf{d}$	dislocation array direction
D	average dislocation spacing
$\mathcal{D}$	functional differential
$\mathbf{e}$	dislocation direction unity vector
E	generic energy
$\mathbf{f}$	Peach-Koehler force
f_0	typical pinning force per unit length
f_p	pinning field
F^{ext}	external force
F_c	critical force

G	shear modulus
$\mathcal{H}$	Hamiltonian
$\mathcal{G}$	Green function for a deforming grain boundary
h	generic thickness
H	Hurst exponent
H_{c_2}	second critical magnetic field
J_c	critical current density
K	isotropic elastic constant (vortex lattice)
K_B	Boltzmann constant
L	deformation length
L_c	weak pinning length (Larkin length)
L_f	strong pinning length (Friedel length)
L_p	grain boundary weak pinning length
n	grain boundary density
N	number of dislocations
N_p	number of pinning centres
N_v	number of vortices
$p(...)$	probability distribution
R_a	vortex lattice weak pinning length
R_g	average grain size
s	avalanche size (swept area)
s_0	avalanche size cutoff
S	grain boundary surface
$S_{ij}(...)$	vortex lattice stress correlator
$\mathcal{S}$	functional action
t^*	correlation time
T	temperature
T_m	melting temperature
$\mathbf{u}$	deformation vector
u_{GB}	grain boundary deformation
v	average collective velocity
z	dynamic exponent
$\mathcal{Z}$	partition function
β	velocity exponent

β_{ij}^{p}	plastic distorsion tensor component
β_{ij}^{r}	relaxation strain tensor component
γ	shear strain
$\dot{\gamma}$	strain rate
γ_0	grain boundary surface energy
γ_E	Euler's constant
γ_T	grain boundary thermal surface energy
$\Gamma(\mathbf{k})$	elastic kernel
Γ_0	line/surface tension
Γ_{ik}	Green tensor component
$\delta(...)$	Dirac's delta function
δF	force fluctuations
ϵ	small increment in expansion
ϵ_0	typical vortex interaction energy
ε	plastic strain (experiments)
ζ	roughness exponent
ζ_{GB}	grain boundary roughness exponent
θ	susceptibility exponent
θ_v	velocity relaxation exponent
Θ	hardening coefficient
κ	avalanche exponent
λ	first Lamè coefficient
λ_{sc}	superconductor penetration depth
μ	mobility coefficient
μ_{pl}	plastic creep exponent
ν	correlation function exponent
ν_P	Poisson ratio
ξ	critical correlation length
$\xi_{\parallel}$	longitudinal disorder correlation length
$\xi_{\perp}$	transversal disorder correlation length
ξ_p	generic disorder correlation length
ξ_{sc}	superconductor correlation length
ξ_τ	dislocation-dislocation correlation length
ρ	dislocation density

σ	stress tensor
σ_{ij}	stress tensor component
σ_m	peak strength variance
τ	resolved shear stress
τ_c	critical/failure stress
τ_{ext}	external/driving stress
τ_f	flow stress
τ_{int}	internal shear stress
τ_m	peak strength
τ_p	pileup back stress
Φ_0	magnetic flux quantum
χ	susceptibility
$\times$	vector product
$\otimes$	dyadic product

Introduction

The balance between elasticity and disorder is responsible for equilibrium properties and dynamic response in a profuse abundance of physical systems exhibiting irreversible deformation. A typical approach to the subject of deformation consists in looking at the problem in terms of transport, either of defects or of the deforming medium itself.

Natural phenomena often involve collective transport, which is often characterised by large-scale critical behaviour, as in slab avalanches, landslides or earthquakes. On smaller length scales, collective transport is encountered in familiar contexts such as fracture, slip-stick events or glide in the presence of friction in general.

In fact, non-equilibrium dynamics can be observed also at microscopic scales. Even when we see "ordinary" and smooth behaviour of materials during deformation, at the micron scale the system undergoes abrupt changes, defects proliferate randomly and rearrange according to complicated patterns. The system deforms in an intermittent manner: what appears as a regular process on the large scales of common observation, is characterised by apparently irregular bursts and intricate spatiotemporal signatures on microscopic scales.

Ordering processes such as recrystallisation, i.e. the restoration of crystalline structure over a lattice, can be described in terms of critical behaviour too. Defects are expected to slide both cooperatively and individually through a series of metastable states, always being subject to instabilities induced by their own mutual interactions.

Even properties of electric and electronic devices are influenced by critical transport in the microscopic domain. Although the transport of conduction electrons is a slow, close-to-equilibrium process, stability and performance of superconductor based devices are undermined by the critical response of the material. In particular, the remarkable class of Type II superconducting crystals and alloys shows an intriguing critical behaviour in the presence of an applied magnetic field, as interacting current vortices and topological defects determine the macroscopic efficiency of the system as well as its phase stability.

Of course, such an abundance of physical examples, including geological events as well as atomistic scale phenomena within its range, may be confusing at first. One may wonder what

earthquakes and crystals have in common, and in which sense criticality observed in the former is "the same" as the one encountered in the latter, if a closer look is taken.

What characterises all the systems that we have briefly introduced, as well as many more, is the role of *randomness* in irreversible deformation. Geological faulting occurs on randomly disordered substrates. Rupture is governed by random forces exerted by defects. Topological defects in deforming crystals are subject to stress fields generated within their random arrangements. Vortices get pinned by random heterogeneities in the underlying superconductor. As the reader may notice, microstructural randomness, i.e. *disorder*, plays a key role. It does not simply perturb the response of the system to an external load. It induces a novel class of phenomena, including intermittency, avalanches, spatial heterogeneity and roughening.

Such phenomena are explained by the theory of collective transport in random media. According to the related theoretical approach, the system perceives the presence of *disorder*, induced by spatial heterogeneities and randomly distributed defects, and deforms according to linear elastic behaviour. An infinitely stiff medium would not allow deformation. Elastic behaviour, instead, allows disorder to perturb the medium in order to reduce energy. In the absence of external loads the system is *pinned* in a stable configuration. Introducing a driving force, critical phenomena such as avalanches appear, as the system is driven through a sequence of metastable states. For strong enough loads, beyond a critical point, the system *depins*, i.e. fails or breaks, generating large scale flow events — the example of an earthquake might be instructive in this case.

In other words, the behaviour of a random medium is governed by three competing effects: (i) disorder tends to corrugate the medium, as deformation allows it to explore lower energy areas randomly disposed in the underlying substrate; (ii) elastic forces counteract deformation in order to minimise elastic energy; (iii) the external force acts on the medium inducing, depending on its intensity, deformation, creep motion or *depinning*.

The generality of such a description allows the so called *pinning theories* to account for the behaviour of a huge variety of diverse phenomena, including earthquake onset, fracture and vortex dynamics, as well as motion of magnetic domain walls or solid-liquid contact lines.

In this thesis we summarise the work which we have done on this field over the past years. We investigate several properties of diverse physical systems and explain their irreversible, or

plastic, behaviour in terms of the interaction between elasticity and disorder.

An elastic description of deforming bodies is appropriate in the case of small deformations. This description holds, for instance, when deformation is induced by immobile defects and spatial heterogeneities embedded in the medium (*quenched disorder*). Determining elastic properties may not be, however, a trivial task. The elastic description of deforming strings and interfaces — the so called *local elasticity* approach — is a powerful tool in several cases. Nevertheless, the elastic response in certain systems is given by long-range interactions, which result in a stiffening of the medium under examination. Such systems fall in the class of *non-local elasticity*. One can in principle assess the type of elasticity by calculating the elastic response to a perturbation. This may not always be easy as several complications may arise, for instance, from anisotropy, but is in general essential as the interaction with disorder depends on the elastic nature of the medium. These aspects are investigated in this work.

In the first place, we consider the problem of dislocation dynamics within a disordered landscape. Dislocations are responsible for plastic deformation of crystalline materials. Due to their long-range interactions, they tend to glide cooperatively, forming in general large assemblies which move through the material according to complicated spatiotemporal patterns. The pinning of an isolated dislocation has been studied in the past, but it does not necessarily account for the real nature of the problem, given the collective nature of dislocation behaviour. Developing an analytical theory of the depinning transition of a generic ensemble of interacting dislocations is of course a formidable task. Linear assemblies, however, such as pileups and low-angle grain boundaries (LAGB) are often encountered experimentally during relaxation processes and provide a nice exemplification for the problem of the interplay between elasticity and disorder.

We develop an elastic theory for such arrangements and conclude that their response to deformations falls into the category of non-local elasticity. Pileups and grain boundaries are thus stiffer than dislocation lines and this affects dramatically their behaviour in the presence of quenched disorder. The problem of depinning is then studied in the light of these results. At stresses close to the depinning threshold, the dynamics exhibit critical behaviour. Referring to previous *renormalisation group* results, we gain a complete quantitative picture of the depinning transition. In the elastic approximation, pileups and low angle grain boundaries are equivalent to a standard interface depinning problem with long-range elasticity. In two dimen-

sions, the problem can be mapped on a contact line or a planar crack, while in three dimensions, the system mimics dynamics of magnetic domain walls.

Next, we examine applications of grain boundary depinning to vortex lattices in Type II superconductors. Experimental observations often show that these systems exhibit polycrystalline ordering under specific conditions. Grain boundaries break topological order into domains of different orientations. In spite of the wealth of observations, no previous theory accounts for the emergence of a vortex polycrystal. However, a polycrystalline arrangement is expected to dramatically modify transport properties in the underlying superconductor. The critical current, below which vortices are pinned and the material conducts without resistance, is expected to change in the presence of a vortex polycrystal. At the same time, the emergence of amorphous and liquid phases in vortex matter is preceded by a metastable polycrystalline arrangement.

In order to investigate properties of vortex polycrystals, we re-derive non-local elasticity in the case of vortex lattice grain boundaries and re-formulate an appropriate pinning theory. We explain the formation of a polycrystal in terms of competition between elastic forces and disorder and accordingly investigate several aspects of the polycrystalline state including the dynamics of grain growth. The validity of our model is assessed by comparing results with experiments. Transport properties are discussed in the light of a numerical implementation of the model. The system shows enhanced critical current and hysteretic behaviour. The technological relevance of a higher critical current is evident, since vortex motion determines resistance and dissipation of the superconductor. A vortex polycrystal is more effectively pinned and ensures absence of resistance at higher induced currents. Finally, the role of grain boundaries in the melting of vortex lattices is examined through phenomenological arguments.

Then our attention turns to larger length scales, where the discrete nature of microstructure defects is averaged over large volumes and plastically deforming materials are described by continuum models in terms of plastic flow. Even on these scales, where the discrete nature of the underlying defected lattice is supposed to homogenise, the system exhibits heterogeneous features. As stated above, plastic flow proceeds through abrupt bursts, or "avalanches", with scale-free size distributions, while surfaces show self-affine morphology. These findings are currently interpreted as signals of the vicinity of a phase transition. In other words, crystals under deformation are envisaged as close to a critical point (*yielding transition*).

In this context, we propose a simple theoretical model, accounting for heterogeneities introduced by fluctuations in dislocation densities, which are supposed to be reminiscent of complex dislocation dynamics on smaller scales. The system proves to be adequately described within the theory of collective transport in random media, as the ensemble behaves like an elastic manifold driven through a disordered landscape. Numerical implementations performed by our co-workers confirm theoretical predictions. The model explains the experimental observation of avalanches as well as the roughening of surfaces according to scale-free patterns, confirming the hypothesis of critical behaviour and corroborating the conceptual framework of a *yielding transition*.

Finally, we examine the problem of slope failure, an irreversible deformation phenomenon which typically occurs on macroscopic length scales. In this regime, deforming bodies have no memory of processes occurring at the micron scale and are suitably described by elastic continua and related discrete approximations. Failure is governed by interface crack nucleation and propagation and disorder at the interface is expected to influence the failure mode.

We focus on the onset of slope failure, which commonly occurs in nature every time a landslide or a slab avalanche take place. We examine elastic properties of a snow or clay slope on a rigid bedrock and demonstrate that failure is governed by pinning of propagating interface cracks. Crack fronts exhibit non-local elasticity, like contact lines or linear dislocation arrays. In the presence of disorder they exhibit critical behaviour and roughen according to scale-free patterns. Numerical simulations performed by our co-workers confirm this picture, allowing us to assess the validity of our description.

Chapter 1
Random media in plastic deformation

This introductory chapter is meant to outline the different theoretical frameworks underlying the present work. Its aim is in particular to emphasise connections between theoretical approaches which describe apparently different physical systems within the common background of elasticity in the presence of disorder and related depinning theories.

1.1 General aspects of plasticity in the presence of disorder.

That of plastic deformation is a very general problem, responsible for a rich phenomenology occurring in diverse physical systems. One of the main aspects of plastic behaviour is its multiscale nature, which makes the formulation of a "definitive" theory a formidable task.

1.1.1 Basic length scales

The behaviour of a deforming crystal is the result of the interplay of processes occurring on length scales extending from the atomistic scale to the macroscopic sizes encountered in experiments. Such process are in general interdependent. As a consequence, the knowledge of microscopic foundations of plastic phenomena is essential for understanding their nature.

Length scales occurring in plastic deformation can be classified as follows [1]:

- The atomistic scale, where the problem comprises motion of individual atoms and their mutual interactions. Plasticity at this scale is explained in terms of dislocation core structures, dislocation mobility and short range interactions.
- The microscopic scale, where dislocations are "quanta" of plastic deformation. From the viewpoint of elasticity theory they appear as singularities in a disordered continuum and interact by long range fields, gliding according to collective patterns. Although assembled in extended arrays, they retain their discrete nature, their average spacing being the

appropriate measure of this length scale. A rich phenomenology is observed, including relaxation of dislocation arrangements, depinning of linear arrays, grain boundary glide and early stages of recrystallisation and grain growth. The typical approach to these problems is thus to investigate dynamics of both isolated and interacting dislocations.

- The mesoscopic scale, where plasticity is mediated by spatial distributions of dislocations described by continuous densities and correlation functions. Internal stress fields come from the statistical summation of stress fields of large numbers of dislocations. Dislocation motion can be described in terms of smooth *flow* or, as recently discovered, intermittent *avalanches*. Continuum models are typically adopted to investigate plasticity on this scale.

- The macroscopic scale, where heterogeneities and incoherent fluctuations are averaged over domains which constitute volume elements of the examined specimen. Plastic behaviour is described by deterministic constitutive laws.

1.1.2 Disorder on different length scales

The nature of disorder varies according to the examined length scale. On the atomistic/microscopic scale, disorder acting on dislocations has two main sources:

- Point defects — Solute atoms and particle inclusions constitute point-like crystal defects, often referred to as sources of *quenched disorder*. They determine pinning providing low energy areas for dislocations which are thus encouraged to roughen in spite of the elastic "cost" of deformation. They exert short-range forces. However, their individual nature is relevant only in the low density limit (strong pinning). For a dense distribution of defects, instead, short-range forces are statistically superimposed and generate a collective *pinning field*.

- Other dislocations — Immobile "forest" dislocations can be responsible for pinning of mobile dislocations. Unlike point defects, dislocations exert long-range stresses. The superposition of dislocation stress fields results in a fluctuating microscopic pinning field.

Turning to mesoscopic length scales, disorder is given by randomness in the dislocation arrangement. Spatial heterogeneities in dislocation densities produce fluctuations in the internal stress field of the same nature as the ones observed on microscopic scales.

Finally, in the case of macroscopic continua disorder is usually provided by spatial heterogeneities, density fluctuations and surface roughness (in the case of tribology problems).

How disorder affects equilibrium of these systems is explained in terms of pinning. An infinitely stiff medium is not affected by disorder. An elastically deformable medium, instead, is perturbed by disorder, which allows the deforming medium to explore lower energy areas. Deformation determines an increase in elastic energy, which is counteracted by the energy gain associated with disorder. In the absence of external forces, the balance between these two effects results in a stable configuration, which corresponds to a minimum in the total energy. The elastic medium is therefore collectively pinned by the disorder. If an external force is introduced, this configuration is no longer stable and the medium moves through a sequence of metastable states, giving rise to avalanche phenomena. If the applied force exceeds a critical value, no more metastable states exist: the medium *depins* and starts moving collectively.

A complex theory lies beyond the qualitative idea of a depinning transition that we have proposed so far. In fact, the theory of pinning, depinning transitions and transport phenomena in random elastic media transcends the context of plasticity and has found several applications over the past years in a wide variety of physical systems.

Pinning theories explain dynamics of complex systems in terms of the competition between elastic properties of the deforming medium and effects of the underlying disorder. This kind of approach can be extended to the case of plasticity and this is in fact one of the guidelines of the present work. To this end, the following section is devoted to a short summary of the current knowledge regarding pinning.

1.2 Pinning theories — an overview

Pinning theories have proven to be successful in describing several phenomena involving elastic media pushed through disorder. Considerable efforts have been made in order to understand how quenched impurities influence equilibrium and transport of, for instance, charge density waves [2–5], flux lines in Type II superconductors [6–11], dislocation lines [12–14], domain walls in ferromagnets [15, 16], contact lines [17, 18], crack fronts [19, 20] and invasion fronts [21, 22].

A rigorous treatment of pinning theories can be found in the vast literature concerning this topic

(see e.g. [5, 23–29]) and predictions have been confirmed by numerical simulations [26, 30–37]. Here we show the basic aspects of the problem and the main results as they turn out useful in the next chapters.

1.2.1 Formulation

Let us consider a d-dimensional manifold (e.g. a line, an interface) moving transversally through a $d+1$-dimensional medium. The d-dimensional vector $\mathbf{r}$ gives the coordinates parallel to the average orientation of the manifold, while u indicates the transversal coordinate. The configuration at a time t is given by $u(\mathbf{r},t)$, which is assumed to be single valued in order to avoid overhangs. The motion of our manifold obeys overdamped dynamics (i.e. viscosity overpowers inertia) and the equation of motion in the presence of an external force F_{ext} acting on the elastic manifold is given by

$$\frac{1}{\mu}\partial_t u(\mathbf{r},t) = F^{ext} + \int \Gamma(\mathbf{r}-\mathbf{r}')[u(\mathbf{r}',t)-u(\mathbf{r},t)]d^d r' + \delta F(\mathbf{r},u)\ , \tag{1.1}$$

where μ is a mobility coefficient, $\Gamma(\mathbf{r}-\mathbf{r}')$ is the kernel characterising the elastic response of the manifold and $\delta F(\mathbf{r},h)$ accounts for the random disorder that "pins" the manifold.

The behaviour of the system depends on three main factors:

- The dimension d. Equation 1.1 describes a non-equilibrium phenomenon. In the following it will become clear that depinning is a non-equilibrium phase transition. As for equilibrium phase transitions, the dimension plays a key role in determining critical behaviour.

- The elastic kernel Γ. In its Fourier representation it assumes the form $\Gamma(\mathbf{k}) \propto |k|^{\tilde{a}}$. If $\tilde{a}=2$, local elasticity (short range) description holds, while $\tilde{a}=1$ signals non-local (long range) elastic response of the manifold to deformations. The case of $\tilde{a}=0$ corresponds to infinite range and is encountered in the mean-field description of the problem.

- The random force field $\delta F(\mathbf{r},h)$. Pinning forces are assumed time-independent. This means that we deal with *quenched disorder*. Statistical properties of $\delta F(\mathbf{r},h)$ are given by

$$\langle \delta F(\mathbf{r},u)\rangle = 0,\ \langle \delta F(\mathbf{r},u)\delta F(\mathbf{r}',u')\rangle = \xi_{\parallel}^{d}\delta(\mathbf{r}-\mathbf{r}')f\left(\frac{u-u'}{\xi_{\perp}}\right) . \tag{1.2}$$

The random force field has zero average and short range correlations. The function f characterises correlations along the transversal direction and decays faster that algebraically. Correlation lengths of disorder along the longitudinal and transverse directions are given by $\xi_{\parallel}$ and $\xi_{\perp}$ respectively.

1.2.2 Critical behaviour and scaling relations

Random elastic media in the presence of an external force are slowly driven non-equilibrium systems. They exhibit critical behaviour in the vicinity of the depinning transition. The external force is thus the control parameter, while the average velocity, which decays as the depinning threshold is reached from above, is the order parameter [38]. Correlation lengths diverge close to the critical point and small scale details become irrelevant. The evidence of critical behaviour, as well as of a non-equilibrium depinning transition, was first found within several numerical [39–46] and experimental [47–50] investigations.

When the applied force F^{ext} is small, the manifold is pinned in one of the many possible states in which $\partial_t u = 0$ at all points. However, if F^{ext} is larger than a threshold value F_c, the manifold is depinned and moves with a constant average velocity v. While approaching the critical force from above, velocity exhibits a power law decay

$$v \sim (F^{ext} - F_c)^{\beta} , \tag{1.3}$$

where β is called velocity exponent. While approaching the threshold from below, instead, the manifold moves in the form of intermittent bursts, each time jumping to the next metastable state. These avalanche-like phenomena have scale-free distribution in size.

The manifold exhibits self-affine morphology and its correlations satisfy the dynamic scaling form

$$\langle [u(\mathbf{r},t) - u(\mathbf{r},t')]^2\rangle = |\mathbf{r}-\mathbf{r}'|^{2\zeta} g\left(\frac{|t-t'|}{|\mathbf{r}-\mathbf{r}'|^{z}}\right) , \tag{1.4}$$

as a function of the roughness exponent ζ and the dynamical exponent z, through the scaling function g which goes to a constant as its argument approaches zero. Scale-free behaviour is cut off at a correlation length ξ which critically diverges as

$$\xi \sim (F^{ext} - F_c)^{-\nu} \tag{1.5}$$

where ν is the correlation length exponent. The probability of having an avalanche of size s (swept area/volume) is

$$p(s) = s^{-\kappa} f_s(s/s_0) \ , \tag{1.6}$$

where f_0 decays faster that algebraically at infinity and the cut-off s_0 is the size of an avalanche of characteristic extension ξ along the transverse direction i.e., after Equations 1.4 and 1.5, $s_0 \sim \xi^{d+\zeta} \sim |F^{ext} - F_c|^{-\nu(d+\zeta)}$.

Critical exponents are not completely independent. A relation between exponents is obtained by simple scaling arguments from the expressions above or by more rigorous arguments (see e.g. [23]), in the form

$$\beta = \nu(z - \zeta) \ , \tag{1.7}$$

while, for the avalanche statistics, one obtains [51]

$$\kappa = 1 + \frac{d + 1/\nu}{d + \zeta} \ . \tag{1.8}$$

As in the case of equilibrium phase transitions [38], the scaling exponents are universal. This means that they do not depend on the small-scale nature of the systems which they describe, but only on the parameters d and $\tilde{a}$ of the model. The critical behaviour of systems with the same values of d and $\tilde{a}$ (i.e. within the same universality class) is described by the same exponents.

Scaling relations provide connections between critical exponents. However, determining the numerical values of these exponents is a complex task, as it will become clear in the following.

1.2.3 Renormalisation group, critical dimension and mean-field behaviour

A field theoretical solution of the dynamic problem in Equation 1.1 is obtained using the MSR formalism (see Reference [52]): various response and correlation functions for the field $u(\mathbf{r},t)$, as well as related critical exponents, can be generated from the functional (partition function)

$$\mathcal{Z} = \int \mathcal{D}u(\mathbf{r},t)\mathcal{D}\hat{u}(\mathbf{r},t)e^{\mathcal{S}} \ , \tag{1.9}$$

where $\mathcal{S}$ is the action obtained form Equation 1.1. The main problem is thus to "calculate" $\mathcal{Z}$. This is possible performing a saddle point expansion of the problem around the Gaussian approximation of $e^{\mathcal{S}}$, which proves to be equivalent to mean-field behaviour. A critical dimension $d_c = 2\tilde{a}$ arises at this point. The Gaussian approximation holds for $d > d_c$, when corrections become irrelevant at large length and time scales and depinning exponents take their mean-field values. At $d = d_c$ the action has an infinite number of marginal terms. However, given the divergence of correlation lengths, the system shows scale-free behaviour and small-scale details can be ignored. The related procedure is called renormalisation group (RG) transformation and is carried out integrating over large momenta and frequencies — corresponding to the small scale spatiotemporal behaviour which one wants to "remove". Once the result at the critical dimension is known, functional renormalisation in $\epsilon = d_c - d$ provides results for $d < d_c$.

In the present work, we are not interested in further technical details, which can be found in the literature (see e.g. [23] and references therein). Results for critical exponents, which will be extremely useful in the following, are compiled in Table 1.1.

As confirmed by numerical simulations (see References in Table 1.1) mean-field behaviour is encountered above the critical dimension, while for $d < d_c$ critical exponents are highly nontrivial. Interestingly, the roughness exponent is zero in the mean-field description. This means that above the critical dimension the manifold is left smooth by disorder and does not exhibit macroscopic fluctuations. Roughness is, however, supposed to grow logarithmically at $d = d_c$, anticipating the self-affine morphology which characterises systems below the critical dimension.

	d	$\tilde{a}$	FRG $\mathcal{O}(\varepsilon)$	FRG $\mathcal{O}(\varepsilon^2)$	simulation
roughness	1	2	1.00	1.43	1.25 ± 0.05 [26]
ζ	2	2	0.66	0.86	0.75 ± 0.02 [26]
	3	2	0.33	0.38	0.34 ± 0.01 [26]
	1	1	0.33	0.47	0.34 ± 0.02 [33]
	MF		0		
correlation length	1	2	0.75	0.98	1.00 ± 0.05 [53]
ν	2	2	0.67	0.77	0.77 ± 0.04 [54]
	3	2	0.58	0.61	
	1	1	1.33	1.58	1.52 ± 0.02 [33]
	MF		$2/d$		
velocity	1	2	0.67	0.31	0.25 ± 0.03 [26]
β	2	2	0.78	0.62	0.64 ± 0.02 [26]
	3	2	0.89	0.85	0.84 ± 0.01 [26]
	1	1	0.78	0.59	0.68 ± 0.06 [33]
	MF		1		

Table 1.1: *Critical exponents for interface depinning as a function of the parameters d and $\tilde{a}$; renormalisation group results (FRG, expansion in $\epsilon = d_c - d$) after [29]; mean-field results after [16]. Courtesy of M. Zaiser.*

1.2.4 Depinning threshold

Existence and uniqueness of the depinning threshold depend on the nature of the elastic kernel Γ in equation 1.1. As discussed above, an infinitely stiff medium ($\Gamma \to \infty$) never gets pinned. For manifolds of finite elastic stiffness ($\Gamma < \infty$), instead, pinning is encountered and the uniqueness of the depinning threshold is ensured if the elastic kernel Γ is positively definite, according to Middleton's *no passing*-theorem (see Reference [55] for details).

Weak pinning

In order to get a qualitative picture of the depinning problem, we present a simple argument, which has been widely used over the past decades, even before a full understanding of the depinning problem was achieved. This argument has been proposed by Larkin for flux lines in Type II superconductors [56], Labusch for dislocation lines [12, 13], Imry and Ma for the random field Ising model [57], and Fukuyama and Lee for charge density waves (CDW) [2].

As previously stated, pinning is determined by the competition between random forces which induce deformation and the elastic term which tries to keep the manifold straight. In the case

of dense pin distribution (weak disorder) pinning forces result in a random pinning field. Let us consider a portion of the manifold of size L. The random field exerts on it a force of the order of $\langle \delta F^2 \rangle^{1/2} (\xi_\parallel / L)^{d/2}$ which tries to deform the manifold over a transversal distance $\xi_\perp$, while the elastic force responds opposing a term which which scales like $\xi_\perp \Gamma_0 L^{-\tilde{a}}$ where Γ_0 plays the role of a line/suface tension. When the two terms balance each other, a critical length can be defined as

$$L_c = \left(\frac{\Gamma_0 \xi_\perp}{\xi_\parallel^{d/2} \langle \delta F^2 \rangle^{-1/2}} \right)^{\frac{2}{2\tilde{a}-d}} . \tag{1.10}$$

Below the critical dimension, disorder always overcomes the elastic term on large scales and the system roughens, as predicted by the FRG approach. The reason why the qualitative approach described above agrees to this extent with results of the formal renormalisation treatment is still not completely understood.

The manifold is depinned when the external force applied on a segment of length L_c exceeds the pinning forces on this segment. At depinning, the applied force equates the pinning force, with $L = L_c$, and the critical force can be derived accordingly as

$$F_c = \left[\frac{\langle \delta F^2 \rangle^{\tilde{a}} (\xi_\parallel)^{\tilde{a}d}}{\Gamma_0^d \xi_\perp^d} \right]^{\frac{1}{2\tilde{a}-d}} . \tag{1.11}$$

Strong pinning

Although widely used, the method illustrated above relies on the assumption of weak pinning, i.e. diffuse pinning centres. This allows the treatment of disorder in terms of a pinning field which is a statistical summation of many individual localised force fields. This approach, however, does not account for disorder produced by diluted distributions of pinning centres. Under such conditions, each obstacle pins the manifold individually and a pinning field cannot be defined. Such problem, often referred to as strong pinning problem, has been studied by Friedel in the context of dislocation pinning [58]. In this case the manifold is one-dimensional ($d = 1$ — a dislocation line in a three-dimensional crystal) and shows local elasticity properties ($\tilde{a} = 2$ — up to negligible logarithmic corrections). Here we report the original formulation, which however will be generalised in the following chapter.

Let us consider the behaviour of a dislocation segment as it depins from a pair of individual obstacles. The length of the segment is L, and it forms a bulge of width u. If the dislocation segment overcomes one of the pins it will travel by an amount which is, again, of the order of u and, hence, sweep an area of the order of Lu. Now we can estimate the depinning threshold by requiring that during this process the freed dislocation segment encounters, on average, precisely one new obstacle. In other words, precisely at the point of depinning the dislocation starts to move through a sequence of statistically equivalent configurations. For a dislocation this leads to the condition $Lu \simeq 1/(c\xi_\perp)$. L and u can be related by equating the work done by the external force F^{ext} in bulging out the dislocation to the concomitant elastic energy increase, $\Gamma_0 u^2/L = F^{ext} uL$, where Γ_0 is a constant line tension. Finally, the depinning force can be obtained by comparing the external force F^{ext} with the typical pinning force f_0. Solving these three equations, one obtains the Friedel length

$$L_f \simeq (\Gamma_0/c\xi_\perp f_0)^{1/2} \tag{1.12}$$

and the depinning force

$$F_c \simeq (c\xi_\perp f_0^3/\Gamma_0)^{1/2}. \tag{1.13}$$

1.3 Disorder and dislocation dynamics

Dislocations are the linear defects which mediate plastic deformation on microscopic scales. Each dislocation is characterised by a direction unit vector $\mathbf{e}$ and a Burgers vector $\mathbf{b}$, which acts as a topological charge, determining the intensity of the long-range stress field produced by the dislocation. Dislocations interact by their anisotropic stress fields σ according to the well known Peach-Koehler formula

$$\mathbf{f} = \sigma \mathbf{b} \times \mathbf{e}\,. \tag{1.14}$$

Dislocation dynamics is influenced by mutual interactions as well as by disorder. Mutual interactions result in intriguing spatiotemporal patterns which are due to the collective nature of dislocation behaviour and give rise to self-induced internal constraints and exotic jammed

configurations [59]. Disorder, on the other hand, determines pinning of dislocation structures.

Quenched disorder in real crystals is given by random distributions of solute atoms, which produce local lattice distortions. Stress fields associated with such distortions act on dislocation lines, inhibiting their mobility. During deformation, dislocations move along their *glide plane* (identified by the vectors e and b) unless solute obstacles hinder this motion. Dislocation pinning hence opposes deformation, explaining what is known as solid solution hardening [60–62] that is, the increase of the yield stress value when solute atoms are present in a crystal.

The analysis of the depinning transition in dislocation theory has often been made in the line-tension approximation [63–67] where dislocations are considered as flexible strings with local elasticity ($d = 1$, $\tilde{a} = 2$ in the current notations). This analogy is not fully accurate. The bending of a dislocation produces long-range stress and strain fields [68, 69] and therefore the energy of a dislocation line segment depends on the overall configuration of the dislocation line. This results in a logarithmic wavevector dependence of the effective line tension [70]. This wavevector dependence does not affect the main features of the depinning transition [14], although numerical simulations indicate a slight change in the roughness exponent which is not completely understood [14, 34].

The knowledge of depinning properties of isolated dislocations, however, does not necessarily lead to the solution of the more realistic case of pinned dislocation assemblies. Long range interactions are expected to modify the behaviour of ensembles of dislocations, resulting in a different critical response. The cooperative nature of dislocation arrangements thus requires an appropriate theoretical approach.

Unfortunately, developing an analytical theory of the depinning transition of interacting dislocation lines and/or loops of generic orientations and Burgers vectors in a random solute distribution may be a formidable task.

However, relatively simple dislocation structures are sometimes observed experimentally (see Fig. 1.1) and provide a nice illustration of the effect of interactions on the depinning transition. Dislocations are often arranged into one-dimensional arrays, such as regularly spaced pileups and low angle grain boundaries (LAGB). An early analysis of the depinning of a dislocation pileup was presented in Ref. [71], considering explicitly the emission of dislocations from a source.

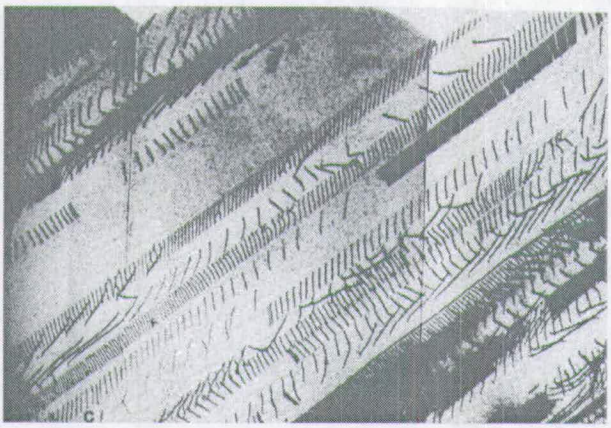

Figure 1.1: *Transmission electron micrograph taken from a Cu-14.4at%Al single crystal deformed at room temperature; the image shows large regularly spaced dislocation pile-ups. Courtesy of J. Plessing and H. Neuhäuser [72].*

Pileups are formed by parallel dislocations disposed on a common glide plane. Burgers vectors are oriented along the glide plane and in the presence of disorder dislocations are supposed to deform along the same direction[1]. In spite of the local elasticity properties of isolated dislocations, a pileup may respond in a different way because of long-range dislocation interactions, resulting in different dynamical properties.

Low angle grain boundaries (LAGB) as well as pileups are linear dislocation assemblies. However, LAGB deform in the perpendicular direction due to a different orientation of Burgers vectors. A surface tension approximation has been adopted in the past to describe pinning of grain boundaries [73, 74] and its impact on grain growth [75]. In the following we shall demonstrate that this is not always appropriate.

Chapter 2 is devoted to the analysis of these aspects, through the formulation of a depinning theory for linear dislocation assemblies [76].

1.4 Disorder and dislocations in vortex lattices

Vortex lattices are observed in Type II superconductors in the presence of an external magnetic field. The field penetrates into the material in the form discrete flux lines (vortices) which rearrange into a quasi two-dimensional triangular lattice. Several analogies can be found in comparison with crystal lattices, including the existence of lattice dislocations. Although length

[1] Motion along the perpendicular direction, known as *climb*, can be neglected for our purposes.

scales might not seem the same at first, since the typical lattice spacing is usually three or four orders of magnitude larger than the one observed in crystals, the problem of dislocations in vortex lattices can be treated by the same methods exploited for plasticity of metals and crystals in general.

Grain boundaries are often observed in vortex lattices, leading to a polycrystalline structure. In spite of the wealth of experiments confirming this aspect, current theories still do not provide an exhaustive explanation for the loss of crystalline order. The emergence of a grain structure, however, is supposed to influence transport properties of the superconducting state. The technological relevance of this aspect has been discussed in the Introduction.

Moreover, it is now accepted that the proliferation of dislocations is responsible for equilibrium phase transitions in the vortex lattice. Under the effect of thermal fluctuations, vortex lattices "melt" into liquid phases, while the increase of the applied magnetic field leads to the onset of amorphous phases. Dislocations are expected to drive this processes, but a definitive theory of dislocation-mediated phase transitions in flux line lattices is still not achieved. Numerical simulations, however, show that phase transitions towards disorder-dominated states are often anticipated by multi-domain arrangements which resemble the polycrystalline structure expected at the onset of melting in thin crystals. Grain boundary densities are supposed to grow, breaking the topological order.

These aspects are examined in detail in Chapter 3, where we investigate the role of grain boundary pinning in vortex lattices and formulate a theory of vortex polycrystals [77, 78].

1.5 Avalanches in plastic deformation

So far we have considered the problem of irreversible deformation on a microscopic scale. Dislocations act as discrete deformation units and the study of their collective dynamics provides the most straightforward approach to the investigation of plastic phenomena. As stated above, however, the general problem of random interacting dislocation arrays in a disordered environment is currently regarded as almost insolvable from an analytic point of view.

Unfortunately several phenomena, including the well known yielding of crystals under the effect of strong enough loads cannot be easily explained in terms of the dynamics of simple and regular dislocation assemblies. The situation is much more complicated as dislocations of dif-

ferent types and directions of motion have to be considered. Such a situation could still be explained in terms of a transition between a stationary and a moving state of the dislocation ensemble, but the microscopic approach does not prove adequate in solving the problem because of the several complications arising from the many degrees of freedom involved.

On the other hand, looking at the system on a mesoscopic scale allows a more complete picture of the problem, avoiding to restrain perspectives to small scale details. Continuum models provide a powerful tool of investigation as they focus on the evolution of large scale quantities such as the *shear strain* γ and the dislocation density ρ. Plastic deformation thus resembles fluid dynamics and proceeds in the so called *plastic flow*.

The appeal of continuum models is usually promoted by the naive assumption that macroscopic regularity of plastic deformation, as commonly experienced, reflects a smooth dynamics on smaller length scales — a laminar flow. However, this viewpoint has recently been questioned by several experimental observations.

Plastic flow on both microscopic and mesoscopic scales proceeds in a strongly heterogeneous and intermittent manner. Spatio-temporal localisation of deformation is obvious at the dislocation scale. However, slip localisation phenomena extend over a wide range of mesoscopic scales and may involve the collective dynamics of very large numbers of defects. This is well known from the observation of the traces left by moving dislocations on the surface of deformed crystals, known as *slip lines* and *slip bands*.

Plastic flow is temporally intermittent and characterised by "deformation bursts" [79, 80]. These events exhibit a scale-free size distribution (see Figure 1.2), as the probability density to observe events with energy release E decreases according to the prediction for mean-field depinning $p(E) \propto E^{-1.5}$ (see Chapter 4 for details on avalanche statistics in the mean-field regime).

In the light of theories of pinning in random media, plastically deforming crystals seem to behave like disordered systems driven close to criticality. The dislocation system in a plastically deforming crystal acts as if always close to a depinning-like transition (*yielding transition* [81]).

Spatial heterogeneities have been investigated in the past, studying three-dimensional patterning of slip on macroscopic scales [82]. The slip burst pattern proved to be fractal. The investigation of surface profiles in deforming metals [83] has shown that samples develop self-affine

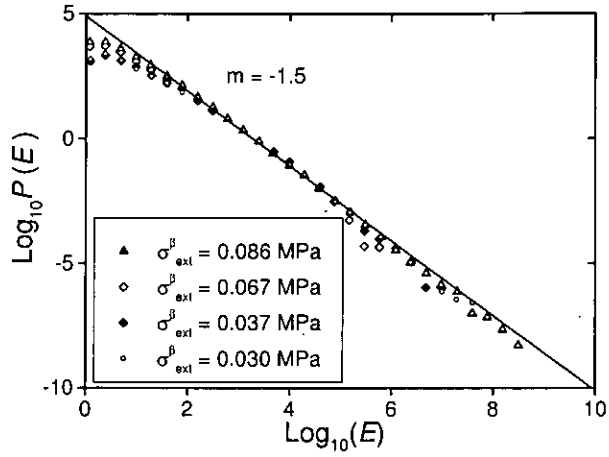

Figure 1.2: *Distribution of energy releases in acoustic emission during creep deformation of ice single crystals; temperature $T = 263$ K, resolved shear stresses on the basal plane as indicated in the inset. After Miguel et al. [79].*

roughness (see Figure 1.3), which is a signature of long-range correlations in the plastic strain pattern.

Over several orders of magnitude, the self-affine behaviour can be quantitatively characterized by a single Hurst exponent H as the average height difference $\langle |y(x) - y(x+L)| \rangle$ between two points on a profile increases as a function of their separation L like L^H with $H \approx 0.8$ (see Figure 1.4).

In order to investigate connections between criticality and plastically deforming crystals, in Chapter 4 we formulate a continuum model accounting for spatial heterogeneities and intermittent behaviour [84]. We show that mean-field results are suggested by pinning theories and confirmed by the numerical implementation of our model, in good agreement with experimental observations.

1.6 Elastic media on a disordered substrate

Plastic deformation on macroscopic length scales is encountered in several phenomena including friction, fracture, failure and crack propagation. The description of these systems usually does not account for microscopic structures and is instead achieved in terms of elastic continua or simple bead-spring models.

Sliding elastic bodies driven on a disordered substrate have been often envisaged as examples

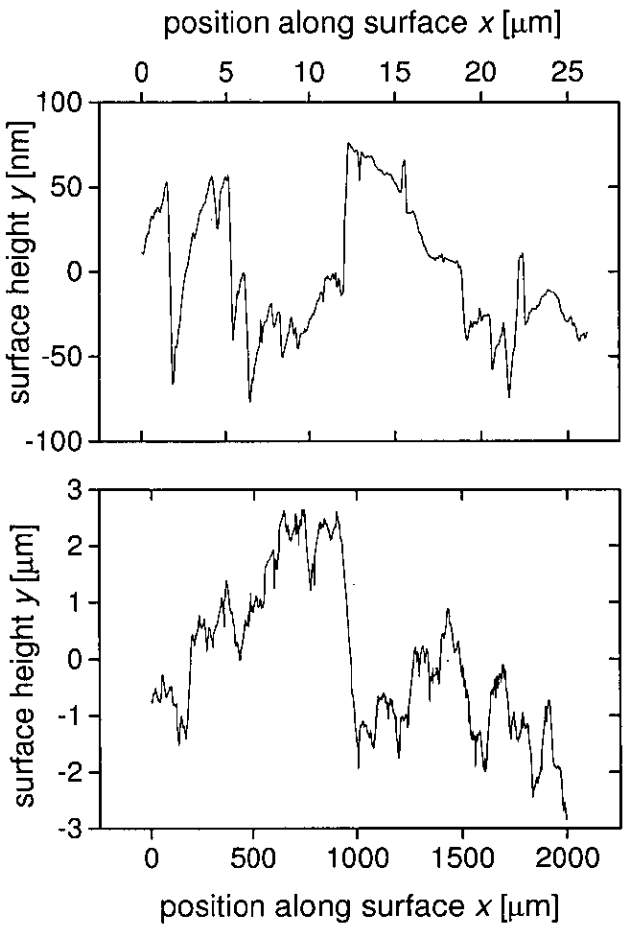

Figure 1.3: *Surface profiles of a Cu polycrystal deformed in tension to a plastic strain* $\varepsilon = 9.6\%$. *Top: AFM profile; bottom: SWLI profile. The* x *direction is parallel to the direction of the tensile axis. After Zaiser et al. [83]).*

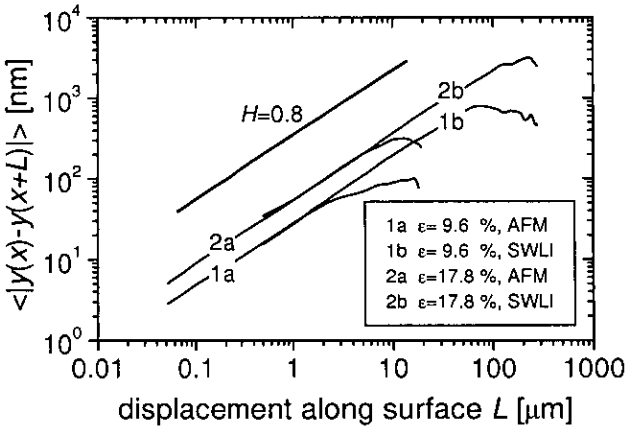

Figure 1.4: *Roughness plots (mean height difference vs. distance along the profile) for AFM and SWLI profiles obtained at strains of 9.6 and 17.8 %. The corresponding profiles for* $\varepsilon = 9.6\%$ *are shown in Figure 1.3.*

of the depinning problem. The original approach was proposed to explain dynamics along an earthquake fault [85] and in spite of its simplicity showed complex response and scaling behaviour (see e.g. [86, 87]). Stick-slip motion belongs to the same category. Slip events exhibit scale-free distribution [88], suggesting a possible description in terms of critical scaling. A theoretical approach to critical scaling has been proposed, for instance, for earthquake fault dynamics [89]. The equivalence between dynamics of a manifold pushed through a random medium and an elastic medium driven on a disordered substrate has been proven both analytically and numerically [36, 37].

However, several natural phenomena such as the initiation landslides and snow avalanches need to be explained in terms of fracture and crack propagation. In Chapter 5 we propose the study of a related problem [90]. Slope failure is governed by crack nucleation and propagation. Randomness is expected to weaken slope stability by facilitating crack nucleation. However we show that weak randomness in the presence of a crack may change the mode of failure, enhancing slope stability. This behaviour is explained in terms of the competition between crack elasticity and disorder and the problem is shown to be analogous to that of pileup depinning discussed above.

Chapter 2
Depinning of dislocation assemblies

As pointed out in the previous chapter, the behaviour of isolated dislocations within a disordered landscape has been widely investigated in the past [14, 63–67]. Pinning of gliding dislocation lines offers a robust explanation of solid solution hardening [60–62] when solute atoms are present in a crystal. The presence of solute atoms changes the local properties of the host material, resulting in a pinning force on nearby dislocations [61, 62]. At the same time, pinning can also be provided by particle inclusions or by dislocations in other slip systems [60].

While the behaviour of an isolated dislocation pushed through a random distribution of obstacles is at present quite well understood, the results do not necessarily carry over to the more realistic case of collective dislocation motion. Dislocations interact via long range stresses and rearrange according to a collective behaviour, which may lead to intriguing jamming and avalanche-like phenomena even in the absence of immobile obstacles [59].

Developing an analytic approach for the solution of the depinning problem of a random distribution of dislocations is at present considered a hard task. It is not infrequent, however, to observe simple and regular dislocation arrangements in deforming metals (see Figure 1.1). Similar arrangements, such as pileups and low angle grain boundaries, have already been introduced in Chapter 1.

In the following, we investigate the depinning transition occurring in such one dimensional dislocation assemblies, interacting with a disordered stress landscape provided by solute atoms, or by other immobile dislocations present in non-active slip systems.

We address the problem by first computing the stress and elastic energy associated with a small deformation of the dislocation arrangement. Local elasticity approximations prove to be inadequate for dislocation arrays since long-range inter-dislocation interactions make pileups and low angle grain boundaries much stiffer than isolated dislocations. The determined elastic energy is then used to estimate the depinning stress within the framework of statistical pinning theories, using collective pinning theory and Friedel statistics for the weak and strong pinning limits, respectively.

Then we focus on the dynamics of dislocation arrays. At stresses close to the depinning threshold, the dynamics exhibits critical behaviour which can be characterised in terms of scaling exponents. Using previous renormalisation group results, we gain a complete quantitative picture of the depinning transition, classifying our systems into the general framework of random manifold models. In the elastic approximation, pileups and low angle grain boundaries are equivalent to a standard interface depinning problem with long-range elasticity. In systems of rigid dislocations the problem is two dimensional, pileups and grain boundaries are one-dimensional arrays ($d = 1$) and the model can be mapped to a contact line or to a planar crack, which have been extensively studied in the literature. In three dimensions ($d = 2$ for the deforming manifold), the self-stress is similar to the dipolar force in magnetic domain walls and leads to logarithmically rough deformations. In more technical terms, $d = 2$ is the upper critical dimension for the transition, which is well described, up to logarithmic corrections, by mean-field exponents.

Results of numerical simulations confirm the validity of the elastic calculations and introduce some interesting dynamical effects. The pileup displays a zero temperature power law creep relaxation which can be interpreted in terms of scaling relations. Below threshold, the power law relaxation terminates into a pinned configuration, while above threshold there is a crossover to linear creep or average constant velocity sliding. As a fingerprint for this class of systems, the motion of the pileup takes place in the form of avalanches whose distribution again can be characterised by scaling exponents.

2.1 Elasticity

Developing a theory for collective dislocation depinning requires the basic knowledge of the elastic properties of the dislocation assembly in the first place. In this section, we determine the elastic response of two particular dislocation assemblies: a regularly spaced pileup and a low angle grain boundary of edge dislocation lines. The two structures are quite similar geometrically; both are one-dimensional arrays of N dislocation lines with the same Burgers vector $\mathbf{b}$ and average line direction $\mathbf{e}$ (for edge dislocations $\mathbf{e} \perp \mathbf{b}$), but they differ in the relative orientation of the Burgers vector and the array direction $\mathbf{d}$. In particular, in a pileup a set of edge dislocations [91] lies in the same slip plane (defined by the dislocation line direction $\mathbf{e}$ and the Burgers vector) so that $\mathbf{d} \parallel \mathbf{b}$ (see Fig. 2.1 for a particular example with $\mathbf{e} = \mathbf{e_z}$ and $\mathbf{e} \parallel \mathbf{b} \parallel \mathbf{e_y}$), whereas in the LAGB the edge dislocations are stacked in the perpendicular plane

such that $\mathbf{b} \perp \mathbf{d}$ (see Fig. 2.2 for a particular geometry). We neglect climb, i.e. the motion of a dislocation perpendicular to its slip plane; hence deformations of the structure can occur solely in the direction of $\mathbf{b}$ both for the pileup and for the LAGB. In this section we derive the shear stress and the elastic energy associated with small deformations of these dislocation assemblies. This is needed in order to derive the yield stress from statistical pinning theories. For completeness, we consider the problem both in two and in three dimensions.

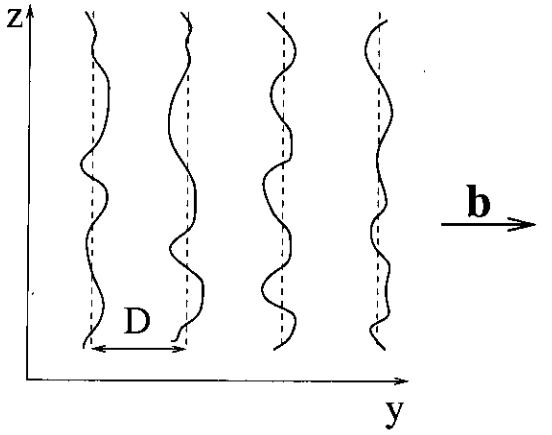

Figure 2.1: *A regularly spaced dislocation pileup with Burgers vector along the y axis. The ideal configuration is plotted with straight dashed lines, whereas the solid lines represent their possible glide deformations within the slip plane yz.*

2.1.1 Two dimensions ($d = 1$)

A two-dimensional model is obtained if we treat the dislocations as rigid lines. In this case, deformations of the dislocation arrangement result only from variations in the position of the dislocations within the one-dimensional ($d = 1$) arrays they form. We consider the case of a LAGB and then directly extend the result to the pileup. In fact, in linear approximation the elastic energy turns out to be the same in both cases.

Here and throughout this work, we consider an ideal LAGB as an infinite set of equally spaced edge dislocations lying on the yz plane (without loss of generality we consider the plane $x = 0$) with Burgers vector pointing along the positive x axis, $\mathbf{b} = b\mathbf{e}_x$ (see Fig. 2.2). In the rigid dislocation approximation, each dislocation is described by the coordinates (x_n, y_n), where $y_n = nD$, D is the dislocation spacing in the LAGB, and x_n is a small displacement out of the $x = 0$ plane. The shear stress at the point (x, y) due to a dislocation at (x_n, y_n) is given by [58, 91]

$$\sigma_{xy}^{n}(x,y) = \frac{Gb}{2\pi(1-\nu_P)} \frac{(x-x_n)[(x-x_n)^2-(y-y_n)^2]}{[(x-x_n)^2+(y-y_n)^2]^2} \tag{2.1}$$

where G is the shear modulus and ν_P is the Poisson ratio. The glide component of the total force per unit length on another dislocation m in the LAGB can be readily obtained from the Peach-Koehler expression $\mathbf{f} = (\sigma \cdot \mathbf{b}) \times \mathbf{e}$ [58, 91]

$$f_x(x_m,y_m) = b \sum_{n=-\infty}^{+\infty} \sigma_{xy}^{n}(x_m,y_m). \tag{2.2}$$

For small deformations $|x_m - x_n| \ll D|m-n|$ we have

$$f_x(x_m,y_m) = -\frac{Gb^2}{2\pi(1-\nu_P)} \sum_{n=-\infty}^{+\infty} \frac{x_m-x_n}{(y_m-y_n)^2}, \tag{2.3}$$

which can be used to obtain the elastic energy

$$E = -\sum_{m=-\infty}^{+\infty} \int f_x(x_m,y_m)\, dx_m = \frac{Gb^2}{8\pi(1-\nu_P)} \sum_{m=-\infty}^{+\infty} \sum_{n=-\infty}^{+\infty} \frac{(x_m-x_n)^2}{(m-n)^2D^2} \text{ with } m \neq n. \tag{2.4}$$

It is instructive to express the elastic energy in Fourier space, where one can easily identify the energy cost of the different modes. For an infinitely long LAGB $N \to \infty$, we can write the dislocation displacements as

$$x_m = \int_{BZ} \frac{dk}{2\pi} e^{-ikDm}\, x(k), \tag{2.5}$$

where because of the periodic dislocation arrangement the integral is restricted to the first Brillouin zone (BZ) of the reciprocal space ($-\pi/D < k < \pi/D$). Using

$$\sum_{d=1}^{+\infty} \frac{1}{d^2} = \frac{\pi^2}{6}, \quad \sum_{d=1}^{+\infty} \frac{cos(\gamma d)}{d^2} = \frac{\pi^2}{6} - \frac{\pi|\gamma|}{2} + \frac{\gamma^2}{4} \tag{2.6}$$

we obtain

$$E = \frac{Gb^2}{8\pi(1-\nu_P)D^2}\int_{BZ}\frac{dk}{2\pi}\left(2\pi|k| - Dk^2\right)\tilde{x}(k)\tilde{x}(-k). \tag{2.7}$$

From this expression, one can see that the elastic interaction kernel $(2\pi|k| - Dk^2)$ is not quadratic in the wavevector, as it would be the case for a local elastic line with a constant tension or stiffness, but grows roughly as $|k|$ for long wavelength deformations. This is a consequence of long range interactions between dislocations in the LAGB which render a much stiffer structure. In the following sections we will explore the consequences of this result in view of the collective pinning of such dislocation structures, something that has been disregarded in previous studies of dislocation depinning.

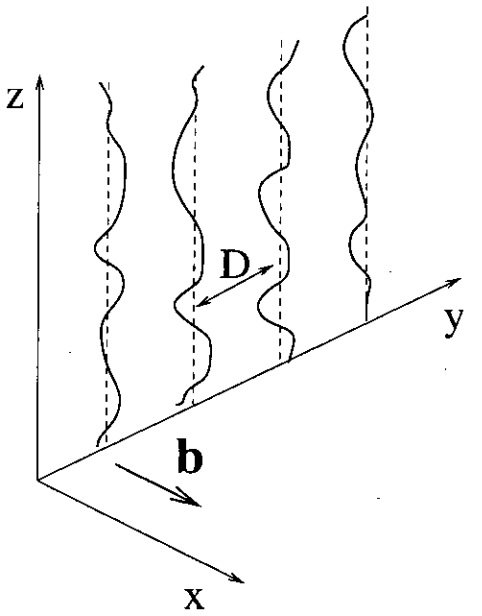

Figure 2.2: *A regularly spaced low angle grain boundary where the dislocations Burgers vector is parallel to the x axis. The ideal configuration is plotted with straight dashed lines in the plane yz, whereas the solid lines represent their possible glide deformations within the slip plane xz.*

The elastic energy associated with perturbations of a regularly spaced dislocation pileup can be obtained in an analogous manner. According to the geometric conditions assumed here, all Burgers vectors are now oriented along the positive y axis, and since the dislocations are all in the same slip plane we can now write $x = x_n = 0$. Proceeding as before, the total Peach-Koehler force on dislocation m along the new glide direction is given by

$$f_y(0, y_m) = \frac{Gb^2}{2\pi(1-\nu_P)} \sum_{n=-\infty}^{+\infty} \frac{1}{y_m - y_n}. \tag{2.8}$$

Note that the Peach-Koehler forces are now repulsive, however the stability of the system is ensured in the case of an infinite pileup where the dislocations located at the extremes (at $\pm\infty$) have fixed positions, or for a finite pileup with periodic boundary conditions. Thus one can also compute the elastic energy cost of small displacements δy_m of the dislocations in the pileup with respect to their stable positions. Up to first order in δy_m, we obtain a restoring elastic force

$$f_y(0, \delta y_m) = -\frac{Gb^2}{2\pi(1-\nu_P)} \sum_{n=-\infty}^{+\infty} \frac{\delta y_m - \delta y_n}{(y_m - y_n)^2} \tag{2.9}$$

equivalent to the one obtained for the case of the LAGB. The corresponding elastic energy cost is given by Eq. 2.7 with $x(k)$ replaced by $\delta y(k)$

Hence, long wavelength distortions of low angle grain boundaries and equally spaced pileups of straight dislocation lines with translational invariance along the dislocation axis have the same nonlocal elastic properties, with eigenvalues that grow linearly with the modulus of the wavevector considered.

2.1.2 Three dimensions ($d = 2$)

Here we consider the more general and realistic case of deformable dislocation lines, forming a planar dislocation array, which behaves as a two-dimensional manifold ($d = 2$) in a three-dimensional space. As before, we consider first the case of a LAGB with Burgers vectors oriented along the x axis, in which each dislocation is now described by a set of coordinates $(x_n(z), y_n, z)$. Again, $y_n = nD$, but now the displacement $x_n(z)$ of the infinitesimal dislocation segment under consideration depends on its position z along the dislocation line (see Fig. 2.2). The elastic stress field due to a general dislocation line or loop can be obtained, for instance, by considering the line as being composed of elementary segments of infinitesimal length [91]. Depending on the relative orientation of the Burgers vector and the local tangent vector $\mathbf{e}(z)$, each segment can either have edge ($\mathbf{e}(z) \perp \mathbf{b}$) or screw character ($\mathbf{e}(z) \parallel \mathbf{b}$), or it can be a combination of both. A first approximation of a general dislocation line can be its

representation in terms of a succession of only edge and screw segments. The mathematical form of the elastic stress fields generated by these two types of elementary segments is simple and renders the problem amenable to analytic treatment. The shear stress created at the point (x, y, z) by an edge dislocation segment of Burgers vector $\mathbf{b} = b\mathbf{e_x}$ and length $\Delta z'$ located at (x', y', z') is given by [91]

$$\sigma_{xy}(x, y, z) = \frac{Gb}{4\pi(1-\nu_P)} \frac{x-x'}{R_0^3} \left[1 - 3\frac{(y-y')^2}{R_0^2}\right] \Delta z', \tag{2.10}$$

where

$$R_0^2 = (x-x')^2 + (y-y')^2 + (z-z')^2, \tag{2.11}$$

and the shear stress field due to a screw segment of length $\Delta x'$ is [91]

$$\sigma_{xy}(x, y, z) = -\frac{Gb}{4\pi} \frac{z-z'}{R_0^3} \Delta x'. \tag{2.12}$$

Equations (2.10) and (2.12) allow us to calculate the glide component of the total Peach-Koehler force $\mathbf{f} = (\sigma \cdot \mathbf{b}) \times \mathbf{e}$ on an edge or a screw segment. The glide force on an edge segment at $(x_m(z), y_m, z)$ has two contributions f_x^{EE} and f_x^{SE} arising from its respective interactions with other edge or screw segments,

$$\begin{aligned} f_x^{EE}(x_m(z), y_m, z) &= \frac{Gb^2}{4\pi(1-\nu_P)} \frac{x_m(z) - x_n(z')}{R_{mn}^3(z, z')} \\ &\quad \left[1 - 3\frac{(y_m - y_n)^2}{R_{mn}^2(z, z')}\right] \Delta z' \, \Delta z, \\ f_x^{SE}(x_m(z), y_m, z) &= -\frac{Gb^2}{4\pi} \frac{z - z'}{R_{mn}^3(z, z')} \frac{\partial x_n(z')}{\partial z'} \Delta z' \, \Delta z. \end{aligned} \tag{2.13}$$

Note that up to first order in the small displacements ($x_m(z) - x_n(z') \simeq 0$), the relative distance among segments can be written as $R_{mn}^2(z, z') = (y_m - y_n)^2 + (z - z')^2$. On the other hand, from the general expression for the Peach-Koehler Force written above, it is straightforward to verify that there are no glide forces acting upon any screw segment on the dislocation line.

After summing up all non-vanishing contributions, we can obtain the elastic energy as for the two-dimensional case (see Eq.(2.4)). The elastic energy can be expressed as the sum $E = E^{EE} + E^{SE}$ of the interaction energies between edge-edge and edge-screw segments. These are given by

$$E^{EE} = -\frac{Gb^2}{32\pi(1-\nu_P)} \sum_{m,n} \int\int dz dz' \left[1 - 3\,\frac{(y_m - y_n)^2}{R_{mn}^2(z,z')}\right] \frac{[x_m(z) - x_n(z')]^2}{R_{mn}^3(z,z')}, \tag{2.14}$$

$$E^{SE} = \frac{Gb^2}{16\pi} \sum_{m,n} \int\int dz dz' \, \frac{z - z'}{R_{mn}^3(z,z')} \, x_m(z)\, \partial_{z'} x_n(z'). \tag{2.15}$$

As we did for the rigid line case, we can also express this elastic energy in Fourier space in order to diagonalise the interaction matrix and to obtain the wavevector dependence of the interaction kernel between the different deformation modes. The detailed calculation is rather lengthy, so we merely indicate the procedure followed and the final results obtained. We evaluate separately the energy contribution due to the self-interaction between the constituent segments of each individual dislocation line, i.e. $n = m$, which we denote by E_0, and the energy contributions due to the interaction of dislocation segments lying on different lines, i.e. $n \neq m$, which we refer to as E_1. Proceeding this way, we find that the total energy is $E = E_0^{EE} + E_0^{ES} + E_1^{EE} + E_1^{ES}$. We express the dislocation displacements in terms of their Fourier modes,

$$x_m(z) = \int_{BZ} \frac{dk}{2\pi} \int \frac{dq}{2\pi} e^{-ikDm} e^{-iqz}\, x(k,q) \tag{2.16}$$

and evaluate the self-interaction contributions for long wavelength deformations $qa \ll 1$ where a is a short-distance cutoff introduced to preclude the interaction of a line segment with itself. The result can be written as

$$E_0^{EE} = \frac{Gb^2}{16\pi(1-\nu_P)} \int_{BZ} \frac{dk}{2\pi} \int \frac{dq}{2\pi} \frac{1}{D} \left[2 \left(\gamma_E - \frac{3}{2} + \ln a|q| \right) q^2 + \right.$$
$$\left. - \frac{a^2}{12} q^4 \right] x(k,q)x(-k,-q) \tag{2.17}$$

$$E_0^{SE} = \frac{Gb^2}{8\pi} \int_{BZ} \frac{dk}{2\pi} \int \frac{dq}{2\pi} \frac{1}{D} \left[2(-\gamma_E - \ln a|q|\,)q^2 + \right.$$
$$\left. + \frac{a^2}{2} q^4 \right] x(k,q)x(-k,-q) \tag{2.18}$$

where γ_E is the Euler constant. We find a quadratic wavevector dependence typical of a local interaction kernel but modified by logarithmic corrections. This a well-known result for isolated dislocation lines, as well as for similar singularities such as vortex lines in high temperature superconductors [8].

The energy contributions due to interactions between segments of different dislocation lines ($n \neq m$) in the LAGB can be expressed as

$$E_1^{EE} = \frac{Gb^2}{16\pi(1-\nu_P)} \int_{BZ} \frac{dk}{2\pi} \int \frac{dq}{2\pi} \frac{1}{D} \left[2 \left(\gamma_E + \ln \frac{D|q|}{4\pi} \right) k^2 + \right.$$
$$\left. + \frac{2\pi}{D} \frac{k^2}{(k^2+q^2)^{1/2}} + \frac{D^2}{2\pi^2} \zeta(3) k^2 q^2 \right] x(k,q)x(-k,-q) \tag{2.19}$$

$$\tag{2.20}$$

$$E_1^{SE} = \frac{Gb^2}{16\pi} \int_{BZ} \frac{dk}{2\pi} \int \frac{dq}{2\pi} \frac{1}{D} \left[2 \left(\gamma_E + \ln \frac{D|q|}{4\pi} \right) q^2 + \right.$$
$$\left. + \frac{2\pi}{D} \frac{q^2}{(k^2+q^2)^{1/2}} + \frac{D^2}{2\pi^2} \zeta(3) q^4 \right] x(k,q)x(-k,-q), \tag{2.21}$$

where $\zeta(x)$ is the Riemann *zeta* function. Naturally, the interaction kernel between the deformation modes for the three dimensional grain boundary case depends explicitly on both the y and z components of the wavevector in an intricate manner. Nevertheless, as in the two dimensional case, for long wavelength deformations the leading term of the interaction kernel is essentially linear in the wavevector, which manifests the non-locality of the interactions.

Finally, we consider the case of a pileup lying on the $x = 0$ plane. Again, we assume small perturbations of the dislocations from their equilibrium positions, $y_m - y_n \rightarrow (y_m + \delta y_m(z)) -$

$(y_n + \delta y_n(z'))$, where the displacements now depend on the z coordinate of the infinitesimal line segment considered. Expanding up to first order in $(\delta y_m(z) - \delta y_n(z'))$, we evaluate the resulting Peach-Koehler glide forces and the corresponding elastic energy. As in the two-dimensional case, the result is equivalent to the one computed for the LAGB, provided that we replace $x_n(z)$ by $\delta y_n(z)$ in Eqs. (2.17) and (2.21). Thus also in this case we find wavevector dependent interaction kernels whose leading terms (for long wavelength deformations) grow either quadratically in the wavevector (with logarithmic corrections) for self-interactions of the same dislocation line, or linearly in the case of interactions between different lines. Thus we may conclude that this particular form of the elastic kernels is characteristic of the long range interactions between different dislocations. As we will see in the following, these long-range elastic properties have significant consequences for the analysis of the depinning transition of dislocation assemblies.

2.2 The effect of disorder: depinning transition

Distortions in a pileup or a LAGB are a result of collective interactions of such dislocation assemblies with various types of impurities such as solute atoms, precipitates or other immobile defects, while, as previously noted, only interactions between individual dislocations and impurities have been computed and are reported in the literature.

In the following, we consider quenched disorder created by a random distribution of immobile impurities with concentration c which interact with dislocations via a force $f_p(r) = f_0 g(r/\xi_p)$, where f_0 is the pinning strength, ξ_p is the interaction range and r is the distance between the impurity and the dislocation. The detailed shape $g(x)$ of the individual pinning force is inessential for most purposes, provided it is of short-range nature.

The dynamics of the dislocation arrays in a random environment is given by

$$\frac{1}{\mu}\frac{\partial u}{\partial t} = \int d^d x' \Gamma(x - x')(u(x') - u(x)) + b\tau_{\text{ext}} + \eta(x, u), \tag{2.22}$$

where μ is a mobility coefficient, τ_{ext} is the applied stress, $\eta(x, u)$ describes the effect of the pinning centres and the elastic interaction kernel Γ, computed in the previous section, scales as $|k|$ in Fourier space.

Our next step will be to discuss how the main theoretical approaches to the depinning transition can be applied to the problem under examination. We will consider the problem of low angle grain boundary pinning, since for pileups the same results are expected to hold.

2.2.1 Weak pinning — Collective pinning theory

Collective pinning theory describes the behaviour of the LAGB in the limit of weak disorder. Defects are dense and pinning is due to the fluctuations of the superposed random forces. As discussed in Chapter 1, the key concept is the introduction of a characteristic length L_c above which pinning becomes energetically advantageous (and thus effective) and consequently the LAGB is distorted. The collective pinning length can be evaluated by simply balancing the elastic energy cost and the pinning energy gain associated with a small displacement of a region of linear size L. On scales below L, the dislocations remain essentially undeformed and, hence, the fluctuations in potential energy follow Poissonian statistics. The effective concentration of the pinning defects along the LAGB is given by

$$\bar{c}_{\text{eff}} = \begin{cases} \bar{c} & , \ \xi_p > D \\ \bar{c}\frac{\xi_p}{D} & , \ \xi_p < D \end{cases} \quad \text{(2 dimensions)}$$

$$c_{\text{eff}} = \begin{cases} c & , \ \xi_p > D \\ c\frac{\xi_p}{D} & , \ \xi_p < D \end{cases} \quad \text{(3 dimensions)} . \tag{2.23}$$

The first expression refers to pinning by columnar defects of areal concentration $\bar{c}$ in $2D$, and the second to pinning by localised defects of volume concentration c in $3D$. In 2D, the characteristic energy of a section of a LAGB of size L displaced by an amount of the order of u can be written as

$$\bar{E} = \frac{Gb^2u^2}{D^2} - \bar{f}_0\xi_p\sqrt{\bar{c}_{\text{eff}}Lu}. \tag{2.24}$$

Here both $\bar{E}$ and $\bar{f}_0$ are defined as quantities per unit length. Note the scale-independence of the nonlocal expression of the elastic energy Gb^2u^2/D^2 in contrast to what would be this energy in the local approximation Gb^2u^2/DL. Essentially the same expression holds for the pileup. Balancing elastic and pinning contributions and imposing that the displacement is of

the order of the pinning range $u \sim \xi_p$, one readily obtains $L_c = (G^2 b^4 \xi_p)/(D^4 \bar{f}_0^2 \bar{c}_{\rm eff})$. The LAGB is depinned when the work done by the external stress in moving a segment of length L_c over the distance ξ_p exceeds the characteristic pinning energy $\bar{E}(L_c)$ of this segment. Equating $\bar{E}(L_c) = \tau_c b L_c \xi_p / D$, for the case above the result is given by $\tau_c b = (\bar{c}_{\rm eff} \bar{f}_0^2 D^3)/(G b^2)$.

A similar calculation in $3D$ is more subtle, since the elastic and the pinning energies scale with the same power of L and thus cancel in the simple dimensional approach discussed above. As we will discuss in the next section, this reflects the fact that in the three dimensional case, the planar dislocation arrays reach the upper critical dimension $d_c = 2$ for the transition (see Chapter 1). To obtain L_c in this case, one should perform a perturbation expansion in the disorder, as discussed in Ref. [6] in the context of the flux line lattice. One essentially computes the typical displacement u for a system of size $|\mathbf{r}| = L$, which for a LAGB is given by

$$\langle |u(\mathbf{r}) - u(0)|^2 \rangle = \int \frac{d^2k}{(2\pi)^2} \int \frac{d^2k'}{(2\pi)^2} (1 - \cos \mathbf{kr}) \, \mathcal{G}(\mathbf{k}) \mathcal{G}(\mathbf{k}') \, F(\mathbf{k}) F(\mathbf{k}') \tag{2.25}$$

where $\mathcal{G}(\mathbf{k})$ is the Green function associated to the elastic kernel determined in the previous section, and $F(\mathbf{k})$ is the pinning force density. In the spirit of collective pinning theory $\langle F(\mathbf{k}) F(\mathbf{k}') \rangle = W \delta^{(2)}(\mathbf{k} + \mathbf{k}')$ with $W = (f_0 \sqrt{c_{\rm eff} \xi_p})^2$. The explicit calculation leads to the characteristic displacement

$$u(L) \simeq f_0 \sqrt{c_{\rm eff} \xi_p} \, \frac{D^2}{G b^2} \, \ln^{1/2} \frac{L}{D} \, . \tag{2.26}$$

This expression can then be inverted, imposing $u \sim \xi_p$, to obtain

$$L_c = D \exp \left[\frac{\xi_p}{c_{\rm eff}} \left(\frac{G b^2}{f_0 D^2} \right)^2 \right] . \tag{2.27}$$

The depinning stress can then be obtained as in 2D and is given by $\tau_c b = (G b^2 \xi_p)/(D L_c)$. Again these results generalise directly to the pileup case. It is however important to note that they refer to the continuum limit, when one can neglect the discrete nature of the dislocation

system. To be consistent with this assumption one should have $L_c \gg D$.

2.2.2 Strong pinning — Friedel statistics

Collective pinning is due to a statistical superposition of the forces created by many obstacles. In the limit of strong and/or diluted pinning centres, however, the characteristic bulge of width ξ_p and extension L_c as envisaged in the previous section may not interact with enough pinning centres for this viewpoint to be valid. Simple estimates for the boundaries of the collective pinning regime are given by the inequalities $L_c\xi_p \geq 1/\bar{c}_{\rm eff}$ and $L_c^2\xi_p \geq 1/c_{\rm eff}$ for the $2D$ and $3D$ cases discussed above, respectively.

In the regime of strong pinning, dislocations are pinned by individual obstacles. The spacing of obstacles along the dislocation and the depinning stress can be obtained by the argument which was, in the context of single dislocations, developed by Friedel [58]. Details have been given in Chapter 1.

As a dislocation segment of length L depins from a pair of strong obstacles, it travels by an amount of the order of u, sweeping an area of the order of Lu. During this process it stumbles upon, on average, precisely one new obstacle. In the present case the external force per unit length (see Chapter 1) is given in terms of the applied shear stress as $\tau_{\rm ext}b$. For a dislocation this leads to the condition $Lu \simeq 1/(c\xi_p)$. The Friedel length reads $L_f \simeq (\Gamma_0/c\xi_p f_0)^{1/2}$ and the depinning stress $\tau_{\rm c}b \simeq (c\xi_p f_0^3/\Gamma_0)^{1/2}$.

This argument can be generalised in a straightforward manner to the case of dislocation arrays. Let us first consider the depinning of a two dimensional LAGB as discussed above in the weak pinning limit: in this case, the Friedel condition reads $Lu \simeq 1/\bar{c}_{\rm eff}$, the elastic energy per unit length of a bulge of width u and extension L is Gb^2u^2/D^2 which must equal the work per unit length $\tau_{\rm ext}bLu/D$, and the force balance (again per unit length) is $\tau_{\rm c}bL/D = \bar{f}_0$. Combining these relations we find that the Friedel length and the depinning stress are

$$L_f \simeq \frac{Gb^2}{D^2\bar{c}_{\rm eff}\bar{f}_0} \quad \tau_{\rm c} \simeq \frac{\bar{c}_{\rm eff}\bar{f}_0^2D^3}{Gb^3} \quad \text{(2 dimensions)}. \tag{2.28}$$

In 3D the Friedel condition is $L^2u \simeq 1/c_{\rm eff}$, the energy balance reads $Gb^2u^2L/D^2 = \tau_{\rm ext}bL^2u/D$, and the force balance is $\tau_{\rm c}bL^2/D = f_0$. This yields

$$L_f \simeq \frac{Gb^2}{D^2 c_{\text{eff}} f_0} \quad \tau_c \simeq \frac{c_{\text{eff}}^2 f_0^3 D^5}{G^2 b^5} \quad \text{(3 dimensions)}. \tag{2.29}$$

Table 2.1 presents a compilation of results for the weak and strong pinning cases in two and three dimensions. For comparison we have also included results obtained under the assumption that the elastic behaviour of the grain boundary can, in local elasticity approximation, be described by a scale-independent surface energy $\Gamma_0 \sim Gb^2/D$.

2.3 Dynamics and critical scaling

A brief introduction to non-equilibrium transitions and in particular to the depinning transition has been given in the previous chapter. As previously stated, our system can be straightforwardly mapped to a more general depinning problem and its critical behaviour can be described by scaling laws and critical exponents.

The control parameter is the applied stress, so that scaling laws depend on the distance $\tau_{\text{ext}} - \tau_c$ from the critical point. In particular, as the system approaches the transition the correlation length diverges as $\xi \sim (\tau_{\text{ext}} - \tau_c)^{-\nu}$. Similarly, one can define a characteristic correlation time t^*, related to the correlation length as $t^* \sim \xi^z$. The average dislocation velocity reaches a steady value, scaling as $v \sim (\tau_{\text{ext}} - \tau_c)^{\beta}$, above the transition, and vanishes below. Before the steady-state the average velocity decays as a power law $t^{-\theta_v}$, for times $t < t^*$. Furthermore the Orowan relation, which relates the rate of plastic deformation $\dot{\gamma}$ to the density ρ and average velocity v of moving dislocations in a crystal, implies that similar scaling laws should hold for the strain rate $\dot{\gamma} \equiv b\rho v$.

The reader may notice the close relationship between quantities involved in this kind of theoretical approach and typical observables in plastically deformed crystals. It is thus tempting to explore the connection between the dynamical behaviour of dislocation systems and the creep laws observed experimentally, i.e. the crossover between primary (power law) to secondary (linear) creep.

Scaling exponents also characterise the morphology of the dislocation arrangement, which exhibits roughening close to the depinning transition. The roughness can be quantified measuring the average displacement correlations $C(x - x') = \langle (u(x) - u(x'))^2 \rangle$. At the transition in the steady-state, we expect a self-affine scaling $C(x) \sim x^{2\zeta}$, where ζ is the roughness exponent

d	type of elasticity	type of pinning	pinning length	critical stress	physical realisation
1	local	weak	$L_c = \left(\frac{\Gamma_0^2 \xi_p}{f_0^2 \tilde{c}_{\rm eff}}\right)^{1/3}$	$\tau_c b = \left(\frac{D^3 f_0^4 \xi_p \tilde{c}_{\rm eff}^2}{\Gamma_0}\right)^{1/3}$	isolated dislocation
1	local	strong	$L_f = \left(\frac{\Gamma_0}{f_0 \tilde{c}_{\rm eff}}\right)^{1/2}$	$\tau_c b = \left(\frac{D^2 f_0^3 \tilde{c}_{\rm eff}}{\Gamma_0}\right)^{1/2}$	isolated dislocation
1	non-local	weak	$L_c = \frac{\Gamma_0^2 \xi_p}{D^2 f_0^2 \tilde{c}_{\rm eff}}$	$\tau_c b = \frac{D^2 f_0^2 \tilde{c}_{\rm eff}}{\Gamma_0}$	dislocation array, rigid dislocations
1	non-local	strong	$L_f = \frac{\Gamma_0}{D f_0 \tilde{c}_{\rm eff}}$	$\tau_c b = \frac{D^2 f_0^2 \tilde{c}_{\rm eff}}{\Gamma_0}$	dislocation array, rigid dislocations
2	local	weak	$L_c = \left(\frac{\Gamma_0^2 \xi_p}{f_0^2 c_{\rm eff}}\right)^{1/2}$	$\tau_c b = \frac{D f_0^2 c_{\rm eff}}{\Gamma_0}$	elastic sheet
2	local	strong	$L_f = \left(\frac{\Gamma_0}{f_0 c_{\rm eff}}\right)^{1/2}$	$\tau_c b = \frac{D f_0^2 c_{\rm eff}}{\Gamma_0}$	elastic sheet
2	non-local	weak	$L_c = D \exp\left[\frac{\Gamma_0^2 \xi_p}{D^2 f_0^2 c_{\rm eff}}\right]$	$\tau_c b = \frac{\Gamma_0 \xi_p}{D} \exp\left[-\frac{\Gamma_0^2 \xi_p}{D^2 f_0^2 c_{\rm eff}}\right]$	dislocation array, flexible dislocations
2	non-local	strong	$L_f = \frac{\Gamma_0}{D f_0 c_{\rm eff}}$	$\tau_c b = \frac{D^3 f_0^3 c_{\rm eff}^2}{\Gamma_0^2}$	dislocation array, flexible dislocations

Table 2.1: *Overview of pinning stresses and pinning lengths obtained from different models and their physical realisations. The parameter d indicates the dimension of the manifold (pileup or low angle grain boundary)*

(see Chapter 1).

What most strongly characterises our system is the long-range nature of the elastic response in the presence of a deformation. The effective elastic energy of the pileup and LAGB scales as $|q|$ in Fourier space, as in the problems of contact line [92] and planar crack depinning [93]. We can thus directly apply to our case the results obtained for a contact line with long-range elastic energy [23, 27].

The renormalisation group analysis predicts that $d_c = 2$ is the manifold critical dimension, above which fluctuations are suppressed. Thus for $d > d_c$ there is no roughening (i.e. $\zeta = 0$) and the other exponents can be computed in the mean-field approximation, yielding $\beta = z = \nu = 1$. These results are valid in the physically interesting dimension $d = 2$ apart from additional logarithmic corrections. For $d < 2$, one-loop renormalisation group expansions in $\epsilon = 2 - d$ performed [27] to compute the exponents at first order in ϵ lead to

$$\zeta = \epsilon/3 = 1/3\,, \tag{2.30}$$

$$\nu = 3/2\,, \tag{2.31}$$

$$\beta = 1 - 2\epsilon/9 + \mathcal{O}(\epsilon^2) \approx 7/9 \quad \text{and} \tag{2.32}$$

$$z = 1 - 2\epsilon/9 + \mathcal{O}(\epsilon^2) \approx 7/9 \tag{2.33}$$

for $\epsilon = 1$. It also worth noting that, using the scaling relation $\theta_v = \beta/(\nu z)$ [16], one obtains $\theta_v = 2/3$. The relevance of this result will be shown in the following.

2.4 Numerical data and experimental evidence

Several kinds of tests can be performed in order to assess the validity of our theoretical approach. In this section we review both numerical and experimental results which provide a robust confirmation for our results and corroborate our predictions. The cases of one- and two-dimensional dislocation pileups will be considered separately. Even though low angle grain boundaries will not be taken into account in the following, it is understood that results holding for pileups also extend to them. The concept of grain boundary depinning is closely related to the problem of *grain growth* and will be extensively analysed in the next chapter, in the context

of vortex matter physics.

2.4.1 One-dimensional pileup

We test our theory for a two dimensional pileup in the light of numerical results and experimental observations. Simulations have been performed by our collaborators for such dislocation assemblies pushed through a random distribution of point obstacles. Even though the analytical treatment assumed equally spaced dislocation pileups, that constraint could be dropped in the case of numerical simulation, allowing us to seek for an even more general confirmation of our theory. For simplicity we consider periodic boundary conditions, so that in absence of disorder the equilibrium configuration is an equally spaced pileup. To test the dependence on the system size, we change the dislocation number N and the system size L keeping the dislocation spacing $D = L/N$ constant.

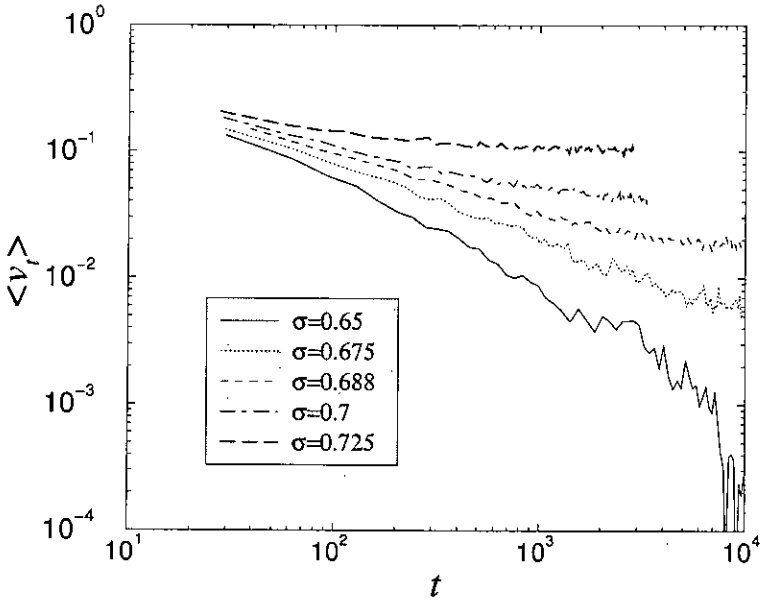

Figure 2.3: *The decay of the average pileup velocities as a function of the applied stress* $\tau_{\text{ext}} = \sigma$. *Units of time, space and forces are chosen so that* $Gb^2 = 1$, $\mu = 1$, $b = 1$, $f_0 = 1$ *and* $\xi_p = 1$. *When the external shear stress exceeds a critical value* $\sigma \simeq 0.675$ *the velocity reaches a steady value and decays to zero otherwise.*

Fig. 2.3 displays the time decay of the average pileup velocity for different values of the applied stress. For large stress values, $\tau_{\text{ext}} > \tau_c$, the initial power law decay is followed by a plateau, while the velocity decays to zero otherwise. This allows the identification of the depinning point τ_c. The finite size analysis shown in Fig. 2.4, indicates that for $\tau_{\text{ext}} = \tau_c$ the power

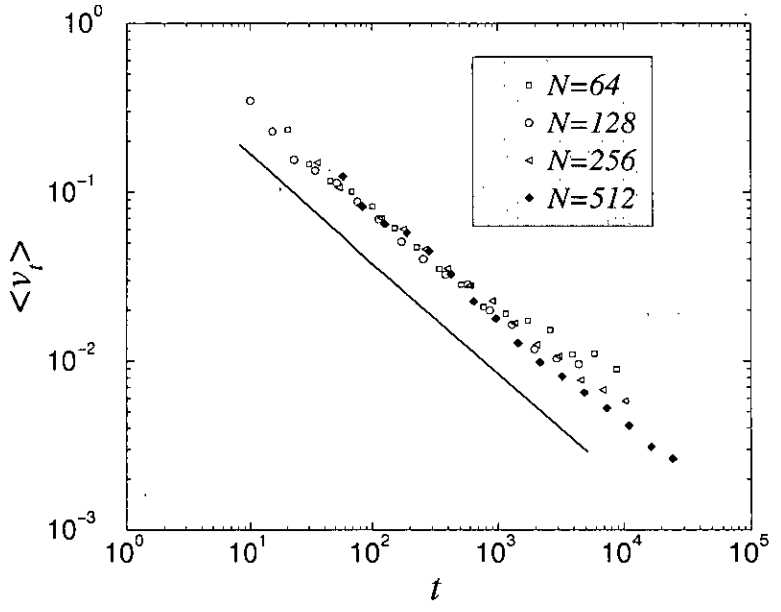

Figure 2.4: *The decay of the velocity at* $\tau_{\text{ext}} > \tau_c \simeq 0.675$ *for different values of* N. *In particular,* $N = 64, 128, 256, 512$ *dislocations with a spacing* $D = 16$ *and average pinning centre spacing* $d_p \equiv L/N_p = 2$ *were considered. As* N *increases the power law scaling region extends. The line has a slope of* $\theta_v = 0.65$.

law extends further as the system size is increased. The exponent of the power law scaling $\theta_v \simeq 0.65$ is in good agreement with the theoretical expectation [59].

Moreover, in order to characterise the growth of correlations at the critical point, one can compute the displacement correlation function $C(i-j,t) = (\langle (u_i(t) - u_j(t))^2 \rangle)^{1/2}$ at different times t for $\tau_{\text{ext}} = \tau_c$ (see Fig. 2.5). The curves can be collapsed using the scaling forms introduced in Chapter 1 with $\zeta = 0.35$ and $z = 0.9$ (see the inset of Fig. 2.5) [76]. To confirm this result one can consider the evolution of the power spectrum $P(k,t) = \int dx C(x) \exp(ikx)$ (see Fig. 2.6). These curves can also be collapsed according to scaling relations with the same exponent values as the correlation function. In summary, all the exponents determined from the simulations are in good agreement with the renormalisation group predictions.

Furthermore, experiments confirm the validity of the elastic theory for two-dimensional pileups. The value of $\theta_v = 2/3$, predicted by the renormalisation group approach and confirmed by simulations, coincides with the exponent of the so-called Andrade creep law, observed in the creep deformation of several materials [58, 59].

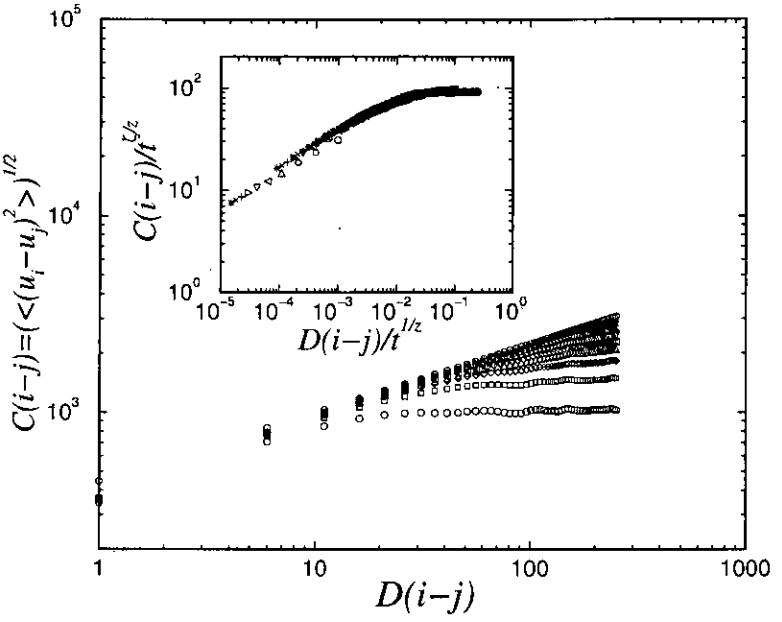

Figure 2.5: *The growth of the correlation function at the depinning transition at different times. The data collapse in the inset allows an estimate of the roughness exponent* $\zeta = 0.35$ *and the dynamic exponent* $z = 0.9$.

2.4.2 Two-dimensional pileup.

In the case of flexible dislocation lines, we expect the depinning transition of a planar dislocation array to be governed by mean-field exponents. A detailed discussion of this case can be found in the literature (see e.g. [16]). The mean-field exponents are

$$\beta = z = \nu = 1 \, . \tag{2.34}$$

Here we provide a possible experimental check in the context of planar dislocation arrangements. Direct experimental observation of the dynamics of planar dislocation arrays may be possible in certain alloys exhibiting so-called planar slip where dislocations form huge pile-ups (see Figure 1.1). The motion of these planar dislocation groups goes along with the formation of large slip steps along the traces where the slip plane of the pileup intersects the surface of the metal specimen. For a moving pileup consisting of roughly equally spaced dislocations, the slip step growth rate is proportional to the dislocation velocity. Since often only a small number of slip steps are growing at a time [94], one may attempt to relate the observed time dependence of slip step growth to the velocity relaxation of a single pileup.

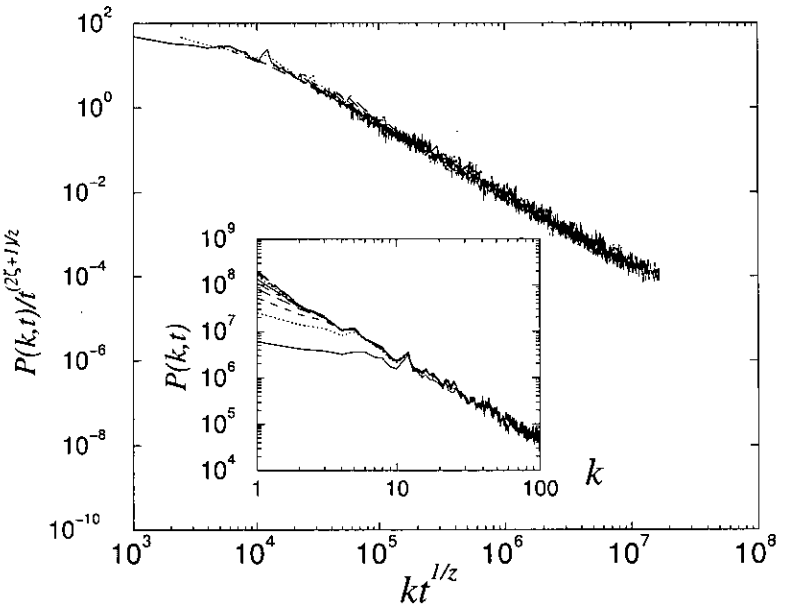

Figure 2.6: *The power spectrum of the pileup at the depinning transition. The data collapse is consistent with the scaling of the correlation function.*

Figure 2.7 shows experimental data with rates of slip step growth as a function of the time after growth has started [62]. The double-logarithmic plot indicates relaxation of the growth rate (the dislocation velocity) according to $v \propto t^{-\theta_v}$ with a characteristic exponent $\theta_v = 1 \pm 0.1$ over six decades. On the other hand, for the depinning transition of a planar dislocation array in 3D we expect according to the scaling relation $\theta_v = \beta/(\nu z)$ the value $\theta_v = 1$. The apparent length of the scaling regime indicates that driving of the dislocation arrays occurs at stresses very close to the critical one. This is in line with the general observation that dislocation arrangements in slowly deforming crystals (where "slow" covers the entire range of strain rates used in typical experiments, [81]) are in a close-to-critical state [79, 81].

2.5 Discussion

In the last part of the present chapter we have focused on the dynamics of the pileups, noting that elastic properties of low-angle grain boundaries would lead to similar results. In fact in certain situations, our results may have some implications for grain growth limited by grain boundary pinning [73, 74]. Numerical studies of the problem often rely on local elasticity approximation (see Reference [75]). If such an assumption was questioned, results would change dramatically as discussed in section 2.2.2. For that reason, it is necessary to point out in which systems local

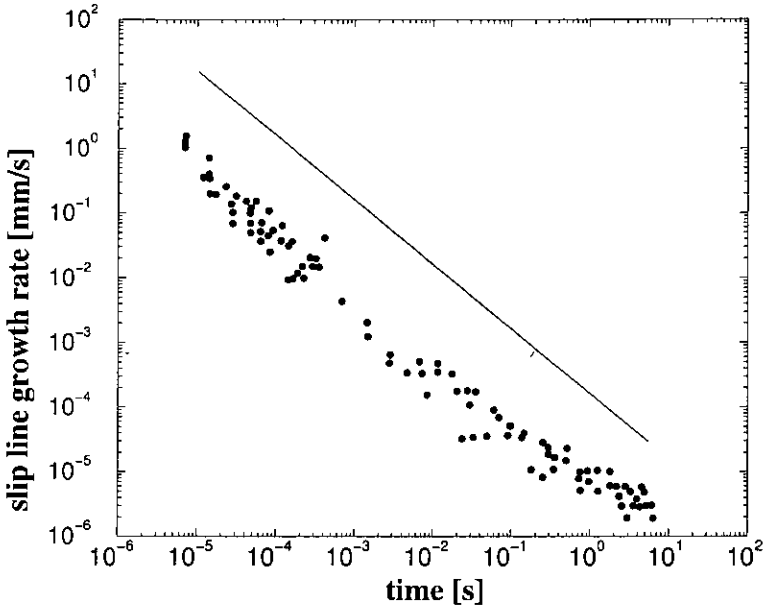

Figure 2.7: *Growth rate of slip steps on the surface of Cu-30at% Zn deformed at room temperature as a function of the time passed after growth has started; after Ref. [62]. The line is a power law with exponent* $\theta_v = 1$.

elasticity can still be considered a reasonably good approximation in the first place.

When grain boundary mobility is governed by glide of the GB dislocations, our formulation of the grain boundary depinning problem provides a correct description. Local elasticity proves inadequate and long range dislocation interactions must be taken into account. The problem of grain growth in this regime will be addressed in the next chapter, as vortex polycrystals provide a nice example. Nonetheless, in the general case where grain boundary motion is controlled by diffusional rearrangements (glide-climb of the grain boundary dislocations) long-range stresses need not occur and local elasticity approximations may retain their validity.

As already pointed out, dynamics of simple dislocation arrays of the kind examined in this chapter provides a nice example of depinning in plastically deforming systems. However, the situation is much more complicated in the general case, when dislocations of different types and directions of motion have to be considered. Under the effect of an external stress, dislocations still move through a series of metastable states, principally due to self induced constraints arising from mutual long-range interactions, until the whole dislocation systems reaches a threshold, the *yielding transition* [59, 81]. The system can still be described in terms of dislocation pinning. However, given the complexity of the problem, an analytic treatment from the point of view of dislocations dynamics remains a hard task, while a continuum approach on larger

length scales seems more adequate, as close to criticality, deforming crystals exhibit a scale-free behaviour over several orders of magnitude in length.

These aspects are examined in further detail in Chapter 4, where we present a theory of plastic flow in the presence of random fluctuations, accounting for the dynamic behaviour of general dislocation systems and the critical features related to the yielding transition.

Chapter 3
Plasticity of vortex lattices

Plastic properties of vortex lattices in Type II superconductors have recently been an active subject area, as the discovery of high temperature superconducting alloys has broadened the phenomenology of flux lines arrays and led to the introduction of novel concepts, such as *field cooling*, *vortex lattice melting* or *vortex glass*. A concise, and inevitably incomplete, introduction to vortex physics will be given in the following, emphasising analogies with plasticity theories and stressing how collective properties of dislocations systems are supposed to determine the phenomenology of vortex matter.

Our study in this field has covered several aspects and phenomena. The starting point is the recurrent observation of polycrystalline order in vortex lattices. Although the role of isolated dislocations in vortex phase diagrams has been extensively studied in the past decades, the evidence of dislocation arrays in the form of grain boundaries leads to a wider class of phenomena which require a suitable theoretical treatment.

In the following, we introduce grain boundaries in flux line lattices as linear arrays of dislocations and analyse their elastic properties and behaviour in the presence of disorder. This allows us to provide an exhaustive description of the polycrystalline state. We first study the growth of a vortex polycrystal in terms of the competition between elastic properties of grain boundaries and disorder. Then we consider the roughening of dislocation walls, along with its effects on depinning transition, creep motion and critical current hysteresis. Finally, we describe the role of polycrystalline ordering in topological order loss at high temperatures and introduce possible implications for a *melting* theory.

3.1 Vortex lattices — a brief introduction

Magnetic fields play an essential role in the behaviour of superconducting materials. Beyond the well known diamagnetic regime obtained for low magnetic inductions (*Meissner* effect), the superconductive state is either broken (Type I superconductors) or characterised by a mixed

phase (Type II superconductors). The scientific breakthrough that came along with the discovery of high temperature superconductors (HTSC or high T_c materials) has significantly moved the attention of the scientific community towards the latter class, as most high T_c materials behave in a magnetic field as Type II superconductors.

As first discussed by Abrikosov for conventional Type II superconductors [97], in the mixed phase magnetic flux is quantised and carried by vortex lines which are arranged in the form of a triangular lattice. As in conventional matter, strong enough fluctuations destroy long range order: when temperature is raised the vortex lattice melts into a vortex liquid [98–100].

Fluctuations are also provided by defects that are intrinsically present in these materials. Vortex density grows linearly with the applied magnetic induction. The theory shows that effects of disorder are stronger for high fields [8] and lead to complex glassy phases [9, 101–105].

3.1.1 Experimental evidences and theoretical background

In comparison to conventional Type II superconductors, high temperature superconducting alloys present an intriguing phase diagram, as the broadening of phase space — in terms of temperature T and field B — gives rise to a rich variety of stable phases and metastable states which couple in peculiar ways with the underlying anisotropic crystal lattices [8, 95, 96]. This leads to a much more complicated scenario for the mixed phase, where magnetic flux penetration is incomplete. While several experimental methods have been used to investigate vortex matter, a direct image of the geometrical and topological properties of the vortices can be obtained by the Bitter decoration technique [106]. Its application to conventional Type II superconductors provided the first direct proof of the vortex lattice [107] predicted by Abrikosov [97].

At the same time, the observed lattice contains topological defects, such as dislocations and grain boundaries. The latter are the signature of a vortex polycrystal with crystalline domains of different orientations [106, 108]. Vortex polycrystals have been observed (see Figure 3.1) in *field-cooling* experiments, in various superconducting materials such as NbMo [106, 108], $NbSe_2$ [109–112], BSCCO [113] and YBCO [114]. More details about experimental procedures will be given below.

The grain size is typically found to grow with applied magnetic field [108, 109]. Moreover, two-sided decoration experiments show that the grain boundaries thread the sample from top to bottom [109, 110]; i.e., one observes a columnar grain structure, as clearly depicted in Figure 3.2.

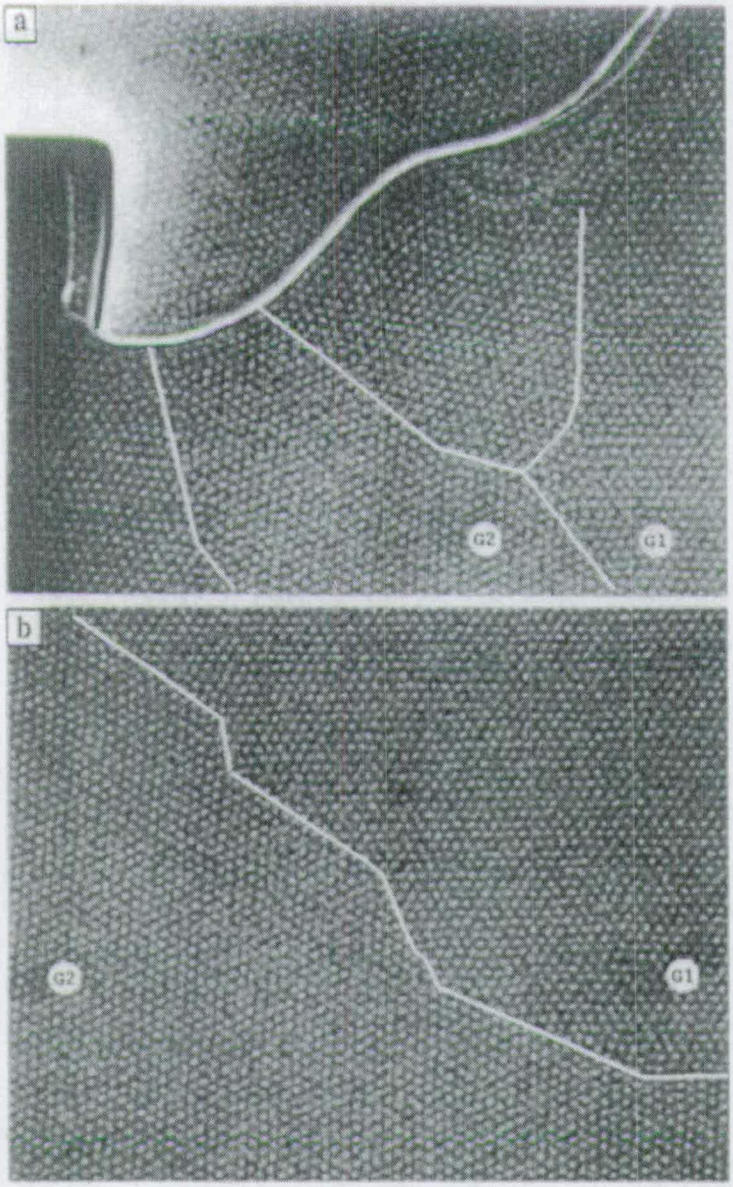

Figure 3.1: *Real space STM image of a vortex polycrystal, as observed in a BSCCO sample, in the presence of a 27 G external field. Grain boundaries are highlighted. The typical vortex spacing is* $a \approx 0.95 \mu m$ *[After Dai et al., Reference [113]].*

Despite the abundance of experimental observations, there is no detailed theory accounting for the formation of vortex polycrystals.

The interaction between vortex matter and disorder represents a general theoretical problem which still remains unsolved. While early theoretical considerations seemed to imply that even a small amount of disorder would lead to the loss of long-range order [56] and to the formation of an amorphous vortex glass phase [104], it is now accepted that at low disorder vortices arrange into a topologically ordered phase: the Bragg glass [9, 10]. The existence of this phase, characterised by long distance ordering, slow relaxation, and other glassy features, has been experimentally confirmed [115]. At high enough disorder, the Bragg glass phase is unstable against dislocation proliferation and the possibility of a transition into an amorphous vortex glass is now commonly accepted. [116–118]. The precise nature of this transition and, more generally, the mechanism underlying vortex lattice thermal melting are still uncertain. Typical melting theories are based on phenomenological criteria with disorder [119], or involve dislocation proliferation mechanisms [120].

3.1.2 Dislocations in vortex matter

Properties and behaviour of isolated dislocations in the vortex lattice have been thoroughly investigated in the past [70, 121–123], but the role of grain boundaries has been often overlooked, although they are often encounterd in numerical simulations [124–128]. For instance, the vortex plastic flow in the Corbino disk geometry is characterised by radial grain boundaries sliding in the tangential direction [124]. In addition, recent numerical simulations indicate the presence of an intermediate polycrystalline stage before the melting transition [125–128]. This behaviour was observed using different numerical methods in two dimensions [125] and in presence of columnar disorder [126–128]. This suggests that, in some conditions, grain boundaries may play a role in the melting process, as in the theory of grain boundary induced melting of two dimensional crystals [129].

3.2 Elasticity of grain boundaries

Properties of grain boundaries in vortex matter determine their response to fluctuations induced by disorder, external stresses or temperature. As in the previous chapter, a grain boundary can be considered as a linear array of dislocations, whose dynamics is ruled by internal stresses.

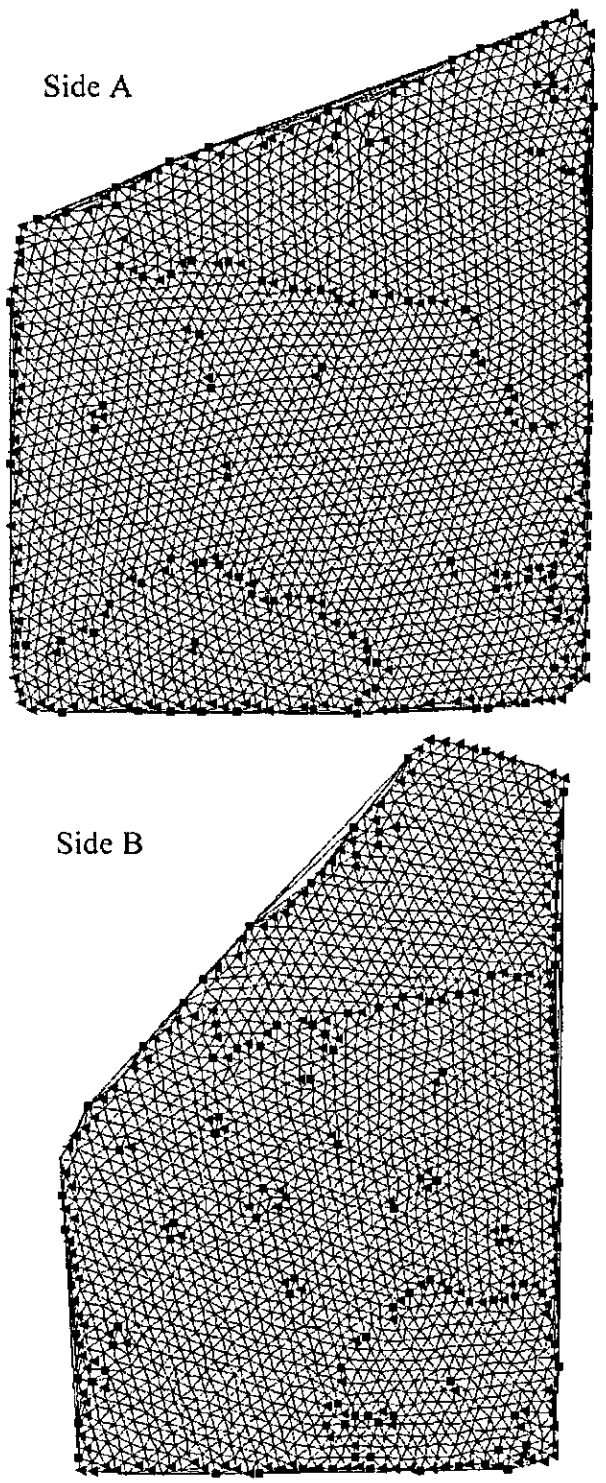

Figure 3.2: *Two sided imaging of a vortex lattice. Real space configurations are reported, corresponding to two parallel surfaces of the sample. Polycristalline structure is unchanged from bottom to top of the sample, up to a rigid rotation. This observation, along with several other, confirms the existence of columnar grain structures and characterises the system as quasi two-dimensional. [After Marchevsky et al., Reference [110].]*

While ideally a grain boundary minimises its energy by remaining flat, the action of external perturbations leads to deformations that can be described by the theory of elasticity. We compute the self-interaction of a deformed grain boundary extending the results obtained for isotropic elasticity (see Chapter 2 to the case of the highly anisotropic vortex lattice.

3.2.1 Analytical approach

A simplified but rather effective description of the vortex lattice is provided by its representation as an elastic crystal of flux lines. On large enough length scales, the elastic energy of the vortex lattice can be expressed in terms of the vortex displacement field $\mathbf{u}$ as follows

$$\mathcal{H} = \frac{1}{2}\int d^3r \left[c_{66}(\nabla \mathbf{u})^2 + (c_{11} - c_{66})(\nabla \cdot \mathbf{u})^2 + c_{44}(\partial_z \mathbf{u})^2\right], \tag{3.1}$$

where c_{11}, c_{44}, c_{66} are the local elastic moduli, and the magnetic induction $\mathbf{B}$ is parallel to the z direction. Within this representation, we shall introduce an ideal low angle grain boundary as an infinite periodic array of straight dislocations in the vortex lattice oriented along the z axis, spatially arranged along the y axis with an array spacing equal to D, and with Burgers vectors $\mathbf{b}$ pointing along the x direction (i.e. edge dislocations [91]). The wandering of the i-th dislocation line can be schematised through the vector $\mathbf{R}_i(z) = (X_i + X_i(z), iD)$, assuming that all displacements take place within glide planes, i.e. the xz plane, so that $X_i + X_i(z)$ plays the role of the displacement field of the grain boundary as well. X_i is a constant term and deals with rigid displacements of the dislocation lines. Its contribution to the elastic Hamiltonian is known since it is the same derived for straight dislocations in isotropic lattices (see Chapter 2). In the following this contribution will be referred to as $\mathcal{H}_0$. $X_i(z)$ has zero average along the z direction.

Defining $\mathbf{r}_\perp = (x, y)$, the vector $\mathbf{u}$ can be decomposed as $\mathbf{u}(\mathbf{r}) = \mathbf{u^r}(\mathbf{r}_\perp, z) + \sum_i \mathbf{u_i^s}(\mathbf{r}_\perp - \mathbf{R_i}(z), z)$, where $\mathbf{u_i^s}(\mathbf{r}_\perp - \mathbf{R_i}(z), z)$ is the singular solution of the two-dimensional problem for each value of z

$$\begin{cases} c_{66}\nabla^2 \mathbf{u}_i^s + (c_{11} - c_{66})\nabla(\nabla \cdot \mathbf{u}_i^s) = 0 \\ \oint d\mathbf{u}_i^s = \mathbf{b}_i \qquad\qquad \forall i, z \end{cases} \tag{3.2}$$

while $\mathbf{u}^{\mathrm{r}}(\mathrm{r}_\perp, z)$ is the regular part of the solution due to the interplane couplings along z.

Minimizing Eq.(3.1) with respect to $\mathbf{u}$ and imposing the first expression of Eqs. (3.2) we find the differential equation

$$c_{66}\nabla^2\mathbf{u}^r + (c_{11}-c_{66})\nabla(\nabla\cdot\mathbf{u}^r) + c_{44}\partial_z^2\mathbf{u}^r = -c_{44}\partial_z^2\sum_i \mathbf{u}_i^s, \tag{3.3}$$

where the field $\mathbf{u}_i^s$ on the right-hand side term of the equation is known from elasticity theory as the displacement field generated by a point edge dislocation at $\mathbf{R_i}(z)$. Performing a first order expansion in the displacement $X_i + X_i(z)$, the derivative removes any dependence on the constant part X_i, and we can rewrite Eq.(3.3) in Fourier space as follows

$$c_{66}q^2\mathbf{u}^r + (c_{11}-c_{66})\mathbf{q}(\mathbf{q}\cdot\mathbf{u}^r) + c_{44}k_z^2\mathbf{u}^r = c_{44}\frac{k_z^2}{q^2}\mathbf{A}, \tag{3.4}$$

where $\mathbf{q} = (k_x, k_y)$, $q^2 = k_x^2 + k_y^2$, and

$$\mathbf{A} = \sum_n e^{ik_yY_n}X_n(k_z)\begin{pmatrix} k_y[r-(1-r)\cos 2\phi] \\ k_x[r+(1-r)\cos 2\phi]\end{pmatrix} \tag{3.5}$$

with $r = c_{66}/c_{11}$, $\cos\phi = k_x/k$ and $\sin\phi = k_y/k$.

$\mathbf{A}$ can be decomposed into its longitudinal and transverse components $\mathbf{A}_L = \mathbf{q}(\mathbf{q}\cdot\mathbf{A})/q^2$ and $\mathbf{A}_T = \mathbf{A} - \mathbf{A}_L$. The Hamiltonian (3.1) thus becomes

$$\mathcal{H} = \mathcal{H}^0 + \frac{1}{2}\,c_{44}\,b^2\sum_{n,m}\int\frac{d^2q}{(2\pi)^2}\int\frac{dk_z}{2\pi}\,k_z^2\,M(q,\phi,k_z)\,e^{ik_y(n-m)D}\,X_n(k_z)X_m(-k_z) \tag{3.6}$$

where we have neglected constant terms and defined

$$M(q,\phi,k_z) \equiv \left[\frac{c_{66}\cos^2 2\phi}{c_{66}q^2 + c_{44}k_z^2} + \frac{c_{11}r^2\sin^2 2\phi}{c_{11}q^2 + c_{44}k_z^2}\right]. \tag{3.7}$$

Defining $X_n(k_z) = \int_{BZ} \frac{dQ_y}{2\pi}\, e^{-iQ_y nD}\, X(Q_y, k_z)$, where the integral is restricted to the first Brillouin zone (BZ), we get

$$\mathcal{H} = \frac{1}{2}\, c_{44}\, \frac{b^2}{D^2} \sum_{G_y} \int_{BZ} \frac{dQ_y}{2\pi} \int \frac{dk_z}{2\pi}\, \Xi(Q_y + G_y, k_z)\, X(Q_y, k_z) X(-Q_y, -k_z) \tag{3.8}$$

where we have introduced the interaction kernel

$$\Xi(Q_y + G_y, k_z) = k_z^2 \int_{-\infty}^{+\infty} M(k_x, Q_y + G_y, k_z)\, dk_x \tag{3.9}$$

with

$$M(k_x, k_y, k_z) = \frac{(k_x^2 - k_y^2)^2}{(k_x^2 + k_y^2)^2 (k_x^2 + k_y^2 + \frac{c_{44}}{c_{66}} k_z^2)} + 4r^2 \frac{k_x^2 k_y^2}{(k_x^2 + k_y^2)^2 (k_x^2 + k_y^2 + \frac{c_{44}}{c_{11}} k_z^2)}. \tag{3.10}$$

Solving the integral in Eq.(3.9) leads to

$$\mathcal{H} = \mathcal{H}^0 + \frac{\pi b^2}{2D^2}\, \frac{c_{66}^2}{c_{44}} \sum_{G_y} \int_{BZ} \frac{dQ_y}{2\pi} \int \frac{dk_z}{2\pi}\, X(Q_y, k_z) X(-Q_y, -k_z)$$
$$\frac{1}{k_z^2} \left[\frac{\left(2k_y^2 + \frac{c_{44}}{c_{66}} k_z^2\right)^2}{\sqrt{k_y^2 + \frac{c_{44}}{c_{66}} k_z^2}} - 4k_y^2 \sqrt{k_y^2 + \frac{c_{44}}{c_{11}} k_z^2} - 2 \left(\frac{c_{44}}{c_{66}} - \frac{c_{44}}{c_{11}} \right) |k_y|\, k_z^2 \right] \tag{3.11}$$

with $k_y = Q_y + G_y$, $\frac{c_{44}}{c_{66}} \gg 1$ and $\frac{c_{44}}{c_{11}} \sim 1$.

Moreover, keeping the leading term of the righthand side in Eq.(3.11) we get

$$\mathcal{H}_{GB} = \frac{\pi b^2}{2D^2} \sum_{G_y} \int \frac{dQ_y}{2\pi} \int \frac{dk_z}{2\pi}\, (2c_{66}|k_y| + \sqrt{c_{44} c_{66}}|k_z|)\, X(k_y, k_z) X(-k_y, -k_z). \tag{3.12}$$

It is a common procedure to rescale the y coordinate by a factor $\frac{1}{2}\sqrt{\frac{c_{44}}{c_{66}}}$ [8], in order to get an isotropic reference frame. The elastic Hamiltonian thus becomes

$$\mathcal{H} = K\frac{\pi b^2}{2D^2}\sum_{G_y}\int\frac{d^2k}{(2\pi)^2}\,|\mathbf{k}|\,X(\mathbf{k})X(-\mathbf{k}), \tag{3.13}$$

being $\mathbf{k} = (k_y, k_z)$ and $K = \sqrt{c_{44}c_{66}}$.

In this limit, the same result is obtained as predicted by the isotropic theory (see Chapter 1). The nonlocal character of the elastic kernel ($\propto k$) implies that long range interactions between dislocations stiffen the grain boundary, and that, once more, a surface tension approximation is not suitable for a correct description of its elastic properties.

3.3 Interaction between grain boundaries and disorder

As in the case examined in Chapter 2, vortex grain boundaries are much stiffer than isolated dislocations, possessing a non-local long-range surface tension. In the presence of disorder, they are expected to roughen less than isolated dislocations.

However, the description of the interaction between elasticity and disorder that was formulated for grain boundaries in crystalline materials needs to be refined in the case of vortex lattices. The strong pinning approach (see Chapter 1) is substantially unchanged, because in the case of dilute pin densities, obstacles interact individually with dislocation lines. Further details are given in the following, in the context of grain growth.

In the case of weak pinning, instead, random forces are mediated by the vortex lattice. Quenched disorder deforms the vortex lattice inducing random strain fields. The corresponding random stress fields act on vortex dislocations and dislocation arrays, determining their pinning.

Following these guidelines, we investigate the problem of grain boundary roughening applying the random stress model introduced in Ref. [123] for vortex dislocations. Using scaling arguments, we also derive the creep law for thermally activated motion and discuss disorder-arrested grain growth.

3.3.1 Random stresses

Point defects such as vacancies or interstitials in the underlying crystalline structure of the superconducting material, and/or substitutional impurities, etc., act as pinning centres for the magnetic vortices. For weak pinning forces, disorder can be theoretically described by a *random pinning potential* acting directly on flux lines. Fluctuations due to pinning in the vortex lattice and the occurrence of depinning under the effect of an applied current have been intensively studied over the last decades (for a review see Reference [8]).

Our aim is to extend those consideration to the case of dislocation assemblies and in particular grain boundaries . The disorder induced vortex lattice displacement field gives rise to elastic shear stresses, which, in turn, generate Peach-Koehler forces on the vortex lattice dislocations [91]. In other words, as the final consequence of these disorder-induced distortions of the vortex lattice, there is an effective pinning stress field $\sigma_{ij}(\mathbf{r})$ acting as well on vortex dislocations (and therefore on grain boundaries). The effects of such a field on isolated dislocations and random dislocation bundles have been already investigated in Reference [123]. In the following, we recall that derivation and provide its equivalent in the case of grain boundaries, adopting the same theoretical framework.

On short length scales, where vortex displacements $\mathbf{u}(\mathbf{r})$ are smaller than the coherence length ξ_{sc} (the so called Larkin regime [6]), a perturbative calculation can be performed. As discussed in Ref. [120], for grain boundaries it is necessary to consider larger scales, $\xi_{sc} < u < a$, where vortices are well described by a *Random Manifold* (RM) model [8, 9] in which flux lines are subject to an uncorrelated pinning potential. In this case, the relative displacements correlation function is

$$\begin{aligned} B_{ij}(\mathbf{r}-\mathbf{r}') &= \overline{[u_i(\mathbf{r})-u_i(\mathbf{r}')][u_j(\mathbf{r})-u_j(\mathbf{r}')]} \\ &\simeq a^2\left(\frac{|\mathbf{r}-\mathbf{r}'|}{R_a}\right)^{2\zeta_{RM}} . \end{aligned} \tag{3.14}$$

Here R_a is the crossover length, also known as *positional correlation length*, at which average vortex displacements are of the order of a. The roughness exponent can be estimated as $\zeta_{RM} \approx 1/5$.

On scales larger than R_a, vortex displacements are of the order of a and the periodicity of the lattice comes into play [9]. Displacements are shown to grow logarithmically, with correlations of the form $B(\mathbf{r}-\mathbf{r}') \simeq \left(\frac{a}{\pi}\right)^2 \ln\frac{e|\mathbf{r}-\mathbf{r}'|}{R_a}$, and topological defects are absent. This quasi-

ordered phase is knwon as the *Bragg glass* (BrG) [9].

As discussed above, vortex displacements act on vortex lattice dislocations through a fluctuating stress field [91]. Statistical properties of this stress field can be obtained from the correlator $B_{ij}(\mathbf{r}-\mathbf{r}')$ applying linear elasticity theory. In particular, the stress correlator $S_{xy}(\mathbf{r}-\mathbf{r}') = \overline{\sigma_{xy}(\mathbf{r})\sigma_{xy}(\mathbf{r}')}$ will read

$$S_{xy}(\mathbf{r}-\mathbf{r}') = (K^2/2)\left[\partial_x\partial_{x'}B_{yy}(\mathbf{r}-\mathbf{r}') + \partial_y\partial_{y'}B_{xx}(\mathbf{r}-\mathbf{r}') + 2\partial_x\partial_{y'}B_{yx}(\mathbf{r}-\mathbf{r}')\right]. \tag{3.15}$$

Replacing previous expressions of $B_{ij}(\mathbf{r}-\mathbf{r}')$ we easily obtain the stress fluctuations over a distance R

$$S_{xy}(R) \approx K^2 \frac{a^2}{R^2} \begin{cases} (R/R_a)^{2\zeta_{RM}} & R < R_a \\ 1 & R > R_a \end{cases} \tag{3.16}$$

where the first case applies to the RM description, while the second corresponds to the BrG regime. The effect of this random stress on isolated dislocations was studied in Ref. [123] where several differences with respect to the case of vortex lines were pointed out. Here we consider the behaviour of grain boundaries, expecting substantial novel features arising from long range interactions between grain boundary dislocations.

The Hamiltonian of a grain boundary in presence of disorder can be written as

$$\mathcal{H}_d = \mathcal{H} + \mathcal{H}_{pin}, \tag{3.17}$$

with $\mathcal{H}$ being the elastic term calculated above and $\mathcal{H}_{pin}$ the pinning term given by

$$\mathcal{H}_{pin} = \sum_i \int dz\, X_i(z)\, b\sigma_{xy}[X_i(z), iD, z]. \tag{3.18}$$

Although there is no explicit expression for $\mathcal{H}_{pin}$, it is possible to derive its fluctuations over a

distance L as

$$E_{pin}^2 = b^2 \sum_{i,i'} \int_0^L dz \int_0^L dz' \, X_i(z) X_{i'}(z') \, \overline{\sigma_{xy}[X_i(z), iD, z] \sigma_{xy}[X_{i'}(z'), i'D, z']}. \quad (3.19)$$

Taking the continuum limit of the sum and integrating for both the RM and the BrG regimes, the typical pinning energy when displacing a grain boundary segment of length L by an amount $\overline{X_i^2}^{1/2} \sim u_{GB}$ will be thus given by

$$E_{pin}^2 \simeq \left(\frac{Kab}{D}\right)^2 L^2 u_{GB}^2 \begin{cases} \left(\frac{L}{R_a}\right)^{\frac{2}{5}} & \text{(RM)} \\ \ln \frac{L}{u_{GB}} & \text{(BrG)} \end{cases} \quad (3.20)$$

A dimensional estimate of the elastic energy cost of fluctuations of a grain boundary fraction of linear dimension L has the form

$$E_{el} = \frac{Kb^2}{D^2} L u_{GB}^2. \quad (3.21)$$

Since we are dealing with static properties of the system, we can impose equilibrium conditions balancing E and E_{pin}, that is, equating the elastic cost of fluctuations and the energy gain due to the interaction with disorder. Defining the roughness exponent of a grain boundary ζ_{GB} from $u_{GB}^2 \sim L^{2\zeta_{GB}}$ we get

$$\zeta_{GB} \approx \begin{cases} \frac{1}{5} & \text{(RM)} \\ \log^{1/2} & \text{(BrG)} \end{cases} \quad (3.22)$$

The long-range stiffness of a grain boundary reduces the values of roughness exponents in comparison with the case of isolated dislocations [123].

exponent	length scale	isolated dislocation	2D bundle	grain boundary
ζ	RM	$15/13$	$5/13$	$1/5$
ζ	BrG	$1-\log^{2/3}$	$1/3$	$\log^{1/2}$
μ_{pl}	RM	$17/11$	$10/21$	$7/4$
μ_{pl}	BrG	1	$2/5$	1

Table 3.1: *Comparison between roughness and creep exponents calculated for isolated dislocations, 2D dislocation bundles [123], and low angle grain boundaries, taking into account non-local effects proven in Section 3.2.*

3.3.2 Depinning and creep

So far we have not considered the effect of driving forces on the dislocation arrangement. Driving forces for grain boundary motion can be externally induced by a current flowing in the superconductor or internally generated by the ordering process during grain growth [138]. In the former case, shear strain is induced in the vortex lattice by current gradients due to boundary effects; in the latter case, ordering is driven by a reduction in elastic energy. In both cases, the presence of a driving shear stress τ_{ext} gives rise to a Peach-Koehler force per unit length of the form $F_{drive} = \tau_{\text{ext}} b$ acting on each dislocation along the grain boundary fraction considered or, in other words, to a total driving force per unit length equal to $F_{drive} = \tau_{\text{ext}} bL/D$.

At low stress grain boundaries are pinned. One can estimate the depinning stress from conventional scaling arguments. The energy associated to the driving force acting on a low-angle grain boundary segment of length L and displaced by an amount u_{GB} is given by

$$E_{drive}(L) = \sum_i \int dz\, F^i_{drive}(z)\, u_{GB}(y_i, z) \sim \frac{\tau_{\text{ext}} bL^2}{D} u_{GB}. \tag{3.23}$$

The depinning stress can be obtained comparing this driving term with the pinning energy reported in Eq. 3.20. The relevant scale to consider is due to the interplay between elasticity and disorder and results from the minimisation of $E_{el} + E_{pin}$ for displacements of the order of $u_{GB} \simeq a \simeq b$, corresponding to the dislocation core. A similar approach is followed in the case of vortices [6], which are pinned for displacements of the order of ξ_{sc}, the size of the vortex core and, hence, the relevant scale for the interaction with impurities. In our case, we obtain the Larkin length as $L_p \simeq (b/D)^5 R_a$, which is typically smaller than R_a. The depinning stress is then identified as the stress necessary to depin a section of dimension L_p:

$$\tau_c \simeq Kb^2/(DL_p) = KD^4/(b^3 R_a). \tag{3.24}$$

For low values of the stress ($\tau_{ext} \ll \tau_c$), the response of a grain boundary is mainly due to thermally activated motion in a disordered environment [8]. In this case, we expect a highly non-linear creep motion with an average velocity $v \sim \exp[-C(\tau_c/\tau_{ext})^{\mu_{pl}}/T]$, where C is a constant, and μ_{pl} is the plastic creep exponent that quantifies the divergence of the energy barriers $U(\tau_{ext}) \sim \tau_{ext}^{-\mu_{pl}}$ separating metastable states. An estimation of the exponent μ_{pl} for a grain boundary can be obtained from a simple dimensional scaling argument, which is confirmed by a more rigorous renormalisation group analysis. The typical energy barrier for a grain boundary section of length L is of the order of $U(L) \sim L^{1+2\zeta_{GB}}$, where we have used $u_{GB} \sim L^{\zeta_{GB}}$. In presence of an applied stress τ_{ext}, we can compute the typical grain boundary length $L(\tau_{ext})$ involved in thermally activated motion minimizing $U(L) + E_{drive}(L)$. The result yields $L(\tau_{ext}) \sim \tau_{ext}^{1/(\zeta_{GB}-1)}$. Using this length, we obtain that the typical energy barrier depends on the stress as

$$U(\tau_{ext}) \sim \tau_{ext}^{(1+2\zeta_{GB})/(\zeta_{GB}-1)}, \tag{3.25}$$

implying that $\mu_{pl} = 2\zeta_{GB}/(2-\zeta_{GB})$. For the RM and BrG regimes the exponents are given by

$$\mu_{pl} \approx \begin{cases} \frac{7}{4} & \text{(RM)} \\ 1 & \text{(BrG)} \end{cases}. \tag{3.26}$$

Now these exponents are larger than their counterparts calculated for isolated dislocations. In other words, the formation of grain boundaries affects vortex dynamics lowering ordinary creep rates. In table 3.1, all previous results are summarised and compared to estimates for different dislocation arrays.

3.3.3 Grain growth and thermal activation

Experimental evidence of polycrystalline order in vortex lattices is provided by direct imaging of the lattice structure in Bitter decoration investigations (see Section 3.1.1 and Figure 3.2). A typical setup for decoration experiments consists in lowering the temperature after a magnetic

field has been applied to the sample at temperatures above the superconducting phase. During this procedure, known as *field cooling*, magnetic flux is already present in the sample as it is cooled into the mixed superconducting phase. It is thus reasonable to expect that vortices are originally disordered and that, due to their mutual interactions, undergo a local ordering process. During this process, many dislocations annihilate, and most of the remaining dislocations arrange themselves into grain boundaries with various orientations. The growth of crystalline vortex grains is due to the motion of these separating boundaries. The resulting polycrystalline structure has been indeed observed experimentally by means of Bitter decorations of both high [113, 114] and low T_c [109–111] superconducting samples. The effect of quenched disorder is to pin the grain boundaries, hindering the growth process. Thus it is important to envisage the growth of vortex polycrystals as the result of the competition between elasticity and disorder.

Grain growth is driven by a reduction in energy: for an average grain size R and straight grain boundaries, the characteristic energy stored per unit volume in the form of grain boundary dislocations is of the order of Γ_0/R, where Γ_0 is the energy per unit area of a grain boundary. Hence, the energy gain achieved by increasing the grain size by dR is $\Gamma_0/R^2 dR$. Physically, the removal of grain boundary dislocations occurs through the motion of junction points in the grain boundary network. As junction points must drag the connecting boundary with them, which may be pinned by disorder, motion can only occur if the energy gain at least matches the dissipative work which has to be done against the pinning forces. The dissipative work per unit volume expended in moving all grain boundaries by dR is $\tau_c b/(DR)dR$, where τ_c is the pinning force per unit area. Balancing against the energy gain yields the limit grain size

$$R_g \approx \frac{D\Gamma_0}{b\tau_c} \,. \tag{3.27}$$

Determining the grain size is thus a matter of finding how the critical stress can be expressed in terms of general properties of disordered vortex matter. To proceed, we have to specify the nature of the "disorder". Several assumptions can be made. In the following we will articulate our discussion around the concept of pin density distinguishing, as usual, weak pinning and strong pinning regimes.

Weak pinning

As discussed above, in this regime the grain boundary perceives a smooth distribution of stresses σ_{xy} due to the elastic straining of the vortex lattice under the effect of quenched disorder [120, 123]. The critical stress, obtained by balancing elasticity and disorder, is given in Equation 3.24. Combining its expression with Eq. (3.27), using $\Gamma_0 \simeq Kb^2/D$, we obtain

$$R_g \sim R_a \,. \tag{3.28}$$

The identification of R_g with R_a was first proposed in Ref. [108], but was not confirmed by experiments (see Fig. 3.3 and Reference [108]). We therefore propose to interpret the experimental data under a strong pinning assumption.

Strong pinning

We are already familiar with this approach. In this regime, pinning centres are strong and localized and one can assume that the dislocations forming the grain boundary are pinned by individual obstacles. We consider here the case of columnar defects, oriented along the z axis. Although not general, this is a sensible assumption, as it holds in a wide variety of experimentally observed vortex arrangements. Its quasi two-dimensional characterisation mimics vortex lattices typically observed in highly anisotropic superconductors, where vortices are split onto weakly coupled layers. This is the case, for instance, in the experiments of Ref. [108] where grain boundary pinning is provided by screw dislocations in the superconducting crystal. Under these circumstances, the problem becomes effectively two dimensional and the grain boundary is a one-dimensional string exhibiting long-range elasticity. Hence we can directly apply the strong pinning theory of Friedel [58] and its extension to grain boundary depinning which we have proposed in Chapter 1.

In the current notations, the elastic energy per unit length of the bulge of width u and extension L is $2c_{66}b^2v^2/D^2$, and should balance the work per unit length $\tau_{\text{ext}}bLv/D$ done by the driving stress τ_{ext} in bowing the boundary. This energy balance provides a relation between L and u. Furthermore, at depinning the total force $h\tau_{\text{ext}}bL/D$ should be equal to the defect strength f_0, where h is the sample thickness. Combining the equations above we obtain the depinning stress $\tau_c b = Df_0/(hL_f)$, where the Friedel length L_f is given by $L_f = 2c_{66}b^2h/(f_0\rho D^2)$. Inserting

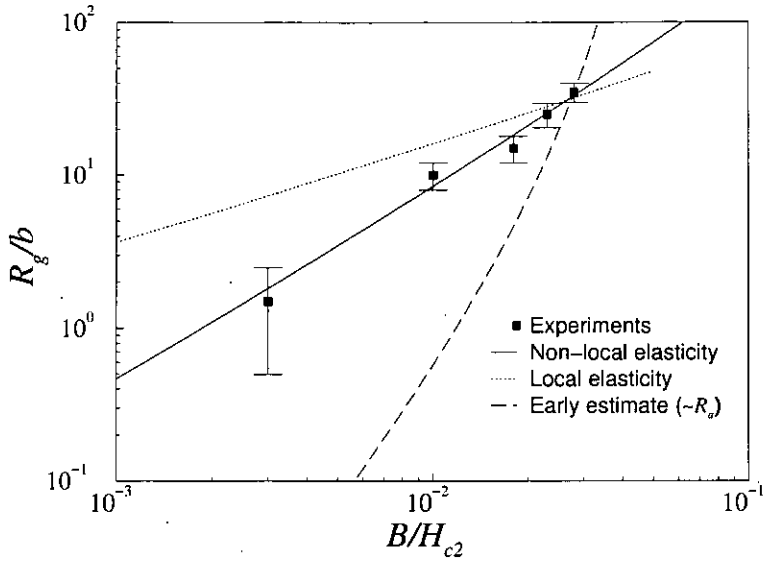

Figure 3.3: *The grain size of a vortex polycrystal experimentally obtained from Bitter decoration of a NbMo sample as a function of the applied magnetic field (Ref. [108]) is compared with the theoretical predictions. The calculation based on Friedel statistics with non-local elasticity compares favorably with the data. For comparison we report as well the result obtained using Friedel theory with local elasticity and the earlier estimate from Ref. [108], formally equivalent to our weak pinning result.*

the expression for the critical stress in Eq. (3.27) together with the scale-independent surface tension $\Gamma_0 = 2c_{66}b^2/D$, we obtain

$$\frac{R_g}{b} \approx \frac{c_{66}^2 b^3 h^2}{D^3 f_0^2 \rho}. \tag{3.29}$$

In order to use this result to fit the data in Ref. [108], we have to express it in terms of the reduced field $\tilde{B} \equiv B/H_{c2}$, where H_{c_2} is the upper critical field of the superconductor. The field dependence is implicit in the parameters b and D, i.e. $b \sim D \sim a \sim \tilde{B}^{-1/2}$, as well as in the shear modulus $c_{66} \sim \tilde{B}$, and in the pinning strength f_0. The pinning force due to a screw dislocation was computed in Ref. [142] and is given by $f_0 \propto \tilde{B}^{1/2}(1-\tilde{B})\ln(\xi_{sc}/2.7b_0\tilde{B}) \approx \tilde{B}^{1/2}\ln(\xi_{sc}/2.7b_0\tilde{B})$, where $\xi_{sc} \simeq 100\dot{A}$ is the coherence length [143], and $b_0 \simeq 5\dot{A}$ is the Burgers vector of the screw dislocation [142]. The resulting expression predicts a linear field dependence of the grain size with logarithmic corrections. In Fig. 3.3 we can corroborate that the agreement of this prediction with magnetic decoration data from Ref. [108] is quite satisfactory, especially if compared to the estimate based on local elasticity assumptions.

Thermally activated motion

In the discussion above we have neglected the effect of temperature. This is an acceptable assumption since in field cooling experiments temperature is rapidly lowered below the vortex melting point and the effects of perturbations due to pinning become predominant. Thermal fluctuations, nonetheless, could induce an activated motion of the grain boundaries, particularly in high T_c materials. This problem can be approached generalizing scaling theories of creep for vortices and dislocations [8, 123]. In the weak pinning regime, the relevant energy barrier that the grain boundaries have to surmount under an applied stress $\tau_{\rm ext} < \tau_{\rm c}$ is given by $U(\tau_{\rm ext}) = U_0(\tau_{\rm c}/\tau_{\rm ext})^{\mu_{pl}}$, where $U_0 \simeq Kb^3R_a$ and $\mu_{pl} = 1$ (Table 3.1). In our case, the applied stress is the ordering stress, so that we have $\tau_{\rm c}/\tau_{\rm ext} \simeq R/R_a$. Using this expression in the energy barrier for thermally activated grain growth, it follows

$$t_0\frac{dR}{dt} = R_a \exp\left[-\frac{U_0}{K_BT}\frac{R}{R_a}\right], \tag{3.30}$$

where t_0 is the appropriate characteristic time. The equation can readily be solved yielding, in the long time limit, a logarithmic growth $R(t)/R_a = kT/U_0 \log(t/t_0)$. This law holds for $R > R_a$ when the grain boundaries would be pinned at $T = 0$. In the initial growth stage $R \ll R_a$, we can neglect pinning forces and the dynamics is ruled by the ordering stress: $\dot{R} \sim 1/R$, yielding a power law growth $R(t) \sim \sqrt{t}$. A similar behaviour is encountered in a wide variety of physical systems exhibiting analogous ordering transitions. In particular, the $\sqrt{t}$ law is known to characterise domain growth phenomena in binary alloys [144].

Besides thermal activation, grain boundaries can move in response to an applied current [123]. Details on this aspect will be given in the following section.

3.4 Effect of grain boundaries on the critical current

The critical current is an important property of Type II superconductors, since it represents the current below which vortices are pinned and the material conducts without resistance. This technological aspect, however, only partly explains the role of critical current in the system under examination. Externally induced currents produce Lorentz-like driving forces in the flux line lattice. This system can be easily mapped into a general depinning model for a random elastic manifold, where the critical current acts as a depinning force. Such a problem has been

carefully pondered and analysed in the past and has led to a further broadening of the vortex phase diagram. An exhaustive review can be found in Ref.[8]. Our concern is to point out how the above scenario changes in the presence of a polycrystalline arrangement.

In Section 3.2 we determined non-local elasticity properties of grain boundaries in vortex matter. This result, determines changes in roughness and creep exponents. It is then reasonable, in the light of results from Table 3.1, to believe that in vortex polycrystals, properties of critical current could change significantly. One can actually expect the critical current to be higher in the presence of grain boundary networks.

In order to assess the validity of that statement, numerical simulations have been run by our co-workers. In the following, we will briefly review their results, emphasising how they confirm predictions based on our theoretical model and match behaviours commonly observed in experiments.

3.4.1 Overview of a numerical approach

In the simulation of arrays of interacting vortices, a polycrystalline vortex structure is obtained by relaxing at zero temperature a random initial vortex arrangement. This process mimics a typical field cooling experiment in which the temperature is rapidly decreased from above T_c in presence of a field. The system moves rapidly towards lower energy configurations corresponding to zero temperature and thermal effects can thus be disregarded. In this case magnetic flux is already present in the material in the form of initially disordered vortices. Once grain growth has stopped, the system has a polycrystalline structure and an external current can be simulated by simply applying a constant Lorenz force. The critical current is then defined as the current at which vortices start to move steadily.

Simulations show that the critical current for a polycrystal is always larger than the one obtained for a perfect lattice. This reflects the fact that a polycrystalline assembly is more effectively pinned than a perfect lattice because it can accommodate better in the disordered landscape. In addition, we find that the corresponding I-V curve is hysteretic upon ramping up and down the current. This result can explain the difference in transport properties between field cooled and zero field cooled samples and the related hysteresis commonly measured experimentally [103, 130–135].

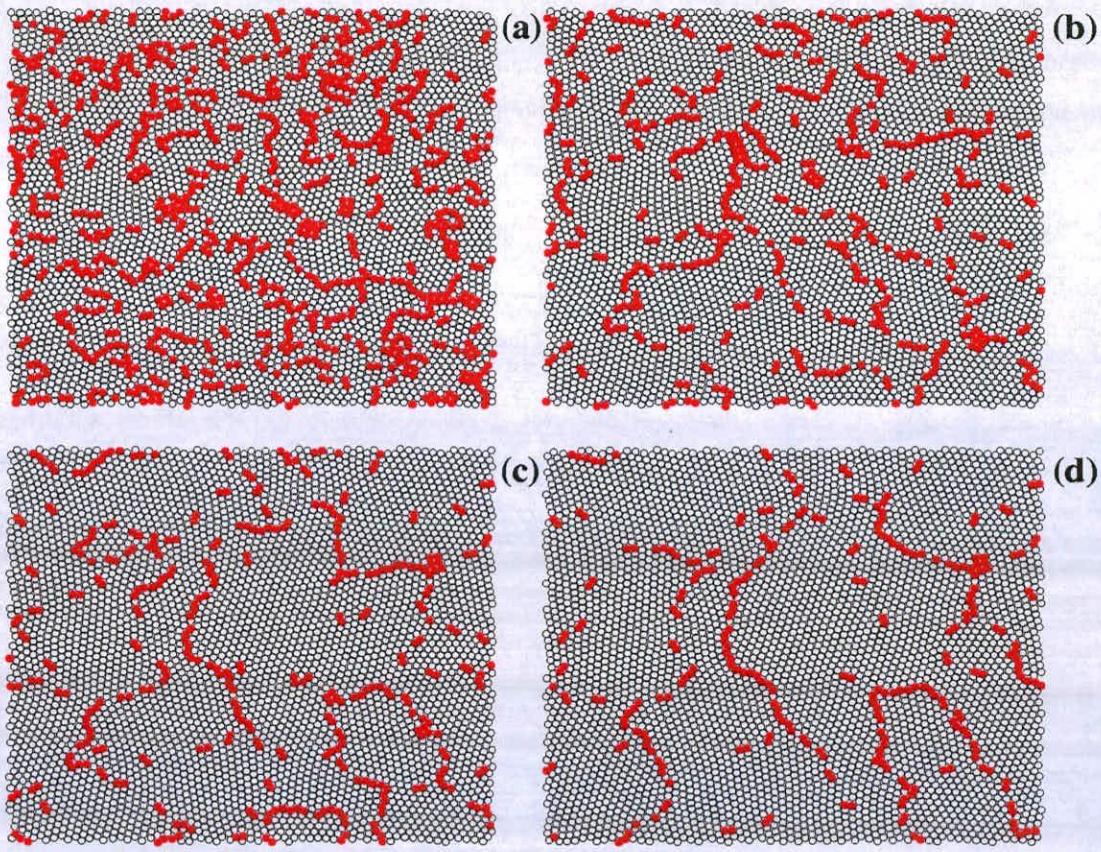

Figure 3.4: *Relaxation of the topological defect structure from a simulation of $N_v = 4128$ interacting vortices after a sudden field cooling from a disordered vortex state in a simulation cell of linear size $L = 36\lambda_{sc}$. The colored five/seven-fold coordinated vortices (filled circles) indicate dislocations in the vortex lattice. The final configuration (snapshot (d)) is completely pinned by disorder. There one can observe a polycrystalline structure with most dislocations arranged into grain boundaries.*

3.4.2 Relaxation of random arrays

Let us first consider the relaxation dynamics of the vortex lines in the absence of driving currents. It is sensible to disregard thermal effects, mimicking the dynamics of the vortex system after a sudden quench of the superconducting sample from high temperatures (or equivalently, random vortex configurations) towards the lower energy states corresponding to zero temperature. After a transient regime, the dynamics stops due to disorder.

The gradual ordering process involves the arrangement of dislocations in grain boundaries (Fig. 3.4). Long range elastic stress fields are screened and the vortex array rearranges into a polycrystal, which evolves in time until the residual stresses accumulated in the distorted vortex lattice drop down below the critical value τ_c. At this point, grain boundaries get pinned by

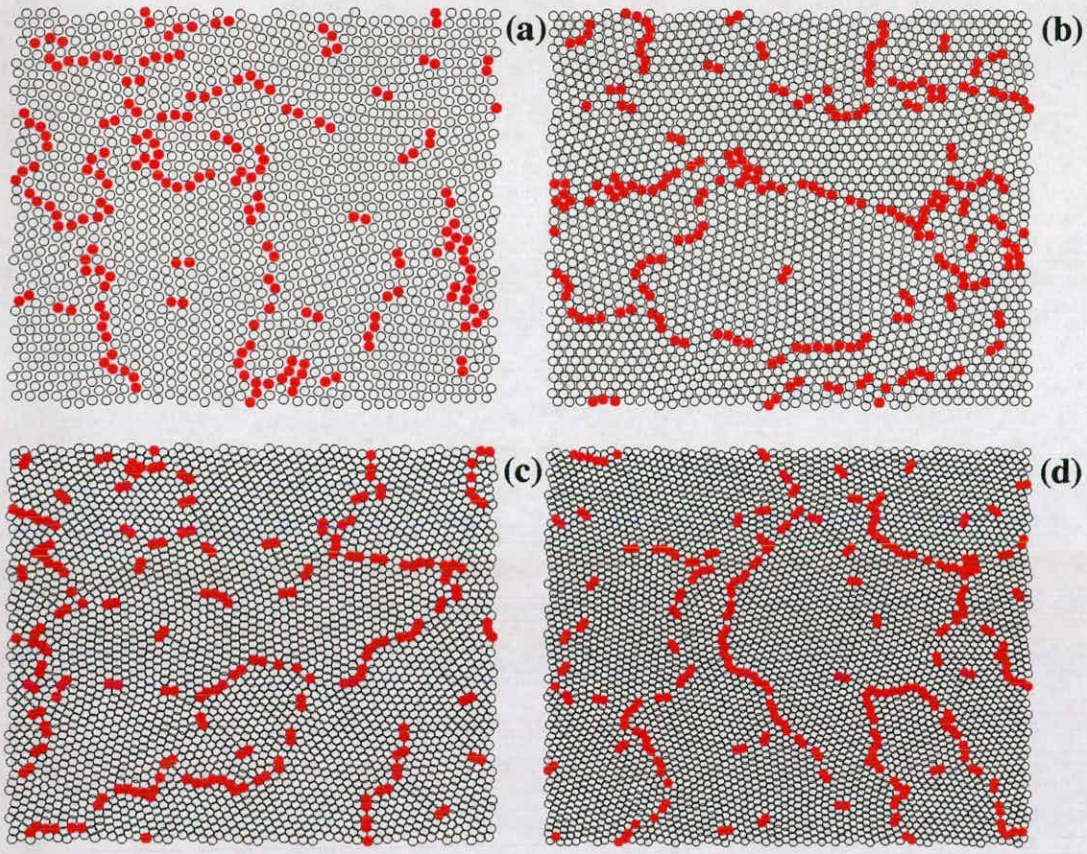

Figure 3.5: *Pinned vortex structure for different values of the magnetic field: (a) $N_v = 1460$, (b) $N_v = 2064$, (c) $N_v = 2919$, (d) $N_v = 4128$, after a sudden field cooling from a disordered vortex state in a simulation cell of linear size $L = 36\lambda_{sc}$. The colored five/seven-fold coordinated vortices (filled circles) indicate dislocations in the vortex lattice. The average grain size in the resulting polycrystalline structure seems to grow with the intensity of the average magnetic field inside the cell.*

disorder limiting the average grain size (see Fig. 3.4(d)). Moreover, the limit grain size R_g/a appears to increase with magnetic field $B \propto N_v$ (see Fig. 3.5), in qualitative agreement with experimental results [108] and confirming the theoretical predictions reported in Section 3.3.3.

3.4.3 Simulated critical current

Once simulations have clarified the mechanism behind polycrystal formation, one can proceed introducing external forces into the system, in order to investigate the behaviour of the critical current $J_c(B)$. An externally applied current may induce the annealing of metastable configurations (see Figs. 3.4 and 3.5), resulting in initial transients of plastic flow, which might eventually cease once a new metastable configuration is found, provided that the current is be-

low the threshold value. As one can observe, for instance, in Fig. 3.6, a small current below the threshold value $J_c(B)$ gives rise to non-trivial changes of the displacement field $\mathbf{u_n}$ of the vortex lattice. This in turn, implies changes of the elastic shear stress distribution responsible for the Peach-Koehler forces acting on grain boundary dislocations that, as a consequence, may move and rearrange in response to the new force field.

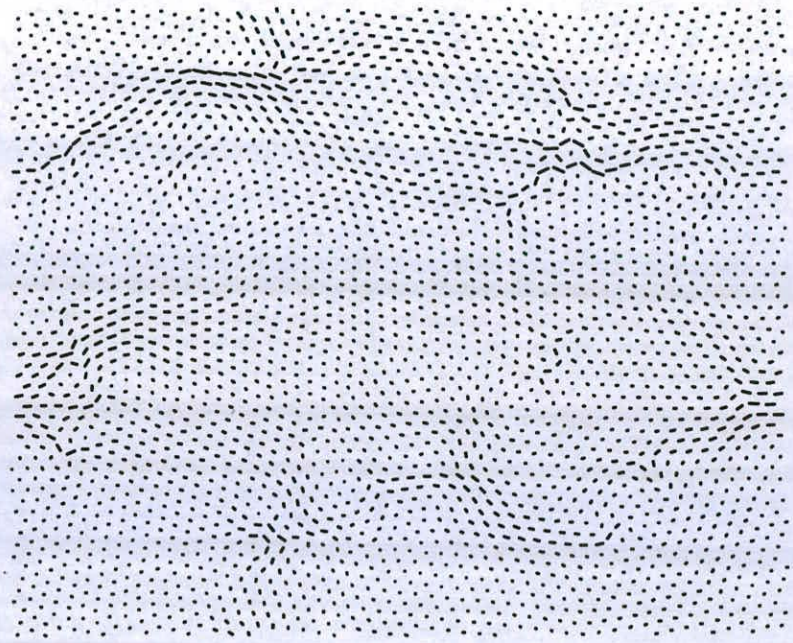

Figure 3.6: *Vortex trajectories between two pinned configurations obtained after the application of a small driving current below the threshold value $J_c(B)$. Small and heterogeneously distributed displacements of the vortex positions are observed in both the parallel and perpendicular direction to the applied force f_L^x. The number of vortices in the simulation cell of linear size $L = 36\lambda_{sc}$ is $N_v = 2919$. The number of pinning points $N_p = 4128$.*

Results for the investigation of the dependence of the critical current on the magnetic field are summarized in Fig. 3.7. Along with the initially polycrystalline arrangement, the study has been also led for a grain boundary-free initial configuration. The qualitative and quantitative differences between the two curves represented in the figure are due to the presence of grain boundaries. The presence of these topological defects in the vortex configuration enhances the critical current needed to give rise to a steady regime of plastic flux flow, that in this case, appears to be controlled by grain boundary motion.

Plastic deformation of crystalline materials is usually mediated by proliferation and motion of dislocations. Nonetheless, another possible mechanism for plastic flow is the glide motion of grain boundaries which, as in this case, can be the most relevant mechanism for small grain

sizes, as in the case of nanocrystals.

According to numerical results, grain boundaries are more efficiently pinned by disorder, as single grains are supposed to adjust better to the disordered landscape than a whole perfectly ordered lattice. In both cases, we observe the decrease of J_c with an increasing magnetic field (i.e. density of vortices) until this reaches a plateau region.

Experiments show that for even higher magnetic fields, the critical current exhibits a sudden increase. Close to the upper critical field $B_{c_2} = \Phi_0/2\pi\xi_{sc}$, the penetration depth λ_{sc} and the coherence length ξ_{sc} are supposed to diverge, and the renormalisation of such parameters is expected to explain that sudden increase [125]. However, the system studied above is far below B_{c_2}, as we are not concerned about the behaviour in the vicinity of that transition.

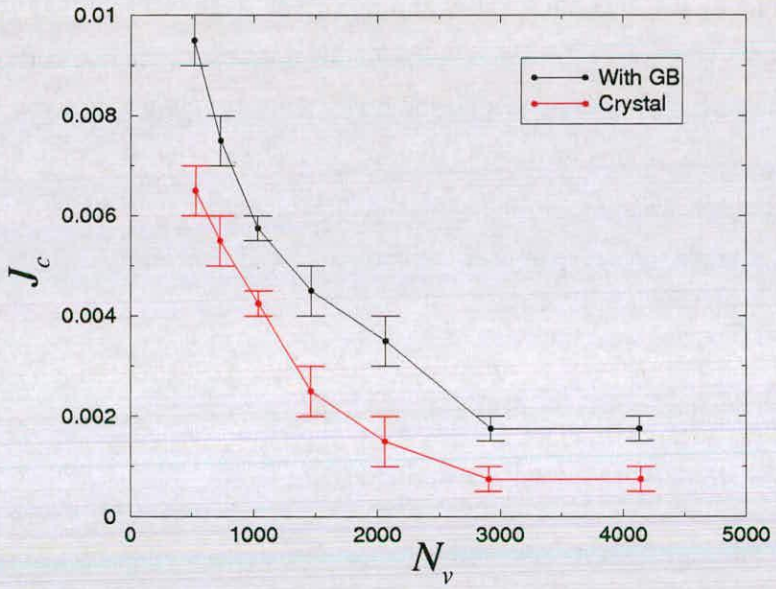

Figure 3.7: *The critical current J_c as a function of the number of vortices N_v in the simulation cell. The number of pinning points is $N_p = 4128$, the cell size $L = 36\lambda_{sc}$. The upper line shows the results obtained starting from initial field-cooled configurations containing grain boundaries (GB), whereas the lower curve shows the numerical results obtained from perfect crystalline initial configurations. Currents are measured in units of Gb^2c/Φ_0.*

3.4.4 Discussion: Hysteresis of the I-V characteristic

Regarding experiments, our results match, at least on a qualitative basis, the behaviour exhibited by vortex matter in critical current measurements at low magnetic fields. As stated above,

grain boundaries are commonly observed in field-cooled (FC) samples. On the other hand, ordered vortex crystals can be obtained in zero field cooling (ZFC) experiments, i.e. applying a magnetic field only after temperature has been lowered to the expected value [103, 130–135]. The FC state is usually characterized by a higher critical current and has been proven to be metastable [131, 133]. These aspects result in a peculiar hysteretic behaviour commonly observed in critical current measurements [131, 133] and $I - V$ characteristics [130, 132]. In our numerical analysis, the evaluation of critical currents in perfect vortex crystals (lower line in Fig. 3.7) fairly mimics the phenomenology of ZFC measurements, while results for the grain boundary model (upper line in Fig. 3.7) can be interpreted as a simulation of FC response. Hysteresis is in fact reproduced by our simulations when we start from the polycrystalline state. As shown in Fig. 3.8, when the current J is ramped up vortices start to move at a current J_{c1}, with a velocity that then increases with the current. If the current is ramped down from the moving state, vortices get pinned at a lower value of the current J_{c2} corresponding to the critical current measured for a perfect crystal upon ramping up the field. Notice the similarity with the experimental results of Refs. [130, 132]. Once more, we should underline that these results hold only for low values of the applied field. As the magnetic induction approaches its critical value, a sudden increase in measured critical currents is observed in both the ZFC and the FC experimental setup [131, 133].

3.5 Grain boundary induced melting

The stability of crystalline order in a vortex lattice beyond the well known Bragg Glass regime is still a matter of investigation. Experimental results suggest that an increase in temperature above a certain critical value T_m determines the transition to a *liquid* phase [98–100], while the effects of disorder associated with high magnetic fields are responsible for the emergence of a *glassy* phase [101–103]. A deep theoretical understanding of such transition phenomena, accounting for their microscopic origin, has not been achieved yet. Nonetheless it has been shown that for strong enough disorder the Bragg glass phase is unstable against dislocation formation [116–118]. This suggests that the melting process could be ruled by topological defects (as discussed in Ref. [120]) in analogy with two dimensional theories of crystal melting. Here we discuss the possibility that, under the effects of fluctuations, dislocations unbind and rearrange in grain boundaries giving rise to a polycrystalline structure [129]. In this framework, the vortex polycrystal can be seen as an intermediate stage in a process that ends in the amorphous

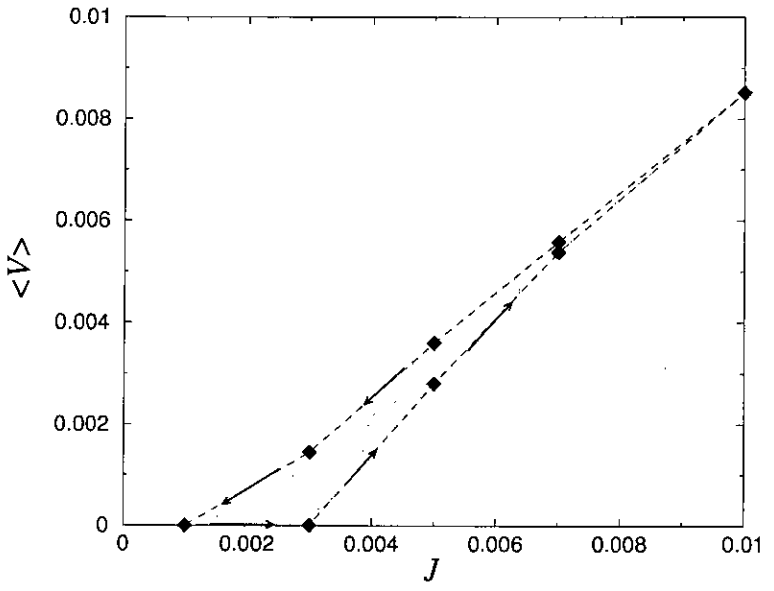

Figure 3.8: *The steady state average velocity of the vortices as a function of the applied current J. The current is ramped up (and down) in steps and is kept constant after each step until the system reaches a steady state. The arrows indicate the direction of the ramp. The number of vortices is $N_v = 2064$, the number of pinning points $N_p = 4128$, the cell size $L = 36\lambda_{sc}$. Currents are measured in units of Gb^2c/Φ_0.*

or liquid phases.

Our purpose is to study the quasi-equilibrium properties of such polycrystalline stage, using the elastic properties of grain boundaries in a vortex lattice derived earlier in this chapter. The main goal of our analysis is to write the free energy density f of the system as a function of different lattice arrangements in configuration space. A minimum in free energy for a polycrystalline configuration in proximity of the melting line would corroborate the hypothesis of a grain boundary mediated transition. For our purposes, we parametrise the configuration space in terms of the linear grain boundary density n, meaning that a $n \to 0$ configuration corresponds to an ordered (grain boundary free) vortex lattice. Our consideration focus on the thermally induced melting transition and the effects of impurities are neglected.

We consider arrays of edge dislocations, parallel to the z axis and arranged in low angle grain boundaries. As in the case of grain growth, all Burgers vectors are in the xy plane, corresponding to a columnar grain structure. Following the aforementioned ideas [129], we can introduce the linear concentration of grain boundaries n and in the low density limit we can expand the free energy functional (per unit volume) in powers of n as

$$f(n) = (\gamma_0 + \gamma_T)\, n + \Gamma\, n^2 - M\, \Gamma\, n^3. \tag{3.31}$$

The different coefficients of the expansion are explained in the following. The linear term is due to the elastic energy of grain boundaries. The zero temperature contribution γ_0 is the elastic energy per unit surface of a flat or smooth grain boundary that, in the limit of low angle grain boundaries, is given by[91]

$$\gamma_0 \simeq \frac{c_{66} b^2}{2\pi D} \ln \frac{e \chi_0 D}{2\pi b}, \tag{3.32}$$

where the $\chi_0 > 0$ factor takes into account core interaction effects. The γ_T term, on the other hand, accounts for thermal fluctuations. Using the elastic Hamiltonian in Equation (3.13), $\mathcal{H} = \int \frac{d^2k}{(2\pi)^2} \phi(\mathbf{k}) X(\mathbf{k}) X(-\mathbf{k})$ with $\phi(\mathbf{k}) = \epsilon |\mathbf{k}|$ and $\epsilon = \pi b^2 K / 2D^2$, the partition function of a thermally perturbed grain boundary over a surface S is

$$\mathcal{Z} = \int \prod_{\mathbf{k}} du_{\mathbf{k}}\, e^{-\beta \phi_{\mathbf{k}} u_{\mathbf{k}}^2} / (K_B T) \tag{3.33}$$

and the corresponding free energy per unit surface is

$$\gamma_T = -\frac{1}{\beta S} \ln \mathcal{Z}\ . \tag{3.34}$$

The above term can be determined explicitly calculating the logarithm of the partition function as

$$\ln \mathcal{Z} = \frac{S}{2} \left[\frac{1}{D a_z} \ln \left(\frac{e^{\frac{3}{2}}}{2\beta\epsilon S \xi^2} \frac{D a_z}{\sqrt{D^2 + a_z^2}} \right) + \frac{1}{D^2} \arctan \frac{D}{a_z} + \frac{1}{a_z^2} \arctan \frac{a_z}{D} \right] \tag{3.35}$$

where we have introduced a short wavelength cutoff $2\pi/a_z$ to delimit the integration domain along the z axis.

The Γ coefficient of the n^2 term is proportional to the energy of a junction between two grain boundaries and details of its computation are given in Appendix A.

The n^3 term captures the case of the intermission of a third grain boundary in a junction, screening the effect introduced by the n^2 contribution. When this is the case, one loses an energy equal to Γn^2 times the probability of such an event. In the low density limit, this probability is Mn, where $M = 2\pi/D$ is roughly the interaction range of a grain boundary [129].

It is convenient to define $\Theta_0 = \ln \mathcal{Z}/S$, so that the free energy functional in Eq. (3.31) can be rewritten as

$$f(n) = K_B\Theta_0 \,(T_m - T)\, n + \Gamma\, n^2 - M\,\Gamma\, n^3, \tag{3.36}$$

defining a melting temperature as $T_m = \dfrac{\gamma_0}{K_B\Theta_0}$. As shown in Fig. 3.9, for values of T close to T_m, $f(n)$ shows a global minimum corresponding to a GB density

$$\frac{1}{R} = \frac{1 + \sqrt{1 + 3K_B\Theta_0(T_m - T)M/\Gamma}}{3M}, \tag{3.37}$$

where R is the average grain size. As discussed above, this suggests the possibility of a poly-

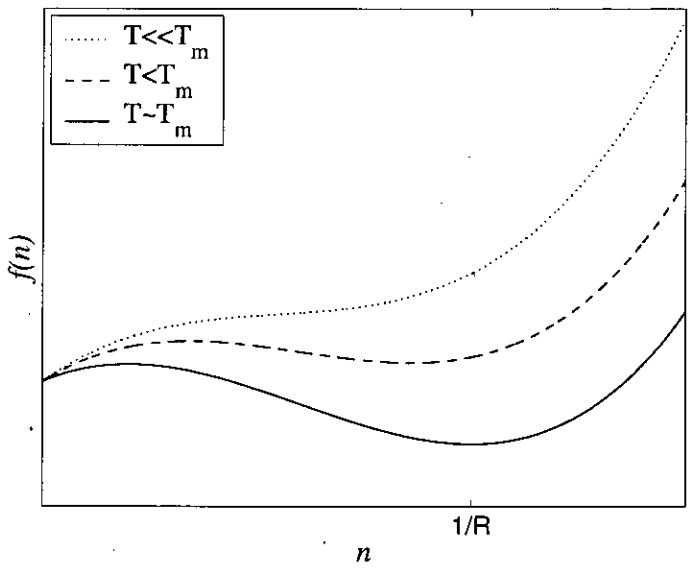

Figure 3.9: *Free energy density as a function of grain boundary density close to thermal melting point.*

crystalline arrangement before the amorphous phase takes over. As soon as T reaches its melting value T_m, the global minimum density becomes of the order of D^{-1}, grains cannot be defined, and the system loses polycrystalline ordering in favor of a liquid-amorphous phase characterized by a typical dislocation spacing of order a.

The considerations above allow us to draw a phase diagram for the vortex array at low applied magnetic fields (i.e. when effects of disorder can be neglected). The resulting plot is shown in Figure 3.10. The melting line is obtained plotting the above temperature T_m as a function of the magnetic induction. Here we use the expression for the local value of c_{66} reported in Ref. [141]. The curve shows reentrant behaviour expected for low fields, due to the exponential decay of the elastic shear modulus in the $B/B_{c_2} \to 0$ limit. The line delimiting lattice and polycrystal phases, instead, is obtained imposing that the free energy minimum shown in Fig. 3.9 is a global minimum. In the presence of disorder, we obviously expect modifications of this schematic phase diagram. Nevertheless, for weak enough disorder (i.e. weak magnetic fields) its main features should remain valid.

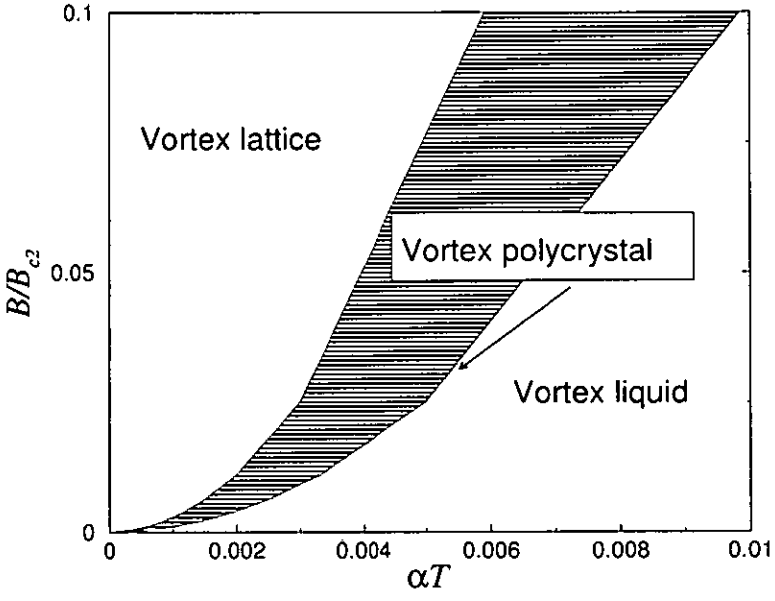

Figure 3.10: *Phase diagram of the vortex ensemble for low values of the reduced field B/B_{c_2}. The temperature is rescaled by the quantity $\alpha = K_B/(\xi_{sc}\epsilon_0)$, where $\epsilon_0 = (\Phi_0)^2/(4\pi\lambda_{sc})^2$ is an energy per unit length along the magnetic field direction, i.e. the typical energy for vortex interactions. The melting line is anticipated by the emergence of a polycrystalline ordering.*

Chapter 4
Fluctuations in continuum crystal plasticity

On mesoscopic length scales, fluctuations induced by the discrete nature of crystal lattice dislocations are averaged out above the scale of a reasonably "small", yet representative volume element. A crystal undergoing deformation is quantitatively described by continuous variables and evolves in terms of plastic flow. Experiments, however, show that plastic flow occurs in a spatially heterogeneous manner and exhibits a pronounced intermittent dynamics (see Chapter 1 and References therein).

The observation of scale invariance in such phenomena suggests a possible approach in the framework of theories of driven elastic media. In this perspective, we propose a generic analytical continuum model which accounts for randomness in the local stress-strain relationships as well as for long-range internal stresses. We show that our system is appropriately described by an elastic manifold characterised by infinite-range elasticity and pushed through a random medium. Mean-field exponents are thus expected for the system, in agreement with experimental observations and numerical predictions.

4.1 Heterogeneity and random stress fluctuations

The rich phenomenology of heterogeneities in plastic flow suggests that the systems evolve within a disordered environment. On typical mesoscopic length scales, disorder is provided by randomness in the arrangements of microstructural defects, such as dislocations, that produce the plastic deformation (see Chapter 1).

In order to provide an appropriate description of the problem we adopt concepts from the dynamics of random media by assuming that the deformation of a given volume element occurs through a random sequence of hardening and softening processes. In other words we define the local flow stress as a fluctuating function of the local strain and regard it as an effective pinning field.

4.2 A continuum model

For our purposes we assume that crystallographic slip occurs on a single slip system only. Dislocations flow into randomly arranged patterns. Randomness introduces fluctuations in the local flow stress which lead to shear strain fluctuations. These, in turn, give rise to long-range stress redistribution which can be expressed in terms of an elastic Green's function. At the same time, dislocation-dislocation correlations give rise to a local back stress which can be expressed in terms of a second-order gradient of strain.

4.2.1 Basic structure

For the single slip system under examination, the plastic distortion tensor is given by $\beta^{\mathrm{p}}(\mathbf{r}) = \gamma(\mathbf{r})\mathbf{n} \otimes \mathbf{s}$ where γ is the shear strain on the slip system, and $\mathbf{n}$ and $\mathbf{s}$ are unit vectors pointing in the direction of the slip plane normal and the slip direction, respectively. In the following we assume without loss of generality that the slip direction corresponds to the x direction of a Cartesian coordinate system and the slip plane is the xz plane. The driving force for plastic flow is the shear stress $\sigma_{xy}(\mathbf{r}) = \tau(\mathbf{r})$ acting in this slip system. For flow to occur, the stress acting in a volume element located at $\mathbf{r}$ must violate the inequality

$$\tau(\mathbf{r}) \leq \tau_{\mathrm{f}}(\mathbf{r}, \gamma(\mathbf{r})) \,. \tag{4.1}$$

Here τ_{f} is the local flow stress, which depends on internal state of the volume element under consideration. It is in general a function of the local strain $\gamma(\mathbf{r})$ and may also depend explicitly on the space coordinate $\mathbf{r}$. The stress $\tau(\mathbf{r}) = \tau_{\mathrm{ext}} + \tau_{\mathrm{int}}(\mathbf{r})$ acting from outside on the considered volume element is a sum of external and long-range internal stresses. The external stress, which acts as an external driving force on the system, is assumed space independent over the region of interest. The space-dependent internal stress field $\tau_{\mathrm{int}}(\mathbf{r})$ is a functional of the (in general spatially non-homogeneous) strain field $\gamma(\mathbf{r})$; it vanishes for a homogeneous deformation state.

If the inequality (4.1) is violated, the local strain $\gamma(\mathbf{r})$ increases quasi-instantaneously until Eq. (4.1) is again satisfied. Impossibility to satisfy this equation implies ductile failure of the system.

4.2.2 Evaluation of long-range internal stresses

We calculate the internal stresses in an infinite three-dimensional body with an arbitrary plastic distortion field $\beta^{\mathrm{p}}(\mathbf{r})$. The external stress is assumed to be zero. (A non-zero external stress simply adds to the internal stresses.) We start out from the elastic equilibrium equation for the components σ_{ij} of the stress tensor:

$$-\partial_j \sigma_{ij} = f_i \ , \tag{4.2}$$

f_i are the body forces and sums are performed over repeated indices. The above equation can be rewritten in terms of the components u_i of the elastic displacement vector as

$$-\partial_j C_{ilkl} \partial_k u_l = f_i, \tag{4.3}$$

where C_{ijkl} are components of Hooke's tensor. The solution of Equation (4.3) has the form

$$u_i(\mathbf{r}) = \int \Gamma_{ik}(\mathbf{r}-\mathbf{r}') f_k(\mathbf{r}') d^3 r' \tag{4.4}$$

where the Fourier transform of the elastic Green's tensor $\Gamma_{ik}(\mathbf{r})$ is $\tilde{\Gamma}_{ik}(\mathbf{k}) = [-C_{ijkl} k_j k_l]^{-1}$.

We now first consider the particular problem of a plastically deformed *inclusion* where the plastic distortion has a constant value β^{p} over a certain volume V and is zero elsewhere. This *inclusion problem* is solved as follows: The volume V is first cut out of the surrounding matrix and deformed plastically in order to produce a stress-free strain β^{p}. To re-insert it into the matrix, interface tractions are applied, such that the original shape is restored. According to Equation (4.2) these interface tractions are

$$f_i = C_{ijkl} \beta^{\mathrm{p}}_{kl} \partial_j H_V(\mathbf{r}), \tag{4.5}$$

where the function $H_V(\mathbf{r})$ is equal to unity within V and zero elsewhere. The volume is then placed in its original position and relaxed. Elastic relaxation proceeds until the tractions produced by the relaxation strain β^{r} balance those given by Equation (4.5). The Fourier transform

of the corresponding displacement field is

$$u_i^r(\mathbf{k}) = i\Gamma_{ik}(\mathbf{k})C_{klmn}\beta^{\mathrm{p}}_{mn}k_l H_V(\mathbf{k}) \; . \tag{4.6}$$

The total elastic distortion is then the sum of the relaxation strain and the initial distortion $-\beta^{\mathrm{p}}_{ij}H_V(\mathbf{r})$ applied to "restore" the original shape before relaxation. The associated total stress reads $\sigma_{ij}(\mathbf{r}) = C_{ijkl}(\beta^{\Gamma}_{kl} - \beta^{\mathrm{p}}_{kl}H_V(\mathbf{r}))$ and its Fourier transform is

$$\sigma_{ij}(\mathbf{k}) = -C_{ijlm}\left(k_m k_o \tilde{\Gamma}_{ln}(\mathbf{k})C_{nopq} + \frac{1}{9}\delta_{lp}\delta_{mq}\right)\beta^{\mathrm{p}}_{pq}H_V \; . \tag{4.7}$$

The angular average

$$\tilde{\Gamma}^0_{ijlm} = \frac{1}{4\pi}\int C_{ijno}[k_o k_q \tilde{\Gamma}_{np}(\mathbf{k})C_{pqlm} + \frac{1}{9}\delta_{ln}\delta_{mo}]d\Omega \tag{4.8}$$

does not depend on the modulus k of the wavevector since $\tilde{\Gamma}_{np}$ scales like k^{-2}. The stress hence can be written as

$$\sigma_{ij}(\mathbf{k}) = [-\tilde{\Gamma}^0_{ijlm} + \tilde{\Gamma}^*(\mathbf{k}/k)]\beta^{\mathrm{p}}_{lm}H_V(\mathbf{k}) \; , \tag{4.9}$$

where the second term is simply defined by $\tilde{\Gamma}^*(\mathbf{k}/k) = C_{ijno}[k_o k_q \tilde{\Gamma}_{np}(\mathbf{k})C_{pqlm} + \frac{1}{9}\delta_{ln}\delta_{mo}] - \tilde{\Gamma}^0_{ijlm}$.

The above procedure can be straightforwardly generalised for an arbitrary distribution of the plastic distortion $\beta^{\mathrm{p}}(\mathbf{r})$ by considering each volume element as a separate *inclusion*. Equation (4.9) becomes

$$\sigma_{ij}(\mathbf{k}) = [-\tilde{\Gamma}^0_{ijlm} + \tilde{\Gamma}^*(\mathbf{k}/k)]\beta^{\mathrm{p}}_{lm}(\mathbf{k}) \tag{4.10}$$

and, in real space,

$$\sigma_{ij}(\mathbf{r}) = -\tilde{\Gamma}^0_{ijlm}\beta^{\mathrm{p}}_{lm}(\mathbf{r}) + \int \Gamma^*(\mathbf{r}-\mathbf{r}')\beta^{\mathrm{p}}_{lm}(\mathbf{r}')d^3r' \; . \tag{4.11}$$

The non-local kernel $\Gamma^*(\mathbf{r}-\mathbf{r}')$ is the inverse Fourier transform of $\tilde{\Gamma}^*(\mathbf{k}/k)$; it scales like $1/r^2$ in two-dimensional space and like $1/r^3$ in three dimensional space and has zero angular average. What has been done so far holds for strain fields that go to zero at infinite distances. If the asymptotic value of the plastic strain assumes a non-zero value $\beta^{\mathrm{p},\infty}$, we have to add the corresponding stress-free strain as follows:

$$\sigma_{ij}(\mathbf{k}) = \tilde{\Gamma}^0_{ijlm}[\beta^{\mathrm{p},\infty}_{lm} - \beta^{\mathrm{p}}_{lm}(\mathbf{r})] + \int \Gamma^*(\mathbf{r}-\mathbf{r}')\beta^{\mathrm{p}}_{lm}(\mathbf{r}')d^3r'. \tag{4.12}$$

For a plastic distortion field which has the *average* value $\langle\beta^{\mathrm{p}}\rangle$, the asymptotic value $\beta^{\mathrm{p},\infty}$ is replaced by the average $\langle\beta^{\mathrm{p}}\rangle$ since the fluctuation contributions average out if integrated over the infinite contour. Hence, the internal stress can be envisaged as the sum of a mean-field contribution and a non-local term with a kernel of zero angular average. For the purpose of a depinning theory built with this type of non-local elastic interaction, one may note that in Fourier space the kernel scales like k^a with $a = 0$, i.e., mean-field theory is expected to be valid in all dimensions.

In the following consider the case where the plastic strain is determined by slip on a single slip system, $\beta^{\mathrm{p}} = \gamma(\mathbf{r})\mathbf{e}_y \otimes \mathbf{e}_x$, and the shear strain γ depends on the x and y coordinates only (such a quasi-two-dimensional model corresponds to a system of straight parallel edge dislocations). In this case, the internal shear stress $\tau_{\mathrm{int}} = \sigma_{xy}$ in Fourier space becomes

$$\tau_{\mathrm{int}}(\mathbf{k}) = -\frac{G}{\pi(1-\nu_P)}\gamma(\mathbf{k})\frac{k_x^2 k_y^2}{|\mathbf{k}|^4}\,, \tag{4.13}$$

and in real space

$$\begin{aligned}\tau_{\mathrm{int}}(\mathbf{r}) &= \frac{G}{2\pi(1-\nu_P)}\int \gamma(\mathbf{r}')\left[\frac{1}{(\mathbf{r}-\mathbf{r}')^2} - \frac{8(x-x')^2(y-y')^2}{(\mathbf{r}-\mathbf{r}')^6}\right]\mathrm{d}^2\mathbf{r}' \\ &+ \frac{G}{4(1-\nu_P)}[\langle\gamma\rangle - \gamma(\mathbf{r})]\,.\end{aligned} \tag{4.14}$$

Here, G is the shear modulus and ν_P the Poisson's ratio. From these expressions, two points may be noted: (i) The elastic kernel is not positively definite in real space. (ii) There exist certain space-dependent strain fluctuations (fluctuations with wavevectors in the x and y direc-

tions) which do not give rise to any long-range internal stresses. The implications of this will be discussed below.

4.2.3 Dislocation-related stresses and internal-stress fluctuations

We now consider the role of the *flow stress* $\tau_{\rm f}(\mathbf{r},\gamma)$, briefly recalling its physical origin. Plastic flow consists, on microscopic scales, in the motion of lattice dislocation lines. In the absence of other defects, dislocations glide through a stress landscape produced by dislocations themselves. The flow stress of a "small" mesoscopic volume is the stress required to push dislocations through the stress landscape within the volume.

The resulting flow stress $\tau_{\rm f} = \delta\tau + \tau_{\rm p}$ can be envisaged as a sum of two contributions [for a more detailed discussion, see References [84, 145–147]]:

(i) A fluctuating stress $\delta\tau(\mathbf{r},\gamma)$. As stated above, spatial fluctuations are given by randomness in dislocation arrangements. At the same time, dislocation glide increases the local strain and modifies the fluctuating stresses within the surrounding mesoscopic volume element. In the absence of detailed information about the individual dislocation positions, we take this evolution of the stress "landscape" into account by introducing a dependence on the local strain γ. Correlation properties of the fluctuation stress are given by

$$\langle \delta\tau(\mathbf{r},\gamma)\rangle = 0 \ , \tag{4.15}$$

$$\langle \delta\tau(\mathbf{r})^2\rangle = K^2 G^2 b^2 \rho(\mathbf{r}) \ , \tag{4.16}$$

$$\langle \delta\tau(\mathbf{r},\gamma)\delta\tau(\mathbf{r}+\mathbf{r}',\gamma+\gamma')\rangle = \langle \delta\tau(\mathbf{r})^2\rangle h(\mathbf{r}'/\xi_\tau) g(\gamma/\gamma_{\rm corr}) \ . \tag{4.17}$$

$K^2 = \ln(\xi_\tau/b)/[8\pi(1-\nu_P)^2]$ is a numerical constant of the order of unity which depends on the elastic properties of the crystal lattice, and logarithmically on the characteristic range $\xi_\tau \approx 1/\sqrt{\rho}$ of dislocation-dislocation correlations. Functions $h(\mathbf{r}'/\xi_\tau)$ and $g(\gamma/\gamma_{\rm corr})$ are dimensionless and characterised by short ranges, respectively $\xi_\tau \approx 1/\sqrt{\rho}$ (see [145]) and $\gamma_{corr} \approx b/\sqrt{\rho}$ (strain produced when all dislocation move by the average dislocation spacing,

see [84]). If $\mathbf{r}'$ is close enough to $\mathbf{r}$, the stress correlator in Equation 4.17 is given essentially by $\langle \delta\tau(\mathbf{r})^2 \rangle$, while for larger distances function h decays rapidly and random stress correlations drop to zero.

(ii) A "back-stress" term, arising from dislocation correlations. Due to long range interactions, small groups of dislocations glide cooperatively, homogenising deformation over the slip plane. This can be seen as the effect of a 'pile-up stress' $\tau_{\mathrm{p}}(\mathbf{r})$ which can be approximated by a second-order gradient of the strain according to

$$\tau_{\mathrm{p}}(\mathbf{r}) = \frac{DG}{\rho}\gamma_{xx} \quad (d=2)\,, \quad \tau_{\mathrm{p}}(\mathbf{r}) = \frac{DG}{\rho}[\gamma_{xx}+\gamma_{zz}] \quad (d=3)\,. \tag{4.18}$$

Here, ρ is the total dislocation density and D a constant of the order of unity [see [146]]. In Eq. (4.18), $d \in [2,3]$ is the dimensionality of the model. The first expression ($d=2$) refers to the special case where deformation is due to the motion of straight edge dislocations in a quasi two-dimensional arrangement, such that the shear strain γ does not depend on the z coordinate.

4.2.4 Plastic flow and elastic manifold depinning

In the light of the above results, one can rewrite Equation 4.1 in the form

$$\tau_{\mathrm{ext}} + \tau_{\mathrm{int}}(\mathbf{r}) + \frac{DG}{\rho}[\gamma_{xx}+\gamma_{yy}] + \delta\tau(\mathbf{r},\gamma) \leq 0. \tag{4.19}$$

The violation of that inequality corresponds to the onset of plastic flow. The asymptotic behaviour of this model for positive external stresses is captured by the equation of motion

$$\frac{1}{B}\partial_t\gamma(\mathbf{r}) = \tau_{\mathrm{ext}} + \tau_{\mathrm{int}}(\mathbf{r}) + \frac{DG}{\rho}[\gamma_{xx}+\gamma_{yy}] + \delta\tau(\mathbf{r},\gamma)\,. \tag{4.20}$$

in the rate-independent limit $B \longrightarrow \infty$.

The analogy with the general problem of depinning is rather straightforward. Formally, Equation (4.20) can be interpreted as describing the overdamped dynamics of an elastic manifold with coordinates $(\gamma, \mathbf{r})$ which moves in the γ-direction through a random medium. In the two-dimensional case where $\gamma = \gamma(x,y)$ depends only on the x and y coordinates ($d=2$),

our model may be considered a continuum approximation of a quasi-two-dimensional system of straight parallel dislocations. If the strain depends on all three spatial coordinates, then the model mimics the large-scale behaviour of a system of three-dimensionally curved dislocations.

In more general terms, the model describes the motion of a d-dimensional elastic manifold through a disordered $(d+1)$-dimensional medium which exerts a fluctuating pinning force $\delta\tau$. Due to the infinite range of the interaction kernel governing the internal stress $\tau_{\text{int}}(\mathbf{r})$, one expects the second-order gradient terms in Equations 4.19 and 4.20 to be irrelevant for the large-scale behaviour, as they scale as $\mathbf{k}^2\gamma(\mathbf{k})$ in Fourier space. It is thus clear, in the light of depinning theories, that the model exhibits mean-field behaviour irrespective of the manifold dimension (see Chapter 1).

The relevance of gradient terms is nonetheless unquestionable from the viewpoint of small-scale morphology, as they break the symmetry existing in the elastic kernel between directions x and y, accounting for slip-line patterns commonly observed in experiments.

4.3 Discussion

In order to assess validity of our theory, numerical simulations of the continuum model detailed above have been performed by our co-workers (see [84]). A lattice automaton model has been implemented, taking into account the two-dimensional case. A generalisation to a three-dimensional approach in is not expected to make any significant difference due to the mean-field behaviour exhibited by the model (see Chapter 1).

Numerical results confirm the validity of our model, allowing us to reproduce several experimental observations and to corroborate the hypothesis of a critical behaviour in a slowly driven non-equilibrium state.

4.3.1 Avalanche dynamics and critical behaviour

In Figure 4.1 a stress-strain curve obtained numerically is reported. Simulated graphs exhibit the typical staircase-like shape observed in experiments (see [148, 149]). At low applied stresses the system becomes pinned in configurations where the fluctuating stress $\delta\tau$ is negative in most volume elements, thereby creating a non-zero average back stress. The increase of plastic strain with increasing stress occurs in discrete *slip avalanches* of varying size. These

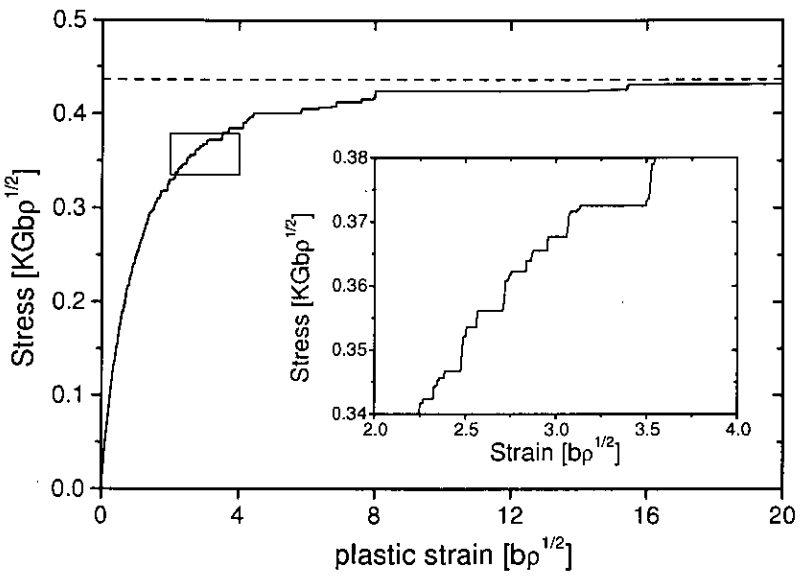

Figure 4.1: *Stress-strain curve as obtained from simulation of a system with 128 × 128 sites; dashed line: critical stress τ_c; Insert: detail of the same stress-strain graph.*

avalanches are visible as steps on the stress-strain curves. The intervals between the larger avalanches divide into avalanches of smaller size, and the characteristic avalanche size diverges as one approaches the yield stress.

The average strain diverges as the stress approaches the yield stress τ_c. A semi-logarithmic plot of γ vs. $\tau_c - \tau_{ext}$ reveals that this divergence is logarithmic in nature (Figure 4.2). The stress susceptibility $\chi = \partial\gamma/\partial\tau_{ext}$ of the plastic strain diverges according to

$$\chi \propto (\tau_c - \tau_{ext})^{-\theta}, \ \theta \approx 1 , \tag{4.21}$$

in line with the expectation for mean-field depinning [16].

Avalanche sizes obey scale free distributions, as in Figure 4.3. The distributions exhibit a power-law decay $p(\Delta E) \propto \Delta E^{-\kappa}$ with $\kappa \approx 1.4$ which is truncated at a characteristic avalanche size ΔE_c. As the stress approaches the critical stress τ_c, this upper limit and hence the average avalanche size diverge. Distributions obtained at different applied stresses τ_{ext} can be collapsed into a single universal distribution if the energy releases are re-scaled by a factor $(1 - \tau_{ext}/\tau_c)^{\nu(d+\zeta)}$ where $\nu(d+\zeta) \approx 2$ (Figure 4.3, right). We therefore expect susceptibility to diverge like $\chi \propto (\tau_c - \tau)^{-\nu(d+\zeta)(2-\kappa)}$. With $\kappa \approx 1.4$, $\zeta \approx 0$ and $\nu \approx 2/d$ we find $\theta \approx 1$ in agreement with Equation (4.21).

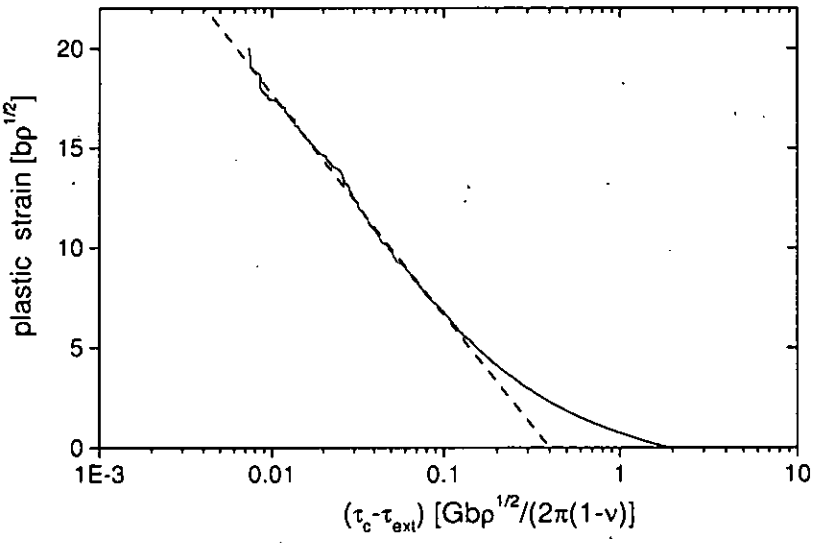

Figure 4.2: *Ensemble-averaged stress-strain graph as obtained by averaging over 60 simulations of systems with 128 × 128 sites. Strain is plotted against distance from the critical stress.*

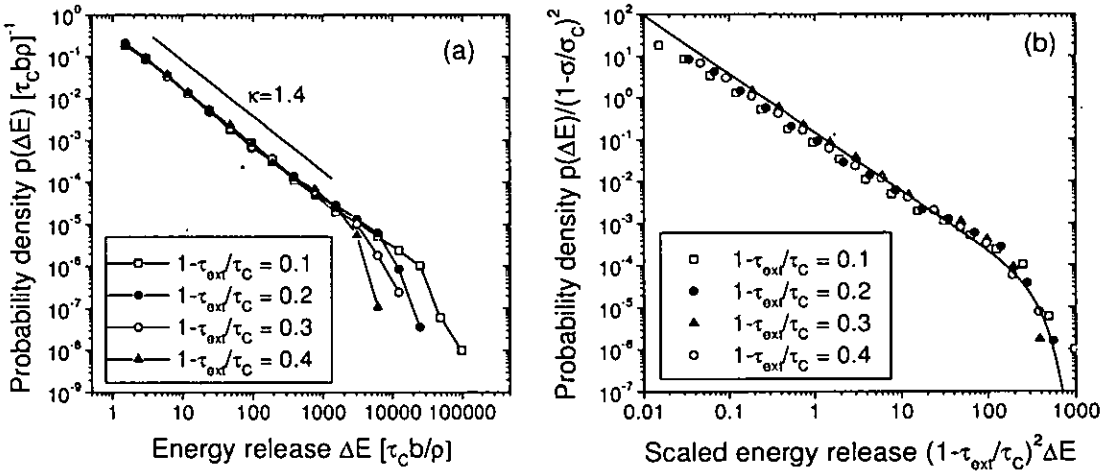

Figure 4.3: *Probability distributions of slip avalanche sizes (probability density $p(\Delta E)$ vs. energy release ΔE) as obtained from an ensemble of systems of size 256×256. Left: distributions corresponding to different stresses; Right: universal distribution obtained by re-scaling $\Delta E \rightarrow \Delta E(1 - \tau_{\mathrm{ext}}/\tau_{\mathrm{c}})^2$; full line: theoretical curve (Equation 4.22).*

The exponents κ, θ, ζ and ν are in good agreement with the hypothesis of mean-field depinning, being the theoretical values $\theta = 1$, $\zeta = 0$, $\nu = 2/d$ and $\kappa = 3/2$ (see e.g. [16, 24]).

Above we have considered avalanche size distributions and energy release distributions as equivalent. This is reasonable, since the total energy release during an event is approximately equal to the product of the applied stress and the strain increment associated with the event (see Reference [1]) and thus proportional to the total slip distance or, equivalently, the avalanche size. Hence, the theoretically predicted energy release distribution for mean-field depinning is

$$p(\Delta E) \propto \Delta E^{-1.5} \exp\left[-\left(\frac{\Delta E}{\Delta E_c}\right)^2\right], \tag{4.22}$$

which again compares well with the results of numerical simulations of our model (Figure 4.3 and Reference [79]).

4.3.2 Influence of hardening

During deformation, the dislocation density often increases with increasing strain, leading to an increase of the stress required to sustain plastic flow (strain hardening). Hardening can be phenomenologically described by a strain dependent "back stress" which is subtracted from the locally acting stress (see e.g. [84]). In the simplest case of linear strain hardening, this stress is given by $\tau_b = -\Theta\gamma$ where Θ is the hardening coefficient.

Our discussions so far, as well as the related simulations, have neglected the effects of hardening. However, it is possible to introduce them in our model and implement them numerically. For a detailed discussion of the problem, the reader may refer to [84]. Here we point out that hardening does not modify the stepwise structure of stress-strain curves, although it suppresses the largest bursts, which in a non-hardening system are supposed to take place close to the critical stress. In other words, hardening tends to hinder the critical behaviour associated with the critical stress, yet leaving many of the scale-invariant properties (such as scale-free avalanche size distributions) basically unchanged.

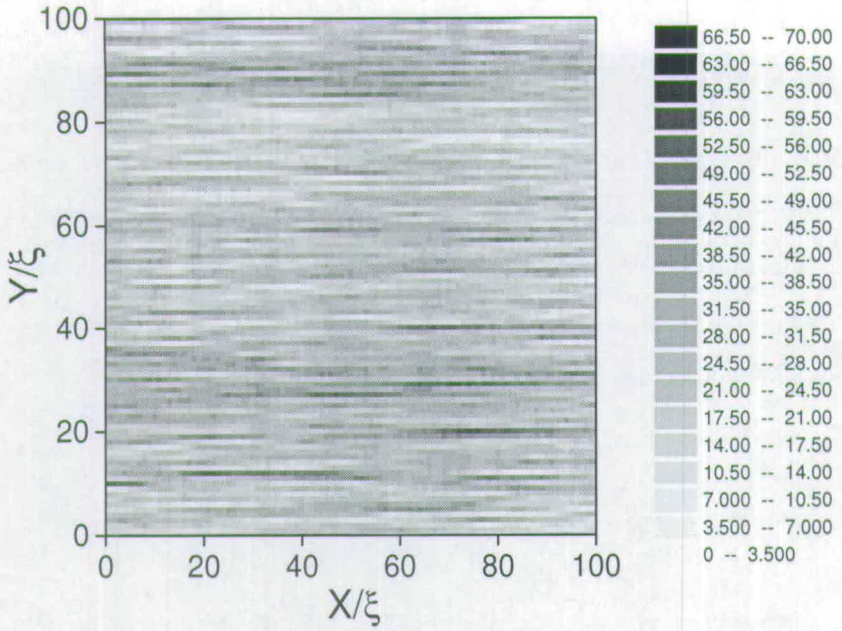

Figure 4.4: *Strain pattern obtained after simulation of a system of size* 256×256 *to an average strain of* $20b\sqrt{\rho}$ *(slip direction from left to right); parameters as in Figure 4.1; greyscale: local strain in units of* $b\sqrt{\rho}$

4.3.3 Slip pattern and surface morphology

Interesting aspects also emerge from the analysis of surface profiles in simulated systems. The observed highly anisotropic strain patterns (see Figure 4.4) with strong correlation along the glide direction and weak coupling in the normal direction are reminiscent of the gradient terms in Equations 4.19 and 4.20. Random fluctuations are weakened along the glide direction by dislocation-dislocation correlations and the model reproduces the experimentally well-known slip anisotropy of deforming crystals.

In more quantitative terms, the roughening of surface profiles can be statistically analysed. Deformation profiles can be calculated by simply integrating strain fluctuations at the surface[1]

$$h(y) = \int_0^y [\gamma(x = 0, y') - \langle\gamma\rangle] \mathrm{d}y' \; . \tag{4.23}$$

Simulated surfaces are self-affine and can be characterised by a strain-independent Hurst exponent $H \approx 0.7$ (see Figure 4.5) whose numerical value is in satisfactory agreement with

[1] Here we tacitly assume that surface effects can be neglected. Near a free surface elastic interactions are, in fact, modified by surface boundary conditions. In the present implementation, however, surface boundary conditions are not taken into account and surface effects can be safely disregarded.

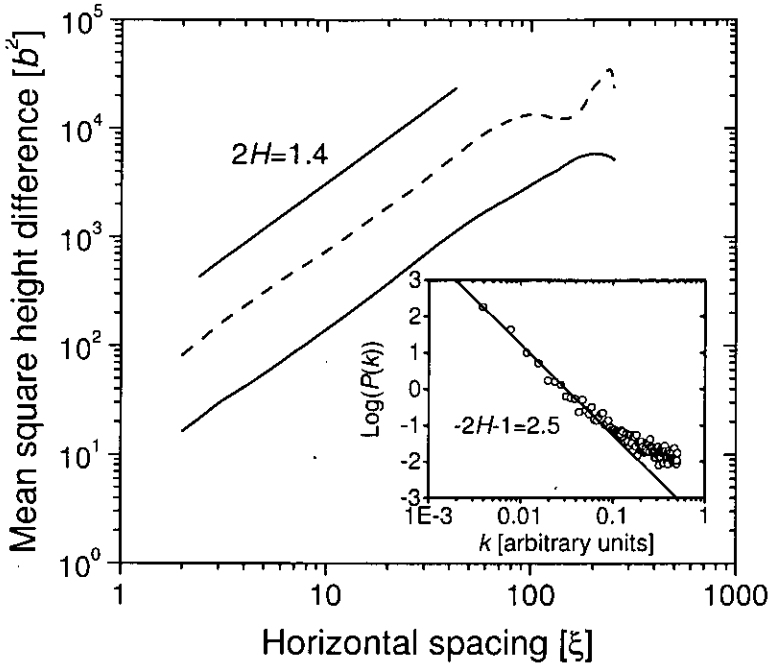

Figure 4.5: *Mean square height difference vs. horizontal distance for surface profiles obtained from a system of size* 512×512 *after simulation to average strains of* $6b\sqrt{\rho}$ *(full line) and* $20b\sqrt{\rho}$ *(dashed line); each graph has been averaged over 10 simulated profiles; insert: average power spectrum obtained from 10 profiles at a strain of* $20b\sqrt{\rho}$

experimental observations (see e.g. Figure 1.4) as well as its strain independence.

4.3.4 Summary

Our simple continuum model captures essential aspects of heterogeneities in plastically deforming metals. By combining a fluctuating local stress-strain relationship with a strain-gradient dependent stress contribution and long-range stresses mediated by the elastic Green's function, the model accounts both for the observed spatial heterogeneities of plastic deformation (slip lines, self-affine surface roughness) and the emergence of "bursts" of plastic activity with a power-law size distribution.

In general terms, our results indicate that fluctuation phenomena in plastic flow of crystalline solids can be envisaged as critical phenomena in driven non-equilibrium systems[2]. However, a crucial difference can be emphasised with respect to ordinary interface depinning problems. In a crystalline solid deforming in single slip, where deformation is restricted to simple shear oc-

[2]An analogous effort has been made in relation with the plasticity of amorphous materials (see [150]).

curring along a single set of planes, the elastic kernel responsible for the long-range interaction is not positively definite. As a consequence, Middleton's *no passing*-theorem (see Chapter 1), ensuring the uniqueness of the depinning threshold, need not hold. Although numerical investigation of the model shows depinning-like behaviour, consequences of this observation remain to be investigated.

Chapter 5
Pinning of interface cracks in slope failure

That of slope failure is a very general problem. The reasons of its interest include implications for glaciology, geology and material science in general. Failure is driven by nucleation and propagation of cracks along the interface between a weak layer (of snow or clay) and the underlying substrate.

We investigate features of slab release introducing spatial heterogeneities (disorder) at the interface with the underlying substrate (see Figure 5.1). Such heterogeneities determine spatial variations in the fracture toughness (a fluctuating pinning field).

These variations affect slope stability and interface failure in two competing ways: (i) If the interface contains a pre-existing shear crack, randomness may lead to crack pinning and thereby enhance slope stability. The pinning of interface cracks is investigated, and the problem is shown to be equivalent to the pinning of a contact line; (ii) Randomness may facilitate crack nucleation and thereby decrease the slope strength. The competition between crack nucleation and propagation is investigated, and it is shown that increasing randomness leads to a cross-over from a failure mode that is controlled by crack propagation to a failure mode that is controlled by the profuse nucleation and coalescence of cracks.

5.1 Slope failure — an overview

Failure may occur either through the propagation of a pre-existing shear crack or by profuse nucleation of multiple flaws. In the former case, the problem is very similar to the problem of shear-band formation in a slope as studied in the work of Palmer and Rice [151]. The criterion for failure by shear band propagation, that was first obtained in that work, has been successfully applied to snow slab avalanches [152]. According to this criterion, for a given load due to the weight of the slope above the plane of shear, the slope starts to slide when the length of the shear band exceeds a critical value.

In real systems, however, one expects significant variations in interface toughness due to the presence of small-scale heterogeneities. In snow slopes, even in an apparently homogeneous snowpack, large fluctuations in the local strength of snow layers have been reported [153]. In the absence of a pre-existing shear crack, such fluctuations facilitate failure by profuse damage nucleation as investigated in the context of snow slab avalanches by Zaiser [83] and Fyffe *et al.* [155].

In the present study we investigate how randomness affects the propagation of an interface crack and demonstrate that increasing randomness leads to a change in failure mode: at small randomness, failure occurs by crack propagation; in this regime, randomness increases slope stability by pinning the crack. If the randomness exceeds a critical value, failure occurs by profuse crack nucleation; in this regime, any further increase of interface heterogeneity deteriorates the stability of the slope.

From the viewpoint of elasticity theory, our system is described by an elastic continuum (the slab) bounded by a rigid substrate (see Figure 5.1). This problem has also been addressed in the past in the different conceptual framework of tribology, in order to explain friction between sliding bodies (see References [36, 37]). It was proven, by statistical considerations, that an elastic body deformed at the interface exhibits non-local elastic behaviour (bulk mediated elasticity) in the short wavelength limit for deformations, under the assumption of large normal loads (see [37]).

Here we address the problem from the point of view of fracture. During crack propagation (see Figure 5.1), shear stresses act on the interface of the slab, causing its deformation. We solve the elastic problem explicitly, deriving the aforementioned crossover between local and non-local elasticity. We show that, in the long wavelength limit, the internal shear stresses acting on the interface are approximated by second order gradients of the shear displacement.

In the presence of disorder, the displacement profile of a crack front at the propagation threshold proves to be self-affine. We demonstrate that a crack front exhibits non-local elastic behaviour and propose a crack front pinning theory in order to explain variations in failure modes.

5.2 Formulation of the model

We consider a clay or snow slope of thickness h (see Figure 5.1). The interface with the bedrock is identified with the plane $z = 0$, the bedrock is considered of infinite stiffness, and the overlying cohesive material is treated as an isotropic linear elastic solid of shear modulus G and Poisson ratio ν_P. The slope is sliding and deforming in the x direction, and the corresponding displacement field in the $z = 0$ plane is denoted by $u(x, y)$. The extension of the slope is assumed much larger than any other characteristic length in the system such that we may neglect boundary effects in the x and y directions.

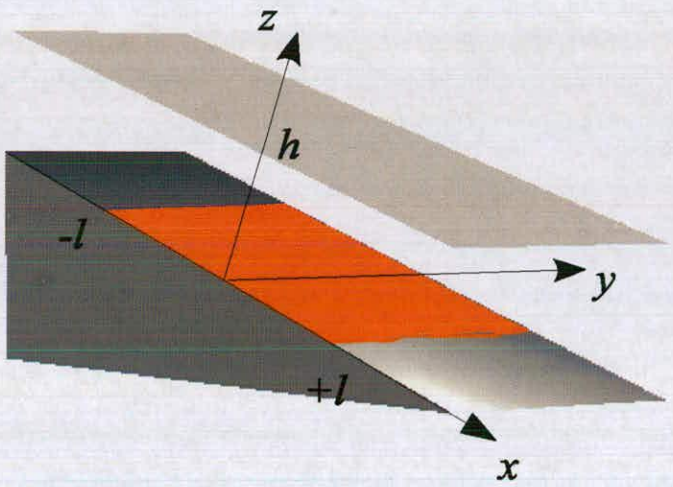

Figure 5.1: *Schematic illustration of our model. A snow or clay slab of thickness h (transparent) is in contact with a stiff bedrock (gray). Shear occurs on the $z = 0$ plane, where a mode-II crack of length $2l$ (orange) propagates (see text below). Spatial fluctuations of the fracture toughness determine roughening of the crack front in $x = +l$.*

The displacement field at the interface produces an internal shear stress distribution τ_{int}. Under the effect of a constant external stress τ_{ext}[1], the slope is stable if the displacement field $u(x, y)$ fulfils the inequality

$$\tau_{int}(u) + \tau_{ext} - \tau_S(u, x, y) \leq 0 \,, \tag{5.1}$$

[1]Since the weight of the slope is the main source of the external stress acting on the slope itself, one has $\tau_{ext} \approx \bar{\rho} g h \sin\vartheta$, where $\bar{\rho}$ is the density of the medium and ϑ is the inclination of the slope. For our purposes, these quantities can be replaced by their average values, over the length and time scales characterising slab release.

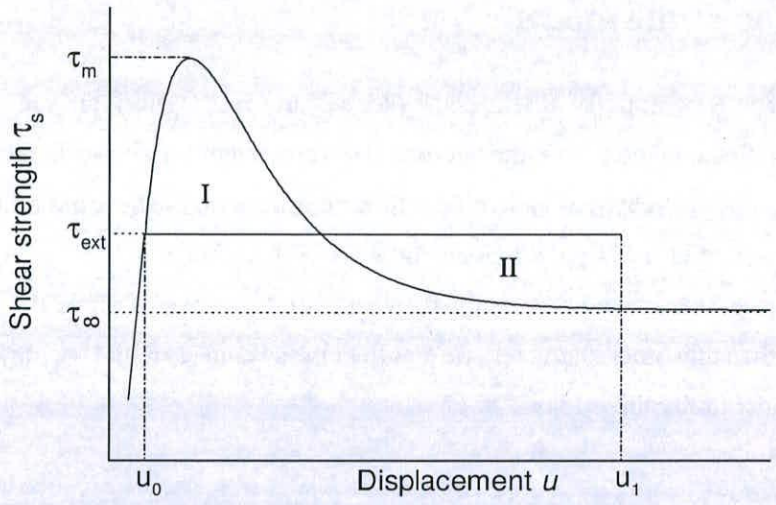

Figure 5.2: *Shear strength versus displacement across weak layer, at a given position (x, y). Areas marked as I and II must be equal, in order to satisfy the "energy conservation" condition described below in the text.*

where $\tau_S(u, x, y)$ is the interface shear strength and, in general, depends on the displacement field $u(x, y)$ and the position along the interface. We assume that the dependence on the shear displacement is characterised by a hardening-softening relationship, as shown schematically in Figure 5.2. The shear strength increases initially towards a peak value τ_m and then drops towards an asymptotic value τ_∞. The spatial dependence of $\tau_S(u, x, y)$, instead, accounts for random heterogeneities at the interface and will be discussed in detail below.

Equation 5.1 is constitutive for our model. In order to get a clearer picture of shear band propagation, we need to evaluate the internal stress distribution $\tau_{int}(u)$ as a function of the displacement field $u(x, y)$. In previous works by Fyffe *et al.* [155] and Zaiser [83] this was done within the framework of a one-dimensional model by using a representation of the internal stress field in terms of interface dislocations. In two dimensions this is not feasible and instead we have to explicitly solve the elasticity problem.

5.2.1 Elastic energy

The elastic energy functional associated with a general displacement vector field $\mathbf{w}(\mathbf{r})$ in an isotropic material can be written as

$$\mathcal{H}(\mathbf{w}) = \frac{G}{2}\int d^3r \left[\left(\frac{2-2\nu_P}{1-2\nu_P}\right)(\nabla\mathbf{w})^2 + (\nabla\times\mathbf{w})^2\right] \tag{5.2}$$

and the associated equilibrium equation is

$$\nabla^2\mathbf{w} + \frac{1}{1-2\nu_P}\nabla(\nabla\mathbf{w}) = 0\,. \tag{5.3}$$

Fluctuations can be introduced by perturbing the elastic medium at the interface. It is convenient to express perturbations in term of their harmonic components $u(k_x, k_y)$, in the form

$$u(x,y) = \int \frac{d^2k}{(2\pi)^2}\, e^{i(k_x x + k_y y)}\, u(k_x,k_y)\,. \tag{5.4}$$

Equation 5.3 can thus be solved in Fourier space, by imposing boundary conditions as $w_x(x,y,0) = u(x,y)$, $w_y(x,y,0) = w_y(x,y,0) = 0$ and allowing a free surface at $z = h$. The problem of an elastic body bounded by a plane has been solved by adopting several diverse methods. Here we follow the procedure due to Boussinesq (see [156] and reference therein).

Let us first introduce the vector $\mathbf{w}_0$ which solves the harmonic problem $\nabla\mathbf{w}_0(\mathbf{r}) = 0$. The expression for w_0 can be easily obtained by simple integration of the differential problem, leading to

$$\mathbf{w}_0 = \int \frac{d^2k}{(2\pi)^2}\begin{pmatrix}1\\0\\0\end{pmatrix}\exp\left[i(k_x x + k_y y) - (k_x^2+k_y^2)^{1/2} z\right]\, u(k_x,k_y)\,. \tag{5.5}$$

Under the assumption of large normal loads, the approximation $\mathbf{w} \approx \mathbf{w}_0$ is often made (see e.g. [37]). However, that may not hold in general and does not apply to our case in particular[2]. By applying results for the theory of Potential [156] to our systems we find an expression for the exact solution $\mathbf{w}$ in the form

[2] In fact, the solution we will adopt in the next sections is exactly the solution of the harmonic problem. However, the reason for that approximation is to be found in the long wavelength assumption instead, as we will show soon.

$$\mathbf{w} = \int \frac{d^2k}{(2\pi)^2} \begin{pmatrix} 1 - \eta z \frac{k_x^2}{(k_x^2+k_y^2)^{1/2}} \\ -\eta z \frac{k_x k_y}{(k_x^2+k_y^2)^{1/2}} \\ -i\eta z\, k_x \end{pmatrix} \exp\left[i(k_x x + k_y y) - (k_x^2 + k_y^2)^{1/2} z\right] u(k_x, k_y) \quad (5.6)$$

where $\eta = 1/(3 - 4\nu_P)$. Comparing this result to the solution of the harmonic problem is quite instructive. One may notice two main aspects: (i) deformation along the normal direction grows linearly close to the interface until it is suppressed by an exponential decay; (ii) although there is no deformation in the y and z directions at the interface, those components are in general non-zero within the bulk. However, they act as higher-order corrections and can be disregarded in the $|kh| \ll 1$ limit, corresponding to the approximation of long wavelengths (or, equivalently, small thickness h of the slab).

Once the assumption $\mathbf{w} \approx \mathbf{w}_0$ has been put in the right perspective, the elastic energy functional can be rewritten as

$$\mathcal{H}(w_x) = \frac{G}{2} \int d^3r \left[\alpha(\partial_x w_x)^2 + (\partial_y w_x)^2 + (\partial_z x_x)^2\right] , \quad (5.7)$$

where $\alpha = (2 - 2\nu_P)/(1 - 2\nu_P)$. In order to express the above energy as a functional of the displacement at the interface, we replace $\mathbf{w}_x$ with the expression found for long wavelengths and, defining Dirac's delta function as

$$(2\pi)^2 \delta(k_x, k_y) = \int dx \int dy \, \exp[i(k_x x + k_y y)] , \quad (5.8)$$

we obtain

$$\mathcal{H}(u) = \frac{G}{2} \int \frac{d^2k}{(2\pi)^2} \left[\alpha k_x^2 + k_y^2 + \frac{1 - e^{-2h(k_x^2+k_y^2)^{1/2}}}{2(k_x^2 + k_y^2)^{1/2}}\right] \times 2h u(k_x, k_y) u(-k_x, -k_y) . \quad (5.9)$$

In the limit of large thickness h of the slab, we recover the approximate result of non-local bulk elasticity [37]. In our case, however, we are interested in the opposite limit $|kh| \ll 1$. Up to

the lowest order the functional reads

$$\mathcal{H}(u) = Gh \int \frac{d^2k}{(2\pi)^2} \left[\left(\frac{1+\alpha}{2} \right) k_x^2 + k_y^2 \right] u(k_x, k_y) u(-k_x, -k_y) \tag{5.10}$$

and reverting to spatial coordinates we find the energy functional

$$\mathcal{H}(u) = Gh \int dx \int dy \left[\left(\frac{1+\alpha}{2} \right) (\partial_x u)^2 + (\partial_y u)^2 \right] . \tag{5.11}$$

5.2.2 Shear stress

To determine the internal shear stress $\tau_{int}(x, y)$ acting on the $z = 0$ interface, we note that the elastic energy must equal the work that has to be expended against the shear stress in order to create the displacement field $u(x, y)$ from an initially displacement-free configuration:

$$\mathcal{H}(u) = \int dx \int dy \left[\int_0^{u(x,y)} \tau_{int}\, du \right] . \tag{5.12}$$

Equating the expressions for $\mathcal{H}(u)$ given in Equations 5.11 and 5.12 and taking on both sides the functional derivative with respect to $u(x, y)$ finally yields

$$\tau_{int} = I_{II} \partial_x^2 u + I_{III} \partial_y^2 u \tag{5.13}$$

where the gradient coefficients relate to mode-II and mode-III crack propagation (see below) and are given by $I_{II} = (1+\alpha)hG$ and $I_{III} = 2hG$. For pure mode-III loading (u is a function of the y coordinate only), Equation5.13 reduces to an expression obtained by Fyffe *et al.* [155] and Zaiser [154] from a completely different line of reasoning.

The constitutive law in Equation 5.1 becomes

$$I_{II} \partial_x^2 u + I_{III} \partial_y^2 u + \tau_{ext} - \tau_S \leq 0 , \tag{5.14}$$

In the following, we consider rate-independent behaviour, i.e., once Equation 5.14 is vio-

lated at some location (x, y), the displacement field $u(x, y)$ increases and re-arranges quasi-instantaneously into a new stable configuration. If no stable configuration is found, u increases indefinitely and the slope fails.

5.3 Shear band profile and crack pinning

The profile of a shear band is obtained by solving Equation 5.14. Let us first neglect disorder, assuming that the shear strength τ_S depends only on the displacement field u, and consider a mode-II crack along the interface. Such a crack is characterised by a displacement field $u(x)$ which is homogenous in the y direction. In the absence of spatial heterogeneities, the displacement field is supposed to start from a value u_0 at $x \rightarrow -\infty$, reach a maximum value u_1 at, let us assume, $x = 0$ and revert to the asymptotic value u_0 in the limit $x \rightarrow +\infty$.

5.3.1 Force acting on a crack

In quantitative terms, the displacement field of a critical mode-II crack satisfies

$$I_{II}\partial_x^2 u + \tau_{ext} - \tau_S(u) = 0 \; . \tag{5.15}$$

Equations of this type have been studied in the context of shear and slip bands in metals plasticity [157, 158]. By analogy, they can be envisaged as describing the un-damped motion of a charged particle of mass I_{II}. Energy conservation therefore implies

$$\int_{u_0}^{u_1} [\tau_{ext} - \tau_S(u)]\, du = 0 \; , \tag{5.16}$$

which means that the areas I and II highlighted in Figure 5.2 must be equal. Approximate solutions of Equation 5.15 can be found in this case applying the appropriate boundary conditions. Assuming that the length $2l$ of the crack is large in comparison with that of the end region where the shear strength is larger than the asymptotic value τ_∞ (see Figure 5.2), one obtains the displacement

$$u_s(x) = \frac{(l^2 - x^2)(\tau_{ext} - \tau_\infty)}{2I_{II}} \; , \tag{5.17}$$

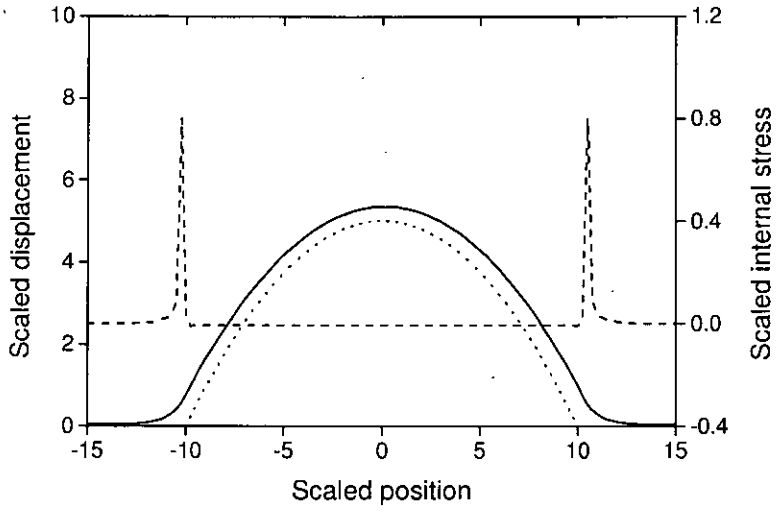

Figure 5.3: *A shear band of scaled length $L = 10$. Full line: displacement profile as a qualitative solution of Equation 5.15. Displacement crosses over to its asymptotic value. Dotted line: parabolic approximation. Dashed line: internal shear stress profile. The strength reaches a constant value (τ_∞ in the text) over most of the crack length. See also [90].*

where we have required the solution to be symmetrical around the origin and imposed $u_0 = 0$, without loss of generality. The parabolic solution is meaningful in the region between $x = -l$ and $x = l$. Close to $x = \pm l$ the displacement smoothly crosses over to the asymptotic value $u_0 = 0$ (see Figure 5.3).

We can assume that u_1 is much larger than the the value u^* where the descending branch of $\tau_s(u)$ crosses the value τ_{ext} in Figure 5.2. Hence, the equal-area condition in Equation 5.16 can be fulfilled only if $\tau_{ext} - \tau_\infty \ll \tau_m - \tau_\infty$. We define $\bar{u}$ such that the area I in Figure 5.2 can be approximated by

$$\int_{u_0}^{\infty} [\tau_S(u) - \tau_\infty] du = (\tau_m - \tau_\infty)\bar{u} \,, \tag{5.18}$$

while the area II can be approximated by $(\tau_{ext} - \tau_\infty)u_1$. Thus, using the expression for u_s at $x = 0$, the equal-area condition for a marginally stable crack becomes

$$\frac{l^2(\tau_{ext} - \tau_\infty)^2}{2I_{II}} = (\tau_m - \tau_\infty)\bar{u} \,. \tag{5.19}$$

This equation can be envisaged as a Griffith-like energy balance criterion. The term on the left-hand side is the force per unit length $F(\tau_{ext}, 2l)$ acting on the crack of length $2l$, as a result of the external stress τ_{ext}, while the right-hand side is an interface toughness. The critical force F_c acting on the crack at failure is defined as the value of $F(\tau_{ext}, 2l)$ which fulfills the condition in Equation 5.19. In terms of energies, the left-hand side in Equation 5.19 can be envisaged as the elastic energy density released as the crack advances by a unit amount, while the right-hand side is the work (density) which has to be done to reduce the interface strength as the the crack advances by a unit amount. Crack propagation occurs when the effective force overcomes the interface toughness by exceeding the critical value or, similarly, when the elastic energy release exceeds the work required to reduce the strength of the interface.

5.3.2 The effect of disorder

Disorder is introduced in this model by allowing the shear strength τ_S to fluctuate, as a result of spatial heterogeneities at the interface. This is expected to perturb the solution for the displacement field derived above and to affect failure.

In order to allow random variations in the interface toughness within our model, we consider the peak strength τ_m in Figure 5.2 as a random function of space. Such strength fluctuations act as a pinning field perturbing the crack front, and the variance $\sqrt{\langle \tau_m^2 \rangle}$ determines the typical pinning force.

The idea of crack front pinning is suggested by numerical results obtained by our co-workers in implementing the analytical model described above (see [90]). These results are briefly summarised below.

5.3.3 Critical stress and profile roughness

Introducing randomness in the system affects the critical behaviour of the system. Average failure stresses of systems containing cracks of different width are plotted in Figure 5.4, as functions of the relative variance

$$\sigma_M = \frac{\langle \tau_m^2 \rangle - \langle \tau_m \rangle^2}{\langle \tau_m \rangle^2} \,. \tag{5.20}$$

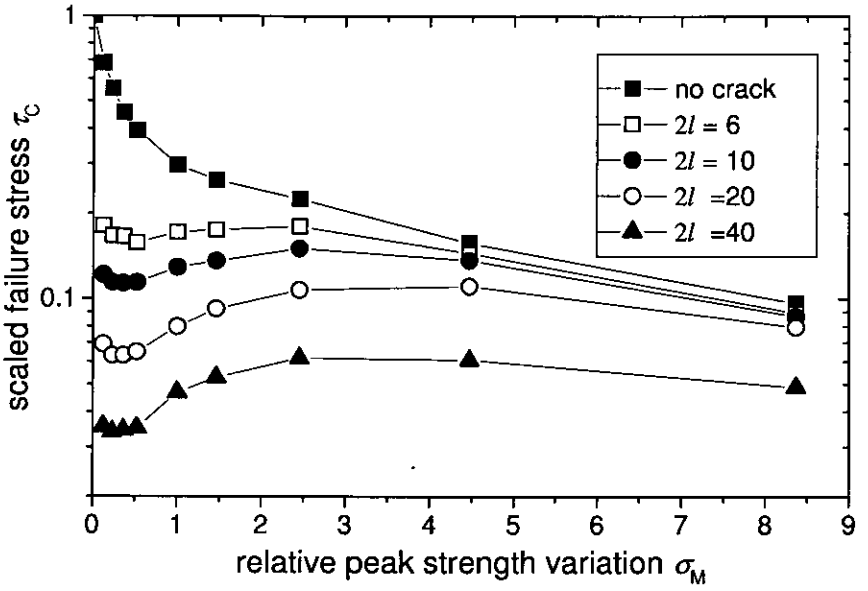

Figure 5.4: *Slope failure stress as a function of peak strength variance.*

For a system without cracks, the failure stress decreases monotonically with increasing peak strength variance since the presence of weak sites facilitates crack nucleation. In the presence of a crack, this behaviour changes. For small degrees of randomness, the behaviour of the system is governed by the propagation of the existing crack. This leads to a failure stress which decreases with increasing crack width but tends to increase with increasing peak strength variance.

This increase is attributed to crack front pinning. At large values of σ_M, we observe a crossover to a decreasing failure stress which is approximately the same as for an initially crack-free system. This crossover corresponds to a change in failure mode; failure in this regime occurs by profuse crack nucleation at particularly weak sites and by crack coalescence, rather than by propagation of the existing crack.

In line with the observation of pinning behaviour, crack fronts assume an irregular shape as the stress approaches the critical stress for crack propagation. The crack profile becomes self-affine. The roughness exponent from the simulated crack profiles can be derived using the Wavelet transform method [159]. The numerical analysis performed on our simulated profiles leads to a roughness exponent $\zeta = 0.28$ [90].

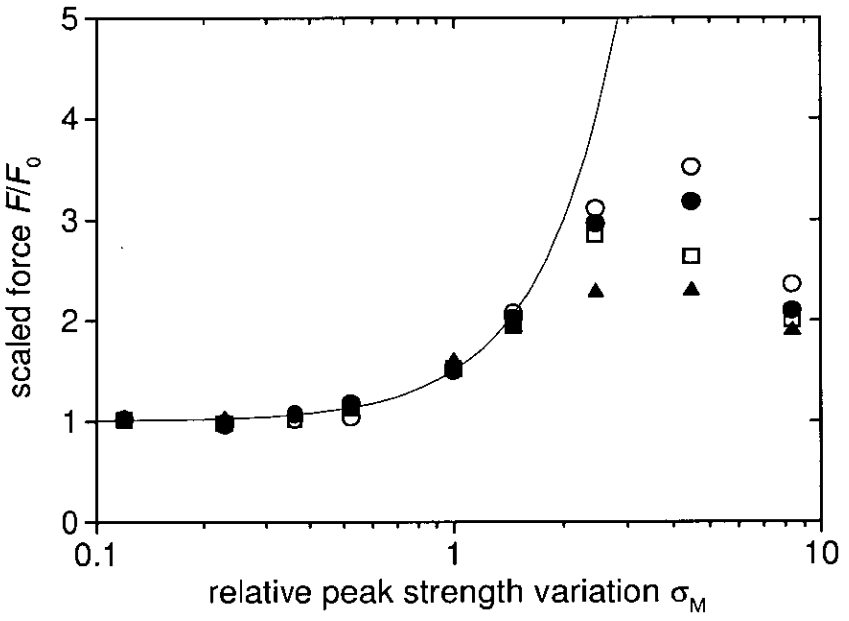

Figure 5.5: *Critical force acting on the crack at failure, normalised by the critical force in a homogeneous system. Symbols as in Figure 5.4. Full line:* $F/F_0 = 0.5\sigma_M$.

5.3.4 Critical force for crack propagation

In a system with increased randomness the crack is able to advance further before failure occurs. Figure 5.5 shows that below $\sigma_M \approx 3$ the critical force for crack propagation F_c increases significantly with increasing degree of randomness, corroborating the hypothesis of crack pinning.

The increase in strength follows a universal curve. Independent of the initial crack width, the critical force (normalised by the critical force for a homogenous system F_0) increases like $F_c/F_0 \approx 0.5\sigma_M$ (full line). For wide cracks, the crack pinning outweighs the force increase due to the widening of the crack, and therefore the overall stability of the slope increases in this regime. At larger values of σ_M, the behaviour becomes non-universal as the critical force reaches a maximum and then apparently decreases. This apparent decrease is due to the fact that in this regime the initial crack gets so strongly pinned that ultimate failure occurs by nucleation and coalescence of cracks at other locations.

5.3.5 A pinning theory

The rich phenomenology shown above corroborates the hypothesis of pinned behaviour of cracks. At the same time, self-affinity and universality suggest, once again, that criticality of our system can be explained in terms of non-equilibrium theories. The observed roughness exponent is close to the value $\zeta = 1/3$ expected for instance for a solid-liquid contact line at the depinning threshold.

A pinning theory for interface cracks can be formulated thanks to simple considerations. The behaviour of the crack front in the presence of disorder is governed by three competing effects: (i) disorder tends to corrugate the crack front, as areas of reduced strength allow the crack front to advance, thereby causing a decrease in total energy of the system (ii) this is counteracted by the elasticity of the system which tends to keep the crack front straight (iii) the external stress leads to an effective force acting on the crack front which tends to move it forward.

The terms of the problem are the same as the ones encountered while studying, for instance, depinning of linear dislocation arrays (see Chapter 2). However, the physics of the problem under examination is different. The external force acting on the crack and driving depinning is the $F(\tau_{ext}, 2l)$ term determined above.

Crack Elasticity

To assess the elastic response of the system, we assume that the crack front in $x = l$ exhibits harmonic perturbations. The solution of the differential problem in Equation 5.14 has the form

$$u(x, y) = u_s(x) + \Delta u(x, y) \ , \tag{5.21}$$

where $u_s(x)$ is the displacement field of a linear crack derived above and perturbations $\Delta u(x, y)$ must fulfill the boundary conditions

$$\Delta u(l, y) = \int \frac{dk_y}{2\pi} e^{ik_y y} \epsilon(k_y) \ . \tag{5.22}$$

By integrating the differential problem, we find

$$u(x,y) = u_s(x) + \int \frac{dk_y}{2\pi} \exp\left[ik_y y + \sqrt{\frac{I_{III}}{I_{II}}} k_y (l-x)\right] \epsilon(k_y) \,. \tag{5.23}$$

However, here we are interested in the energy variations ΔE introduced by disorder. Hence, the u_s term can be ignored, as it gives no contribution to fluctuations. We calculate variations in the elastic energy replacing Δu in Equation 5.12, i.e. defining $\Delta E(\Delta u) \equiv \mathcal{H}(\Delta u)$, and obtain the expected result

$$\Delta E[\Delta u(k_y)] \approx \frac{1}{2} \int \sqrt{I_{II} I_{III}} |k_y| \epsilon^2(k_y) dk_y \,, \tag{5.24}$$

that is, non-local elasticity for a perturbed interface crack.

Depinning and increase in the critical force

The above result allows us to locate crack front pinning in the same universality class as, for instance, linear dislocation arrays (see Chapter 2) and contact lines [160].

Given the nature of the problem, an estimate of the critical force due to pinning can be given in terms of competition between elasticity and disorder, by exploiting the well known Larkin-type argument introduced in Chapter 1. A similar problem has been addressed in the past (see Reference [93]) in terms of crack trapping by periodic arrays of obstacles in brittle solids. Here we consider the more general problem of a random distribution of pinning centres and apply its results to the shear crack model introduced above.

The average pinning force fluctuation per unit length, perceived by a crack front segment of length $L > \xi_p$ is

$$f_p(L) = \sqrt{\langle \tau_m^2 \rangle \bar{u}^2 \frac{\xi_p}{L}} \,, \tag{5.25}$$

where ξ_p is the characteristic range of the fluctuating force. The elastic energy associated with bulging a crack front segment of length L over the distance ξ_p is of the order of

$$\Delta E \approx \frac{I}{2} \epsilon^2 \approx \xi_p^2 l^2 \frac{(\tau_{ext} - \tau_\infty)^2}{2I} \,, \tag{5.26}$$

where ϵ approximately relates to the oscillation amplitude of the crack front by $\epsilon \approx \xi_p \, \partial_x u_s|_{x=l} \approx \xi_p \, l(\tau_{ext} - \tau_\infty)/I_{II}$ and the approximation $I \sim I_{II} \sim I_{III}$ is introduced. The associated elastic force acting on a segment of length L follows as

$$F_{el} = \xi_p \, l^2 \frac{(\tau_{ext} - \tau_\infty)^2}{2I} \, . \tag{5.27}$$

By equating elasticity and disorder at a length $L = L_c$

$$f_p(L_c) L_c = \Delta E \tag{5.28}$$

we obtain the pinning length L_c

$$L_c = \frac{\xi_p \, l^4 (\tau_{ext} - \tau_\infty)^4}{I^2 \langle \tau_m^2 \rangle \bar{u}^2} \approx 4 \xi_p \frac{(\tau_m - \tau_\infty)^2}{\langle \tau_m^2 \rangle} \, , \tag{5.29}$$

where we made the assumption that fluctuations are weak such that Equation 5.19 still holds. The depinning force ΔF_c is obtained by replacing L_c in f_p. In this model, the depinning force is not the critical force for crack propagation. It is, instead, the increase in critical force produced by disorder (see Figure 5.5). It is easy to see that

$$\Delta F_c \propto \sigma_M^2 \, . \tag{5.30}$$

This result is in remarkably good agreement with simulation results, as shown in Figure 5.5.

5.4 A generalisation of the theoretical approach

In the theoretical model presented at the beginning of the present chapter, several assumptions have been made in order to ensure solvability of the main elastic problem. Certainly, the hypothesis of long wavelength deformations is reasonable since we are have to bear in mind that we are dealing with a macroscopic system and the length scales involved, as well as time scales, allow us to make such an assumption rather safely.

A possible improvement consists in formulating a similar problem in a slightly different geom-

etry. So far we have considered gliding motion of an elastic slide (a slab) on a rigid substrate (the bedrock). However, we can consider the case of the formation of a weak layer within the elastic continuum, resulting in the glide motion of an elastic slab on another, with random fluctuation at the interface. Deformations in this case would be given by the relative displacement of the two media at the contact surfaces. In other words, a further complication would arise from the necessity to know the elastic displacements of two media instead of one as before. The medium on the top, however, behaves as the single slab considered above, since one of the two surfaces is still free.

Instead, trying to describe what happens to the underlying elastic medium may appear less straightforward, since neither of its surfaces is left free. In mathematical terms, one has to solve the elastic problem 5.3, imposing boundary conditions on both surfaces, as displacement at the contact surface with the bedrock is supposed to vanish. This is known in elasticity theory as the problem of a body bounded by two parallel planes and has been given attention in the past (for a review, see [156] and references therein). Solutions have been found in different forms. However they are given in the form of very general expansions, which may not be the best choice in our case, where we seek for Fourier components of deformation.

We found a general solution of this problem using the method of the Fourier transform, basing our procedure on the early work of Tedone [161]. For the sake of completeness, we report our work on this topic in Appendix B, focusing on the method of integration, as results do not differ from the ones obtained for a body bounded by one plane.

Conclusions

We investigated properties and implications of the interplay between elasticity and disorder in various physical systems undergoing plastic deformation. Independent of the length scale considered, order is constantly perturbed by fluctuations arising from the atomistic nature of matter on small scales or spatial heterogeneities in macroscopic continua. The competition between elastic behaviour and disorder introduced by random fluctuations is expected to rule equilibrium properties and drive dynamic response of a wealth of deforming systems which are amenable to an elastic description. These aspects have been thoroughly investigated in the past in the conceptual framework of pinning theories.

We performed a theoretical analysis of elastic properties in disordered materials on different length scales and proposed an interpretation of their behaviour in terms of pinning and collective transport in random media. Our aim was to emphasise how several aspects of statics and dynamics can be, sometimes easily, explained by balancing fluctuations which produce disorder and elastic forces which tend to restore order.

On microscopic scales, we investigated the dynamics of microstructure defects, such as dislocations and dislocation arrays, which are responsible for plastic deformation of crystalline materials. Dislocation dynamics exhibits a complex behaviour due to both self-induced constraints and embedded *quenched disorder*. If subject to small fluctuations, dislocations assemblies such as pileups and low-angle grain boundaries behave like elastic manifolds. We showed that, taking into account the long nature of the interactions involved, elastic properties of pileups and grain boundaries are appropriately described within the framework of non-local elasticity and line/surface tension approximations prove inadequate. This affects their response induced by disorder and their critical behaviour when an external stress is applied. In order to assess this picture we investigated the properties of pinning and the dynamics at the depinning transition. Our results, confirmed by experiments and numerical simulations, allow to map our problem on that of a contact line or a magnetic domain wall and provide a microscopic description of a wealth of plastic phenomena involving dislocation dynamics including certain types of recrystallisation.

Next, we considered an application to grain boundary depinning in flux line (vortex) lattices

in Type II superconductors. Grain boundaries and grain structures are often observed in these systems. However no theory currently accounts for polycrystalline ordering. We derived the exact solution for the elastic problem of a grain boundary in a flux line lattice and formulated a theory of a vortex polycrystal in the presence of disorder. Grain growth is first examined and the derived average grain size is found in good agreement with experiments. Then the problem of transport in the underlying superconductor is addressed. Pinning of topological defects in the vortex lattice is expected to influence the response to an applied current. Currents act in the form of external Lorentz forces driving vortex motion. Below a critical current, the vortex lattice is pinned by disorder and conduction takes place without resistance. Above the critical current, instead, vortices start gliding in the transversal direction, causing dissipation. We found that in the presence of a polycrystalline arrangement, a higher critical current is expected, and the region characterised by zero-resistance is broader. The hysteretical behaviour commonly observed in experiments proves to be a natural consequence of grain boundary depinning. Finally, we analysed the role of grain boundaries in a phenomenological approach to vortex lattice melting. In agreement with various recent numerical results, we found that a polycrystalline arrangement is energetically advantageous at high temperatures, thus constituting an early stage of the transition to the liquid phase, which is observed at higher temperatures.

On larger length scales, we formulated a continuum theory accounting for spatial heterogeneities and intermittent behaviour observed in deforming crystals in the form of self-affine roughening of surfaces and stick-slip avalanche phenomena. We mapped the system to a general depinning problem, in which disorder is introduced by random fluctuations in dislocation densities. We proved that the pinning approach predicts mean-field behaviour, as the system can be envisaged as an elastic manifold slowly driven through a random medium above the critical dimension and constantly close to criticality. Depinning occurs at the onset of yielding, corroborating the picture of a non-equilibrium *yielding transition*, as recently suggested by experimental evidence of critical scale-free behaviour, observed in a wide variety of examples, from ice crystals to metals. Our expectations were confirmed by the numerical implementation of our model, performed by our co-workers. Avalanche size distribution was found consistent with the mean-field prediction and simulated surface profiles agreed quantitatively with the ones obtained experimentally.

Finally, we investigated the possibility of a pinning theory in the general context of slope failure. We considered the propagation of cracks under the effect of internal and external stresses.

We derived the internal shear stress by solving the elastic problem of a body bounded by a disordered plane and formulated a constitutive equation for the model. We found that if on one hand randomness facilitates the nucleation of cracks — hence decreasing the slope strength — on the other hand pre-existing cracks can get pinned by disorder, enhancing stability of the slope. Pinning of cracks is expected to occur at low degrees of randomness, while for highly random substrates diffuse crack nucleation overwhelms pinning effects. In order to get a quantitative picture of the problem, we formulated a depinning theory for crack fronts. Crack fronts show non-local elastic properties and the problem can be easily mapped to the pileup depinning approach recalled above, in good agreement with numerical implementations.

In the light of the results which have been presented and discussed throughout this work, we conclude that several aspects of plasticity can be described in terms of the competition between elasticity and disorder. In spite of its undoubted conceptual simplicity, this kind of approach proves to be a powerful tool in studying complex systems. The ubiquity of randomness — in the various disguises which it assumes on different length scales — turns out essential in understanding the intriguing dynamics of plastically deforming media.

Appendices

Appendix A

Grain boundary junction energy

The presence of a n^2 term in the free energy functional [3.31] was first suggested by Chui [129], in order to take into account grain boundary crossing in the framework of a crystal melting theory. Such a crossing energy consisted of a thermal contribution due to coupling between fluctuations of dislocations of crossing grain boundaries. Nonetheless, Bitter decoration experiments show that in vortex polycrystals, grain boundaries primarily rearrange forming junctions, instead of simply crossing. The formation of such junctions determines variations in the overall free energy of the system due to two different contributions, a zero temperature junction elastic energy and a thermal part related to fluctuations. In the following, we will address to these contributions respectively as Γ_0 and Γ_T, being $\Gamma = \Gamma_0 + \Gamma_T$.

A.1 Zero temperature energy

We assume that because of the short range nature of a grain boundary stress field, grain boundary interactions are screened for long distances and we show that forming a junction leads to a zero-temperature elastic energy gain $\Gamma_0 \neq 0$.

The idea is to focus on what happens when two grain boundaries come so close that they can form a junction. Let us consider a first grain boundary, e.g. directed along $\mathbf{j}$ with Burgers vectors $\mathbf{b}_n$ such that, $\mathbf{b}_n \cdot \mathbf{i} = b_n$, and a single dislocation, belonging to the other grain boundary, whose Burgers vector is $\mathbf{b}' \cdot \mathbf{i} = -b' \cos\varphi$, being φ the junction angle.

Since grain boundary interactions are short-ranged, we expect misorientations effects to make no difference in the energy computation until dislocations come close to a distance that we will call $\bar{s}$. If, on a distance $\bar{s}$, the interaction energy for $\varphi = 0$ is lower than for $\varphi \neq 0$, there in no reason for the system to make a junction. Otherwise, if there is an energy gain, grain boundaries are likely to join.

Considering the general expression for dislocation interactions

$$V = -\frac{K}{2\pi}\left[\ln\frac{e\alpha\,|\mathbf{r}-\mathbf{r}'|}{b}\,\mathbf{b}\cdot\mathbf{b}' - \frac{\mathbf{b}'\cdot(\mathbf{r}-\mathbf{r}')\,\mathbf{b}\cdot(\mathbf{r}-\mathbf{r}')}{|\mathbf{r}-\mathbf{r}'|^2}\right], \tag{A.1}$$

where $\mathbf{r}$ and $\mathbf{r}'$ are the positions of interacting dislocations, the energy (per unit length) of our system (GB and rotated dislocation) is

$$E_s(\varphi) = \frac{Kb^2}{4\pi}\left[\left(\sum_{n=-\infty}^{+\infty}\ln\frac{e^2\alpha^2(s^2+n^2D^2)}{b^2} - 2\sum_{n=-\infty}^{+\infty}\frac{s^2}{s^2+n^2D^2}\right)\cos\varphi - \left(\sum_{n=-\infty}^{+\infty}\frac{snD}{s^2+n^2D^2}\right)\sin\varphi\right], \tag{A.2}$$

where s is the distance between the rotated dislocation and the grain boundary. Moreover, after summing the series,

$$E_s(\varphi) = \frac{Kb^2}{2\pi}\left[\ln\left(\frac{e\alpha D}{\pi b}\sinh\frac{\pi s}{D}\right) - \frac{\pi s}{D}\coth\frac{\pi s}{D}\right]\cos\varphi. \tag{A.3}$$

Assuming that we have M dislocations within the range of $\bar{s}$, the energy gain due to a junction will be

$$\Gamma_0 = \sum_{m=1}^{M} E_{s_m}(\varphi) - M E_{\bar{s}}(0) < 0 \tag{A.4}$$

Since the stress field generated by a grain boundary is exponentially suppressed beyond a distance of the same order of the dislocation spacing, we can give a rough estimate of the sum taking $M = 1$ and $s_1 = D$, i.e.

$$\Gamma_0 \simeq -\frac{Kb^2}{2\pi}(1-\cos\varphi)\ln\left(\frac{e\alpha D}{2\pi b}\right). \tag{A.5}$$

A.2 Thermal fluctuations

The Γ_T contribution, due to the coupling between fluctuations of dislocations belonging to different grain boundaries in a junction can also be estimated following Ref. [129]. After performing the thermal average of the interaction potential (A.1), calculated on the cylinder of radius $|r| < (2/\sqrt{3})D/\pi$ and taking the short range logarithmic part of V

$$\Gamma_T = \mathcal{N}\int dz\int_A dr\, rV\, e^{-\beta V}, \tag{A.6}$$

being $\mathcal{N}$ a normalisation constant. Evaluating the integral for $T \simeq T_m$ leads to

$$\Gamma_T \simeq -\frac{Kb^2}{2\pi} \cos\varphi \, \ln^2\left(\frac{D}{b}\frac{2}{\pi\sqrt{3}}\right), \tag{A.7}$$

where φ is the average junction angle. In the estimate of the lattice-polycrystal crossover we have assumed $\varphi \simeq \pi/3$, as it is often observed in decoration experiments.

Appendix B
Body bounded by two planes

We show a method of integration for the general elastic problem of a body bounded by two planes, given the displacements at the surfaces.

B.1 General properties

Following the reasoning in Reference [161] the elastic problem

$$\nabla^2 \mathbf{w} + \frac{1}{1-2\nu_P}\nabla(\nabla \mathbf{w}) = 0 \tag{B.1}$$

for a continuum of thickness h within two planes is solved if the auxiliary harmonic fields ϕ_n and ϕ'_n that satisfy

$$\frac{\lambda+3G}{4\pi G}\sum_{n=-\infty}^{+\infty}\partial_z(\phi'_n-\phi_n)+\frac{\lambda+G}{2\pi G}h\sum_{n=-\infty}^{+\infty}n\partial_z^2(\phi_n+\phi'_n)=\nabla \mathbf{w}_0, \tag{B.2}$$

are found. Here λ is the first Lamè coefficient, G the shear modulus and $\mathbf{w}_0$ the solution of the harmonic problem $\nabla \mathbf{w}_0 = 0$ for the assigned boundary conditions. The solution in that case would read

$$\begin{aligned}
w_x &= w_{0x} + \frac{\lambda+G}{4\pi G}\sum_{n=-\infty}^{+\infty}\left[(2nh+z)\partial_x\phi_n + (2nh+h-z)\partial_x\phi'_n\right] \\
w_y &= w_{0y} + \frac{\lambda+G}{4\pi G}\sum_{n=-\infty}^{+\infty}\left[(2nh+z)\partial_y\phi_n + (2nh+h-z)\partial_y\phi'_n\right] \\
w_z &= w_{0z} - \frac{\lambda+G}{4\pi G}\sum_{n=-\infty}^{+\infty}\left[z\partial_z(\phi'_n-\phi_n) + h\partial_z\phi'_n\right] .
\end{aligned} \tag{B.3}$$

Equations B.3 give a great deal of insight into the physical nature of the problem. Each point within the medium "sees" its infinite reflections on the two planes. Up to constants, the solutions can be qualitatively envisaged as an infinite sum of solutions for the single plane problem.

Once given the above solution, we only need to determine the auxiliary fields to replace in B.3. The rest of the Appendix is devoted to this task.

B.2 Calculating the fields ϕ_n and ϕ'_n

Given the structure of the system, which recalls the simpler problem of the single plane, we can write the auxiliary fields in the forms [161]

$$\begin{aligned}
\phi_0(r) &= \int \frac{d^2k}{(2\pi)^2} e^{i(k_x x + k_y y)} \Phi(k_x, k_y) e^{-Qz} \\
\phi'_0(r) &= \int \frac{d^2k}{(2\pi)^2} e^{i(k_x x + k_y y)} \Phi'(k_x, k_y) e^{-Q(h-z)} \\
\phi_n(r) &= \int \frac{d^2k}{(2\pi)^2} e^{i(k_x x + k_y y)} \Phi(k_x, k_y) e^{-Q(2nh+z)} \\
\phi'_{-n}(r) &= \int \frac{d^2k}{(2\pi)^2} e^{i(k_x x + k_y y)} \Phi(k_x, k_y) e^{-Q(2nh-z)} \qquad \text{(B.4)} \\
\phi'_n(r) &= \int \frac{d^2k}{(2\pi)^2} e^{i(k_x x + k_y y)} \Phi'(k_x, k_y) e^{-Q(2nh+h-z)} \\
\phi'_{-n}(r) &= \int \frac{d^2k}{(2\pi)^2} e^{i(k_x x + k_y y)} \Phi'(k_x, k_y) e^{-Q(2nh-h+z)} \ ,
\end{aligned}$$

(B.5)

where we have expressed the dependence on the x and y coordinates in terms of the Fourier transforms Φ and Φ' and the behaviour along z as a sum of exponentials. Here $Q = \sqrt{k_x^2 + k_y^2}$

In order to obtain the desired functions from Equation B.2 we need the explicit solution of the harmonic problem w_0. For our system we choose appropriate boundary conditions in the form

$$\begin{aligned}
w_x(x, y, h) = u(x, y) \ , w_y(x, y, h) = w_z(x, y, h) = 0 \\
w_x(x, y, 0) = w_y(x, y, 0) = w_z(x, y, 0) = 0 \qquad \text{(B.6)}
\end{aligned}$$

assuming that no displacement takes place at the interface with the bedrock. We obtain that the only nonzero component is

$$w_{ox} = \int \frac{d^2k}{(2\pi)^2} e^{i(k_x x + k_y y)} \left[\frac{e^{Qz} - e^{-Qz}}{e^{Qh} - e^{-Qh}} \right] u(k_x, k_y) \, , \tag{B.7}$$

which, once replaced in Equation B.2 allows to determine, after tedious calculations

$$\Phi = i\frac{k_x}{Q}(e^{Qh} - 1)\frac{M(e^{Qh} - e^{-Qh}) + NQh(e^{Qh} + e^{-Qh} + 1)}{M^2(e^{Qh} - e^{-Qh}) + (NQh)^2} u(k_x, k_y) \, , \tag{B.8}$$

$$\Phi' = i\frac{k_x}{Q}(e^{Qh} - 1)\frac{M(e^{Qh} - e^{-Qh})(e^{Qh} + e^{-Qh} + 1) + NQh}{M^2(e^{Qh} - e^{-Qh}) + (NQh)^2} u(k_x, k_y) \, , \tag{B.9}$$

with $M = (\lambda + 3G)/(4\pi G)$ and $N = (\lambda + G)/(2\pi G)$. The problem is then solved. An explicit result can be found replacing these functions in B.4, inserting the resulting fields in B.3 and differentiating accordingly.

Here we meant to focus on the method we adopted to find a solution explicitly accounting for Fourier components of deformation on the xy plane. The result is briefly discussed in Chapter 5.

References

Publications

Book Articles

S. Zapperi, M.-C. Miguel, P. Moretti and M. Zaiser, *Jamming and yielding of dislocations: From crystal plasticity to superconducting vortex flow*, Springer, Lecture Notes in Physics, in press.

Articles in International Journals

P. Moretti, M.-C. Miguel, M. Zaiser, and S. Zapperi, *Depinning transition of dislocation assemblies: Pileups and Low angle grain boundaries*, Phys. Rev. B **69**, 214103 (2004).

P. Moretti, M.-C. Miguel, M. Zaiser, and S. Zapperi, *Growth of a Vortex Polycrystal in Type II Superconductor*, Phys. Rev. Lett. **92**, 257004 (2004).

M.-C. Miguel, P. Moretti, M. Zaiser, and S. Zapperi, *Statistical dynamics of dislocations in simple models of plastic deformation: Phase transitions and related phenomena*, Mater. Sci. Eng. A **400-401**, 191198 (2005).

P. Moretti, M.-C. Miguel, and S. Zapperi, *Grain boundaries in vortex matter*, Phys. Rev. B **72**, 014505 (2005).

M. Zaiser, and P. Moretti, *Fluctuation phenomena in crystal plasticity - a continuum model*, J. Stat. Mech. P08004 (2005).

Papers in Conference Proceedings

M. Zaiser, B. Fyffe, P. Moretti, A. Konstantinidis and E.C. Aifantis, *Pinning and propagation of interface cracks in slope failure: 1D and 2D considerations*, In: Modelling of Cohesive-Frictional Materials, Eds. P.A. Vermeer, W. Ehlers, H.J. Herrmann & E.Ramm, Taylor and Francis, London 2004, pp. 435-446.

S. Zapperi, P. Moretti, M.-C. Miguel and M. Zaiser, *Depinning of a Dislocation Pileup*, In: Dislocations, Plasticity and Metal Forming, Proceedings of the Plasticity 2003 Conference, Ed.

Bibliography

[1] M. Zaiser, *Habilitation Thesis*, University of Stuttgart (2001).

[2] H. Fukuyama, and P. A. Lee, Phys. Rev. B **17**, 535 (1978).

[3] D. S. Fisher, Phys. Rev. B **31**, 1396 (1985).

[4] U. Narayan, and D. S. Fisher, Phys. Rev. B **46**, 11520 (1992).

[5] O. Narayan and D. S. Fisher, Phys. Rev. B **48**, 7030 (1993).

[6] A. I. Lar'kin and Yu. N. Ovchinnikov, J. Low Temp. Phys. **34**, 409 (1979).

[7] S. Bhattacharya and M. J. Higgins, Phys. Rev. Lett. **70**, 2617 (1993).

[8] G. Blatter, M. V. Feigel'man, V. B. Geshkenbein, A. I. Larkin, and V. M. Vinokur, Rev. Mod. Phys. **66**, 1125 (1994).

[9] T. Giamarchi, and P. Le Doussal, Phys. Rev. Lett. **72**, 1530 (1994).

[10] T. Giamarchi and P. Le Doussal, Phys. Rev. B **52**, 1242 (1995).

[11] R. Surdeanu, R. J. Wijngaarden, E. Visser, J. M. Huijbregtse, J. H. Rector, B. Dam, and R. Griessen Phys. Rev. Lett. **83**, 2054 (1999).

[12] R. Labusch, Cryst. Lattice Defects **1**, 1 (1969).

[13] R. Labusch, Phys. Status Solidi **41**, 659 (1970); Acta Metall. **20**, 917 (1972).

[14] S. Zapperi and M. Zaiser, Mat. Sci. and Eng. A **309-310**, 348 (2001).

[15] S. Lemerle, J. Ferré, C. Chappert, V. Mathet, T. Giamarchi, and P. Le Doussal Phys. Rev. Lett. **80**, 849 (1998).

[16] S. Zapperi, P. Cizeau, G. Durin and H. E. Stanley, Phys. Rev. B **58**, 6353 (1998).

[17] E. Schäffer and P.-Z. Wong Phys. Rev. E **61**, 5257 (2000).

[18] E. Rolley, C. Guthmann, R. Gombrowicz, and V. Repain Phys. Rev. Lett. **80**, 2865 (1998).

[19] E. Bouchaud, J Phys. C **9**, 4319 (1997).

[20] J. Schmittbuhl and K. Maaløy, Phys. Rev. Lett. **78**, 3888 (1997).

[21] R. Bruinsma, and G. Aeppli, Phys. Rev. Lett. **52**, 1547 (1984).

[22] J. Koplik, and H. Levine, Phys. Rev. B **32**, 280 (1985).

[23] M. Kardar, Phys. Rep. **301** 85 (1998).

[24] D. S. Fisher, Phys. Rep. 301, 113-150 (1998).

[25] T. Nattermann, S. Stepanow, L. H. Tang, and H. Leschhorn J. Phys. II (France) **2**, 1483 (1992).

[26] H. Leschhorn, T. Nattermann, S. Stepanow, and L. H. Tang, Ann. Physik **6**, 1 (1997).

[27] D. Ertas and M. Kardar, Phys. Rev. E **49**, R2532 (1994).

[28] P. Chauve, T. Giamarchi, and P. Le Doussal Phys. Rev. B **62**, 6241 (2000).

[29] P. Le Doussal, K. J. Wiese, and P. Chauve Phys. Rev. B **66**, 174201 (2002).

[30] F. Lacombe, S. Zapperi and H. J. Herrmann, Phys. Rev. B **63**, 104104 (2001).

[31] A. Rosso, A. K. Hartmann, and W. Krauth Phys. Rev. E 67, 021602 (2003).

[32] J. Schmittbuhl, S. Roux, J.P. Villotte, and K. J. Maloy, Phys. Rev. Lett. **74**, 1787 (1995).

[33] S. Ramanathan and D. Fisher, Phys. Rev. Lett. **79**, 877 (1997); Phys. Rev. B **58**, 6026 (1998).

[34] A. Tanguy, M. Gounelle and S. Roux, Phys. Rev. E **58**, 1577 (1998).

[35] A. Rosso and W. Krauth Phys. Rev. E **65**, 025101 (2002).

[36] D. Cule, and T. Hwa, Phys. Rev. Lett. **77**, 278 (1996).

[37] D. Cule, and T. Hwa, Phys. Rev. B **57**, 8235 (1998).

[38] S. K. Ma, *Modern theory of critical phenomena*, Benjamin Press (1976).

[39] P. Sibani, and P. B. Littlewood, Phys. Rev. Lett. **64**, 1305 (1990).

[40] A. A. Middleton, and D. S. Fisher, Phys. Rev. Lett. **66**, 92 (1991).

[41] A. A. Middleton, and D. S. Fisher, Phys. Rev. B **47**, 3530 (1993).

[42] C. R. Myers, and J. P. Sethna, Phys. Rev. B **47**, 11171 (1993).

[43] B. Koiller, H. Ji, and M. O. Robbins, Phys. Rev. B **46**, 5258 (1992).

[44] M. Dong, M. C. Marchetti, A. A. Middleton, and V. Vinokur, Phys. Rev. Lett. **70**, 662 (1993).

[45] H. Leschhorn, and L.-H. Tang, Phys. Rev. Lett. **70** 2973 (1993).

[46] L. A. N. Amaral, A.-L. Barabasi, and H. E. Stanley, Phys. Rev. Lett. **73**, 62 (1994).

[47] M. A. Rubio, C. A. Edwards, A. Dougherty, and J. P. Gollub, Phys. Rev. Lett. **63** 1685 (1989).

[48] V. K. Horváth, F. Family, and T. Vicsek, Phys. Rev. Lett. **67**, 3207 (1991).

[49] S. He, G. L. M. K. S. Kahanda, and P.-Z. Wong, Phys. Rev. Lett **69**, 3731 (1992).

[50] S. V. Buldyrev *et al.*, Phys, Rev. A **45**, R8313 (1992).

[51] M. Paczuski, S. Maslov, and P. Bak, Phys. Rev. E **53**, 414 (1996).

[52] P. C. Martin, E. Siggia, and H. Rose, Phys. Rev. A **8**, 423 (1973)

[53] U. Nowak, and K.D. Usadel, Europhys. Lett. **44** 634 (1998).

[54] L. Roters, A. Hucht, S. Lübeck, U. Nowak and K.D. Usadel, Phys. Rev. E **60**, 5202 (1999).

[55] A. A. Middleton, Phys. Rev. Lett. **68**, 670-673 (1992).

[56] A. I. Larkin, Sov. Phys. JETP **31**, 784 (1970).

[57] Y. Imry and S. K. Ma, Phys. Rev. Lett. **35**, 1399 (1975).

[58] J. Friedel, *Dislocations*, Pergamon Press (1967).

[59] M.C. Miguel, A. Vespignani, M. Zaiser and S. Zapperi, Phys. Rev. Lett. **89**, 165501 (2002).

[60] F. R. N. Nabarro (Ed.), *Dislocations in Solids*, Vol. **4**, North-Holland (1979).

[61] M. Z. Butt and P. Feltham, J. Mat. Sci. **28**, 2557 (1993).

[62] H. Neuhäuser, Phys. Scr. **T49** 412 (1993).

[63] F. R. N. Nabarro, Proc. R. Soc. Lond. A **381**, 285 (1982).

[64] E. H. Brandt, Phys. Rev. Lett. **56**, 1381 (1986).

[65] L. B. Ioffe and V. M. Vinokur, J. Phys. C **20**, 6149 (1987).

[66] J. G. Sevillano, E. Bouchaud and L. P. Kubin, Scr. Metall. Mater. **25**, 355 (1991).

[67] G. D'Anna, W. Benoit and V. M. Vinokur, J. Appl. Phys. **82**, 5983 (1997).

[68] A. J. E. Foreman, Phil. Mag. **15**, 1011 (1967).

[69] G. De Wit and J. S. Koeheler, Phys. Rev. **116**, 1113 (1959).

[70] M.C. Miguel and M. Kardar, Phys. Rev. B **56**, 11903 (1997).

[71] S. I. Zaitsev and E. M. Nadgorny, Sov. Phys. Solid State **21**, 804; *ibid* 1934 (1979).

[72] J. Plessing, *PhD thesis*, University of Braunschweig (1995).

[73] C. S. Smith, Trans. AIME **175**, 15 (1948).

[74] P. A. Manohar, M. Ferry and T. Chandra, ISIJ Intern. **38**, 913 (1998).

[75] P. M. Hazzledine and R. D. J. Oldershaw, Phil. Mag. A **61**, 579 (1990).

[76] P. Moretti, M.-C. Miguel, M. Zaiser, and S. Zapperi, Phys. Rev. B **69**, 214103 (2004).

[77] P. Moretti, M.-C. Miguel, M. Zaiser, and S. Zapperi, Phys. Rev. Lett. **92**, 257004 (2004).

[78] P. Moretti, M.-C. Miguel, and S. Zapperi, Phys. Rev. B **72**, 014505 (2005).

[79] M.-C. Miguel, A. Vespignani, S. Zapperi, J. Weiss and J. R. Grasso, Nature **410**, 667 (2001).

[80] J. Weiss *et al.*, Mater. Sci. Eng. A **309-310**, 360 (2001).

[81] M.Zaiser, Mater. Sci. Engng. **A 309/310**, 304 (2001).

[82] J. Weiss, and D. Marsan, Science **299**, 89-92 (2003).

[83] M. Zaiser, F. Madani, V. Koutsos, and E. C. Aifantis, Phys. Rev. Lett. **93**, 195507 (2004).

[84] M. Zaiser, and P. Moretti, J. Stat. Mech. P08004 (2005).

[85] R. Burridge, and L. Knopoff, Bull. Seismol. Soc. Am. **57**, 341 (1967).

[86] J. Carlson, and J. S. Langer, Phys. Rev. Lett. **62**, 2632 (1989).

[87] H. Nakanishi, Phys. Rev. A **41**, 7086 (1990).

[88] H. J. S. Feder, and J. Feder, Phys. Rev. Lett. **66**, 2669 (1991).

[89] D. S. Fisher, K. Dahmen, S. Ramanathan, and Y. Ben-Zion, Phys. Rev. Lett. **78**, 4885 (1997).

[90] M. Zaiser, B. Fyffe, P. Moretti, A. Konstantinidis, and E. C. Aifantis, *Pinning and propagation of interface cracks in slope failure: 1D and 2D considerations*, In *Modelling of Cohesive-Frictional Materials*, Eds. P.A. Vermeer, W. Ehlers, H.J. Herrmann & E. Ramm, Taylor and Francis, London 2004, 435-446 (2005).

[91] J.P. Hirth and J. Lothe, *Theory of Dislocations*, McGraw Hill (1968).

[92] J.F. Joanny and P.G. de Gennes, J. Chem. Phys. **81**, 552 (1984).

[93] H. Gao and J. R. Rice, ASME J. Appl. Mech. **56**, 828 (1989).

[94] H. Neuhäuser, In: F. R. N. Nabarro (Ed.), *Dislocations in Solids*, Vol. **6**, North-Holland (1983), p. 319.

[95] E. H. Brandt, Rep. Prog. Phys. **58**, 1465 (1995).

[96] T. Giamarchi and S. Bhattacharya, In *High Magnetic Fields: Applications in Condensed Matter Physics and Spectroscopy*, p. 314, C. Berthier *et al.* Eds., Springer-Verlag, (2002).

[97] A. A. Abrikosov, Zh. Eksp. Teor. Fiz. **32**, 1442 (1957).

[98] H. Safar, P. L. Gammel, D. A. Huse, D. J. Bishop, J. P. Rice, and D. Ginsberg, Phys. Rev. Lett. **69**, 824 (1992).

[99] F. Bouquet, C. Marcenat, E. Steep, R. Calemczuk, W. K. Kwok, U. Welp, G. W. Crabtree, R. A. Fisher, N. E. Phillips, A. Schilling, Nature **411**, 448 (2001).

[100] N. Avraham, B. Khaykovich, Y. Myasoedov, M. Rappaport, H. Shtrikman, D. E. Feldman, T. Tamegai, P. H. Kes, M. Li, M. Konczykowski, K. van der Beek, E. Zeldov, Nature **411**, 451 (2001).

[101] R. Cubitt, E. M. Forgan, G. Yang, S. L. Lee, D. McK. Paul, H. A. Mook, M. Yethiraj, P. H. Kes, T. W. Li, A. A. Menovsky, Z. Tarnawski, K. Mortensen, Nature **365**, 407 (1993).

[102] P. L. Gammel, U. Yaron, A. P. Ramirez, D. J. Bishop, A. M. Chang, R. Ruel, L. N. Pfeiffer, and E. Bucher, Phys. Rev. Lett. **80**, 833 (1998).

[103] X. S. Ling, S. R. Park, B. A. McClain, S. M. Choi, D. C. Dender, and J. W. Lynn, Phys. Rev. Lett. **86**, 712 (2001).

[104] D. S. Fisher, M. P. A. Fisher and D. A. Huse, Phys. Rev. **B 43**, 130 (1991).

[105] D. R. Nelson and V. M. Vinokur, Phys. Rev. B **61**, 5917 (2000).

[106] I. V. Grigorieva, Supercond. Sci. Technol. **7**, 161 (1994).

[107] U. Essmann and H. Trauble, Phys. Lett. A **56**, 596 (1967).

[108] I. V. Grigorieva. Sov. Phys. JETP **69**, 194 (1989).

[109] M. V. Marchevsky *PhD Thesis*, (Leiden University, 1997).

[110] M. Marchevsky, A. Keurentjes, J. Aarts, and P. H. Kes, Phys. Rev. B **57**, 6061 (1998).

[111] Y. Fasano, M. Menghini, F. de la Cruz, Y. Paltiel, Y. Myasoedov, E. Zeldov, M. J. Higgins, and S. Bhattacharya, Phys. Rev. B **66**, 020512 (2002).

[112] F. Pardo , F. De La Cruz, P. L. Gammel, C. S. Oglesby, E. Bucher, B. Batlogg, and D. J. Bishop, Phys. Rev. Lett. **78**, 4633 (1997).

[113] H. Dai, J. Liu and M. Lieber, Phys. Rev. Lett. **72**, 748 (1994).

[114] J. A. Herbsommer, G. Nieva and J. Luzuriaga, Phys. Rev. B **62**, 678 (2000).

[115] T. Klein, I. Joumard, S. Blanchard, J. Marcus, R. Cubbit, T. Giamarchi, and P. Le Doussal, Nature (London) 413, 404 (2001).

[116] D. Carpentier, P. Le Doussal and T. Giamarchi, Europhys. Lett. **35**, 379 (1996).

[117] J. Kierfeld, T. Nattermann and T. Hwa, Phys. Rev. B **55**, 626 (1997).

[118] D. S. Fisher, Phys. Rev. Lett. **78**, 1964 (1997).

[119] G. P. Mikitik and E. H. Brandt Phys. Rev. B **68**, 054509 (2003).

[120] J. Kierfeld and V. M. Vinokur, Phys. Rev. B **61**, 14928 (2000).

[121] F. R. N. Nabarro and A. T. Quintanilha, In: F. R. N. Nabarro (Ed.) *Dislocations in Solids*, Vol. **5**, North-Holland, (1980).

[122] E. H. Brandt, Phys. Rev. B **34**, 6514 (1986).

[123] J. Kierfeld, H. Nordborg and V. M. Vinokur, Phys. Rev. Lett. **85**, 4948 (2000).

[124] M.-C. Miguel and S. Zapperi, Nature Mat. **2**, 477 (2003).

[125] M. Chandran, R. T. Scalettar, and G. T. Zimnyi, Phys. Rev. B **69**, 024526(2004).

[126] C. Dasgupta and O. T. Valls, Phys. Rev. Lett. **91** 127002 (2003).

[127] C. Dasgupta and O. T. Valls, Phys. Rev. B **69**, 214520 (2004).

[128] C. Dasgupta and O. T. Valls, Phys. Rev. B **72**, 094501 (2005).

[129] S. T. Chui, Phys. Rev. B **28**, 178 (1983).

[130] Z. L. Xiao, E. Y. Andrei, P. Shuk, and M. Greenblatt, Phys. Rev. Lett. 86, 2431 (2001).

[131] W. Henderson, E. Y. Andrei, M. J. Higgins, and S. Bhattacharya, Phys. Rev. Lett. **77**, 2077 (1996).

[132] Z. L. Xiao, E. Y. Andrei, P. Shuk, and M. Greenblatt, Phys. Rev. Lett. **85**, 3265 (2000).

[133] S. S. Banerjee, N. G. Patil, S. Ramakrishnan, A. K. Grover, S. Bhattacharya, G. Ravikumar, P. K. Mishra, T. V. Chandrasekhar Rao, V. C. Sahni, and M. J. Higgins, Appl. Phys. Lett. bf 74, 126 (1999).

[134] I. Joumard, T. Klein, J. Marcus, and R. Cubitt, Physica C **341-348**, 2131 (2000).

[135] B. Sas, F. Portier, K. Vad, B. Keszei, L. F. Kiss, N. Hegman, I. Puha, S. Mszros, and F. I. B. Williams, Phys. Rev. B **61**, 9118 (2000).

[136] G. I. Menon Phys. Rev. B **65**, 104527 (2002); Mod. Phys. Lett. B **15**, 1023 (2001).

[137] U. Divakar, A. J. Drew, S. L. Lee, R. Gilardi, J. Mesot, F. Y. Ogrin, D. Charalambous, E. M. Forgan, G. I. Menon, N. Momono, M. Oda, C. D. Dewhurst, and C. Baines, Phys. Rev. Lett. **92**, 237004, (2004).

[138] P. M. Hazzledine and R. D. J. Oldershaw, Phil. Mag. A **61**, 579 (1990).

[139] P.-G. de Gennes, *Superconductivity of metals and alloys* (Benjamin, New York, 1966).

[140] M. Menghini, Y. Fasano, and F. de la Cruz, Phys. Rev. B 65, 064510 (2002).

[141] M.-C. Miguel and M. Kardar, Phys. Rev. B **62**, 5942 (2000).

[142] E. Schneider, J. Low. Temp. Phys. **31**, 357 (1978).

[143] G. H. Kruithof, P. C. van Son, and T. M. Klapwijk, Phys. Rev. Lett. **67**, 2725 (1991).

[144] M. K. Phani, J. L. Lebowitz, M. H. Kalos, and O. Penrose, Phys. Rev. Lett. **45**, 366 (1980).

[145] M. Zaiser, and A. Seeger, *Long-range internal stresses, dislocation patterning and work hardening in crystal plasticity*, In: F. R. N. Nabarro and M. S. Duesbery (Eds.), *Dislocations in Solids*, Vol. **11**, North-Holland, pp. 1-100.

[146] I. Groma, F. Csikor, and M. Zaiser, Acta Mater. **51**, 1271-1281 (2003).

[147] M. Zaiser, and E. C. Aifantis, *On the theory of gradient plasticity III: Random effects and slip avalanches*, Int. Journal of Plasticity (in press).

[148] M. D. Uchic, D. M. Dimiduk, J. N. Florando, and W. D. Nix, Science **305**, 986-989 (2004).

[149] M. D. Uchic, Mater. Sci. Eng. A **400-401**, 268 (2005).

[150] J.-C. Baret, D. Vandembroucq, and S. Roux, Phys. Rev. Lett. **89**, 195506 (2002).

[151] A. C. Palmer, and J. R. Rice, Proc. R. Soc. London, Ser. A **332**, 527-548 (1973).

[152] D. M. McClung, J. Geophys. Res. **84**, 3519-3526 (1979).

[153] H. Conway, and J. Abrahamson, J. Glaciol. **34**, 170-177 (1988).

[154] M. Zaiser, Annals of Glaciol. **38**, 9-14 (2004).

[155] B. Fyffe, M. Zaiser, and E. C. Aifantis, J. Mechan. Behav. Materials **15**, 185 (2004).

[156] A. E. H. Love, *A treatise on the mathematical theory of elasticity*, Dover Publications (1944).

[157] M. Zaiser, M. Avlonitis, and E. C. Aifantis, Acta Materialia **46**, 4143-4151 (1998).

[158] H. M. Zbib, and E. C. Aifantis, Scripta Metall. Mater. **22**, 703-708 (1988).

[159] I. Simonsen, A. Hansen, and O. M. Nes, Phys. Rev. E **58**, 2779-2787 (1998).

[160] J. F. Joanny, and P. G. de Gennes, J. Chem. Phys. **81**, 552 (1984).

[161] O. Tedone, Annali di Matematica Pura ed Applicata, serie 3, tomo **10**, 13-64 (1904).